

DMS – RE 2009

The nineteenth joint seminar

**DEVELOPMENT
OF MATERIALS SCIENCE
IN RESEARCH AND
EDUCATION**

PROCEEDINGS OF THE 19th JOINT SEMINAR

August 31 - September 4, 2009

Z á v a ž n á P o r u b a

DMS – RE 2009

The nineteenth joint seminar

**DEVELOPMENT
OF MATERIALS SCIENCE
IN RESEARCH AND
EDUCATION**

August 31 – September 4, 2009

Z á v a ž n á P o r u b a

Organized by

Slovak Expert Group of Solid State Chemistry and Physics
Czech and Slovak Association for Crystal Growth
Faculty of Chemical and Food Technology STU
Faculty of Materials Science and Technology STU
Crystallographic Society
Slovak Society for Industrial Chemistry
Regional Committee of Czech and Slovak Crystallographers

Sponsor of **DMS-RE 2009**

Slovak Society for Industrial Chemistry

Anamet s.r.o. instruments for material testing

1. Maja 29, 900 01 Modra, Slovak Republic

ITES Vranov, s. r. o.

Čemernianska 137

093 03 Vranov nad Topľou, Slovak Republic

ISBN 978-80-89088-81-2

GUARANTEES

Prof. Ing. Marian Koman, DrSc., STU Bratislava

Ing. Karel Nitsch, PhD., Institute of Physics of the AS ČR, Prague

PROGRAM COMMITTEE

M. Koman (chairman)

M. Behúlová

D. Mikloš

M. Rodová

ORGANIZING COMMITTEE

B. Papánková (chairman)

M. Behúlová

M. Koman

D. Mikloš

V. Jorík

Secretary

Ľ. Dlháň

Department of Inorganic Chemistry, FCHPT STU Bratislava

e-mail: lubor.dlhan@stuba.sk

Editors

M. Koman

D. Mikloš

FOREWORD

The seminar "Development of Materials Science in Research and Education" is already the nineteenth in the series started at Gabčíkovo in 1991 by the initiative of the Czech and Slovak Association for Crystal Growth and the Slovak Expert Group of Solid State Chemistry and Physics.

The objective of this meeting is to offer an opportunity to Czech and Slovak teachers and scientists as well as guests from other countries who are working in the field of Materials Science to present their recent results and experience and to exchange new ideas and information.

The scientific session will cover the following topics on materials science:

- Trends in development of material research
- Education in materials science at the universities
- Information on research program of individual institutions
- Information on equipments for preparation and characterization of materials
- Results of materials science research

This workshop is aimed at creation of a stimulating atmosphere of cooperation and at the support of patient dissemination of scientific ideas and propagation of materials science in education.

Organizers

CONTENTS

<i>T. Bazyláková, D. Ondrušová, M. Pajtášová, S. Lalíková, M. Olšovský</i>	12
STUDY OF ZEOLITES AS FILLER IN THE RUBBER COMPOUNDS	
<i>M. Behúlová</i>	14
APPROACHES TO THE MODELLING OF METALLIC MATERIAL PROCESSING IN SEMI-SOLID STATE	
<i>O. Blahož, M. Kursá</i>	16
EFFECT OF THERMOMECHANICAL CYCLING ON CHARACTERISTIC OF Ni – Ti SHAPE MEMORY ALLOYS	
<i>V. Brožek, P. Ctibor, H. Boldyryeva, D.-I. Cheong, S.-H. Yang</i>	18
COMPATIBILITY OF PLASMA SPRAYED TUNGSTEN BASED MATERIALS WITH GRAPHITE SUBSTRATES	
<i>P. Demo, Z. Kožíšek, A. M. Sveshnikov, P. Tichá, J. Krňanský</i>	20
STIMULATED NUCLEATION ON POLYMER NANOFIBRES	
<i>L. Dlháň, R. Boča, N. Hassan, P. Weinberger, W. Liner</i>	22
SPIN CROSSOVER IN Fe(II) COMPLEXES MONITORED BY DSC CALORIMETRY	
<i>J. Drápala, A. Kroupa, B. Smetana, J. Urbánek</i>	24
LEAD-FREE SOLDERS ON THE TIN – ZINC - ALUMINIUM BASIS FOR HIGH-TEMPERATURE APPLICATIONS	
<i>J. Gutwirth, T. Wágner, M. Frumar</i>	26
BASIC ASPECTS AND TRENDS IN DEVELOPMENT OF NON-VOLATILE REWRITABLE PHASE-CHANGE BASED MEMORIES - OPTICAL DISCS AND PC-RAM MODULES	

<i>J. Hužvár , P. Nemeč</i>	28
PROPOSAL OF HEAT EXCHANGER IN MICRO-COGENERATION UNIT, CONFIGURATION WITH BIOMASS COMBUSTION	
V. Jorík	30
ZEOLITES AND POWDER DIFFRACTION	
<i>J. Juřica, M. Losertová</i>	32
MICROSTRUCTURE PROPERTIES OF TiAl-Nb ALLOY	
<i>M. Koman, J. Moncol'</i>	34
NEW HALOGENCARBOXYLATES OF Cu(II) WITH NICOTINAMIDE	
<i>Z. Kožíšek, P. Demo, A. M. Sveshnikov, P. Tichá</i>	36
NUCLEATION BARRIER IN SMALL VOLUMES	
<i>R. Král, A. Cihlár</i>	38
STUDY ON GROWTH OF LEAD HALIDES SINGLE CRYSTALS FOR SOLID- STATE LASERS IN MID-IR	
<i>S. Lalíková, M. Pajtašová, D. Ondrušová, T. Bazyláková, M. Olšovský</i>	40
THE PROPERTIES OF NATURAL RUBBER/CLAY COMPOUNDS	
<i>J. Lipták</i>	42
STRUCTURE AND ELECTRICAL PROPERTIES OF COMPOSITES OF POLYSTYRENE WITH MODIFIED CARBON BLACK	
<i>R. Dvorský, J. Luňáček, A. Slíva, K. Píksová</i>	44
MORPHOLOGY ANALYSIS OF SILICON NANOPARTICLES PREPARED BY CAVITATION DISINTEGRATION	

<i>D. Lysáček, L. Válek</i>	46
THERMAL STABILITY OF UNDOPED POLYSILICON LAYERS	
<i>J.A. Mareš, P. Průša, M. Nikl, M. Kučera, K. Nitsch, A. Beitlerová</i>	48
SCINTILLATION PROPERTIES OF Ce³⁺-DOPED (Y-Lu) ALUMINUM GARNETS GROWN BY LPE METHOD IN DIFFERENT FLUXES	
<i>M. Martinkovič</i>	50
COMPARISON OF PLASTIC DEFORMATION AND GRAIN BOUNDARIES ORIENTATION OF STEEL	
<i>P. Nemeč, J. Hužvár</i>	52
MATHEMATICAL CALCULATION OF TOTAL HEAT POWER OF THE SODIUM HEAT PIPE	
<i>K. Nitsch, A. Cihlář, M. Rodová, R. Král</i>	54
GROWTH OF RARE EARTH GARNET LAYERS BY LIQUID PHASE EPITAXY	
<i>J. Nováček, S. Štastník</i>	56
COMPREHENSIVE TESTING OF STRUCTURAL POWDER MASS WATER REPELLENTS BASED ON SILICONE	
<i>B. Papánková, R. Boča, L. Dlháň, J. Titiš, I. Svoboda</i>	58
THE ZERO FIELD SPLITTING OF PARAMAGNETIC TRANSITION METAL COMPLEXES	
<i>A. Pavlová, N. Pavlišáková, J. Černák</i>	60
COMPLEXES OF Ni(II) WITH 2,2'-DIPYRIDYLAMINE	
<i>I. Pilarčíková, J. Hampl, S. Jirků</i>	62
MODELLING OF CONSTRICTION PHENOMENON IN COMPOSITE CONTAINING CONDUCTIVE CARBON PARTICLES	

<i>M. Rodová, A. Cihlář, R. Král, K. Nitsch</i>	64
PREPARATION AND PROPERTIES OF LITHIUM YTTRIUM PHOSPHATE - $\text{LiY}(\text{PO}_3)_4$ GLASS	
<i>I. Šabová, J. Černák</i>	66
HETEROBIMETALLIC COORDINATION COMPOUNDS BASED ON COPPER AND NICKEL	
<i>V. Brožek, P. Ctibor, D.-I. Cheong, S.-H. Yang, J. Sedláček</i>	68
STRUCTURE AND ELECTRIC RESISTIVITY OF SINTERED AND PLASMA SPRAYED TUNGSTEN – BASED CERMETS	
<i>J. Šitek, J. Lipka</i>	70
PARAMETERS OF SPENT RADIOACTIVE SOURCE	
<i>J. Šik, M. Lorenc, P. Kostelník</i>	72
BOND AND ETCH-BACK SOI	
<i>P. Štěpán, M. Losertová</i>	74
SHAPE MEMORY ALLOYS ON THE BASE OF TiNi	
<i>L. Válek, D. Lysáček, J. Šik</i>	76
ENGINEERING OF DEFECTS IN HEAVILY BORON-DOPED SILICON	
<i>M. Vavra, I. Potočňák</i>	78
SPECTRAL-STRUCTURAL CORRELATIONS IN COPPER(II) TETRACYANIDOPLATINATE COMPLEXES WITH BI- AND TRIDENTATE N-DONOR LIGANDS	

<i>R. Yatskiy, J. Zavadil, L. Pekarek</i>	80
INFLUENCE OF RARE-EARTH ELEMENTS ON ELECTRICAL AND OPTICAL PROPERTIES OF INP BULK CRYSTALS	
<i>I. Čulák</i>	82
ANAMET s.r.o. INSTRUMENTS FOR MATERIAL TESTING	
PROMOTION OF SPONZORS	83
PROGRAM	85
AUTHOR INDEX	89
REMARKS	91
POST DEADLINE ABSTRACT	92

STUDY OF ZEOLITES AS FILLER IN THE RUBBER COMPOUNDS

T. Bazyláková^(a), D. Ondrušová^(a), M. Pajtášová^(a), S. Ľalíková^(a), M. Olšovský^(a)

(a) Faculty of Industrial Technologies, Trenčín University of Alexander Dubček,
020 01 Púchov, Slovak Republic

Zeolites are microporous crystalline oxides with a high surface to volume ratio. Strictly speaking, they are aluminosilicates of form $M_x^*(Si_{1-x}+Al_x)O_2*yH_2O$. Zeolites have many useful purposes. They can perform ion exchange, filtering, chemical sieve and filler. The zeolite clinoptilolite is a natural silicate mineral with internal channelling, a large surface area and high cation exchange capacity¹.

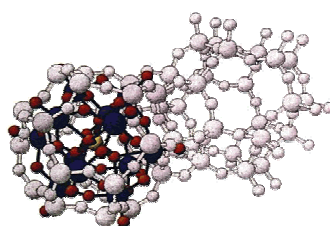


Figure 1. Structure of zeolite

Minerals can be only identified absolutely by x-ray analysis. The x-ray analysis determines the structure of the mineral.

Present paper deals with the preparation of modified rubber compounds in the presence of nanoadditive on the base of clinoptilolite and give the information about their rheology, vulcanization performance and physical-mechanical properties.

The nanofiller of natural zeolite used in the experiments was obtained from region of Majerovce SR. It was ground and fraction of 0 - 0,2 mm was selected.

Individual amounts of mixed components and used conditions are given in the Table 1. Sample 1 – modified rubber compound with the substitution of all amount of filler clinoptilolite. Sample 2 – modified rubber compound with the substitution of 1/2 amount of filler clinoptilolite.

Table 1. Condition of prepared model rubber compound in g

Ingredient of compound	standard	sample 1	sample 2
SMR 20	59,40	59,40	59,40
ZnO	2,73	2,73	2,73
CBS	0,89	0,89	0,89
N660	5,94	0	2,97
Zeolite	0	5,94	2,97
Sulphur N	0,89	0,89	0,89

Selected sample of newprepared modified rubber compounds were studied by methods of thermal analysis - DTA, TG. Differential thermal analysis and Thermogravimetry were measured in the temperature range of 40 °C – 900 °C with heating rate of 10 °C.min⁻¹. Rheology and vulcanization performances (M_L , M_H , t_s , t_{90} , R_V) of prepared rubber

compounds with the addition of nanofiller – clinoptilolite were tested and physical-mechanical properties of vulkanized rubber was studied^{2, 3}. The values of prepared modified rubber compounds was compared with the standard (commercial rubber compound).

X-ray analysis of natural zeolite show that confirmed the major presence of clinoptilolite with structural formula $(\text{Na}_{1,32}\text{K}_{1,28}\text{Ca}_{1,72}\text{Mg}_{0,52})$. The XRD pattern of the natural zeolite sample is given in Fig. 2.

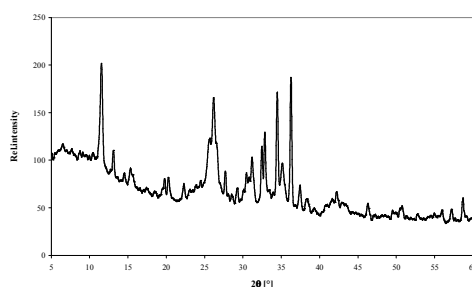


Figure 2. X-ray of natural zeolite

From results of thermal measurements given in Fig. 1-2 follows a similarity of thermogram in the case of sample 2 with the thermogram of standard. The thermal decomposition of all studied rubber compounds was observed in the temperature range of cca 300 °C – 700 °C.

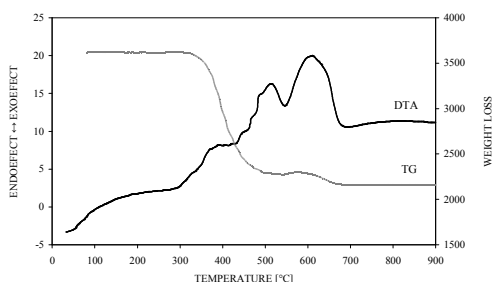


Figure 1. DTA-TG standard rubber compound

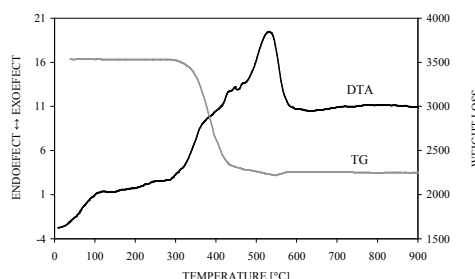


Figure 2. DTA-TG of sample 2

From study of properties of modified rubber compounds with the addition of natural zeolite nanofiller follow that natural zeolite – clinoptilolite may be used for the application in the rubber compounds improving the properties studied.

Acknowledgements

The authors sincerely thank the Slovak Grant AV 4/2014/08 for the financial support.

References

- [1] ŠAMAJOVÁ E.: Z histórie výskumu zeolitových surovín Slovenska, Seminár Prírodné a syntetické zeolity, FCHPT STU Bratislava, 2003.
- [2] DUCHÁČEK V.: Gumárenské suroviny a jejich zpracovávání. VŠCHT Praha, (1999), 96.
- [3] PREKOP Š. a kol.: Gumárska technológia I. Žilinská univerzita Žilina, (1998), 78.

APPROACHES TO THE MODELLING OF METALLIC MATERIAL PROCESSING IN SEMI-SOLID STATE

M. Behúlová

Slovak University of Technology in Bratislava, Faculty of Materials Science and Technology in Trnava, Paulínska 16, 917 24 Trnava, Slovak Republic, maria.behulova@stuba.sk

1. Introduction. Innovative technologies of semi-solid material processing cover particularly the processes of thixoforming and rheocasting. They exploit thixotropic behaviour of two-phase mixtures containing quasi-globular solid particles uniformly distributed in a liquid matrix at the temperatures between solidus and liquidus [1-3]. Thixotropic behaviour of metallic slurries is characteristic by decreasing viscosity with increasing shear rate and shear time. It provides possibilities for manufacturing high-quality parts with complex geometries, very fine homogenous microstructures and significantly improved material properties [1-6]. Comparing with conventional die casting, the lower process temperatures and laminar flow of the melt lead to less shrinkage porosity and entrapped pores in parts produced by semi-solid casting. Thixoforming allows to produce complicated components applying single forming operation with considerably lower forces than in conventional hot forging. In both processing routes, semi-solid material is filling a die cavity. This paper briefly summarizes approaches to the numerical modelling of material flow in semi-solid state.

2. Numerical modelling of metallic material flow in semi-solid state. During the process of filling a die cavity, the flow of semi-solid metallic material is influenced by complex shear-thinning thixotropic material behaviour, occurrence of the yield stress and segregation effects [6, 7]. Moreover, the temperature of slurry material decreases with time what results in the changes of material properties, solid fraction distribution and complete solidification of material near a die wall. Due to the complex behaviour of material flow and solidification under compression, the exact solution of equations describing the semi-solid material processing is impossible and application of numerical modelling is apparent necessity. Numerical analysis and simulation of material flow during semi-solid processing takes advantages of rapid development in the field of computational fluid and solid dynamics. In the dependence on the solid fraction of a material under investigation, the approach derived from computational fluid dynamics or solid mechanics can be applied to model flow phenomena [6-9]. In addition, the micro-macro modelling approach based on the idea of coated inclusions has been developed [10].

Computational fluid dynamics (CFD) is applied mostly for semi-solid materials with a solid content less than 60 % [6-7]. Such materials exhibit a non-Newtonian history-dependent flow behaviour. Models based on CFD can take into account one- or two-phase material flow. In one-phase modelling, material is considered as a continuum. Applying two-phase approach, the coexistence of both liquid phase and solid globular particles is assumed. Each phase has its own behaviour which can be affected by the presence of the other phase through conditions at liquid/solid interface. Solid phase is obviously modelled as viscous compressible or incompressible material, liquid phase as Newtonian fluid. Usually, the two-phase models require the simultaneous calculation of a solid fraction field, a pressure field, two velocity fields (for solid and liquid phase) and a temperature field. In this reason, the computation time can be quite long.

Solid body mechanics is more suitable for highly concentrated slurries which behave similarly as nonlinear elasto-plastic or visco-plastic solids [6-7]. The yield stress is described by the flow curve and depends on the current state of deformation, strain rate and temperature. The viscoplastic constitutive equation defines the velocity dependence of plasticity. In micro-macro modeling [7,10], spherical inclusions (particles) containing entrapped liquid are surrounded by liquid and solid bonds. Particles are assumed to deform very little and deformation takes place mostly in liquid. During deformation, the bonds are broken and the liquid is released.

From the mathematical point of view, models describing the thixotropic material flow consist of a system of partial differential equation for mass conservation (continuity equation), momentum conservation and energy conservation completed by initial and boundary conditions and constitutive equations [7-9]. The properties of semi-solid material flow are characterized by extra stress tensor depending on the viscosity and deformation rate tensor. In some cases, the specific interface friction force is defined supposing that it is proportional to the slip velocity difference.

Obviously, the finite difference, finite volume or finite element discretization methods are used to predict thixotropic material flow applying some commercial program code such as MAGMAsoft, FLOW3D, PAMCAST, ProCAST, FORGE3, DEFORM3D, ABAQUS, PETERA and others [5-8]. Comparing numerical techniques, the finite element method is the most flexible in formulation of the problem for the complex geometrical domains and definition of time and variable dependent material and boundary conditions.

3. Conclusion. Using a suitable approach and experimentally verified material properties and models, the numerical simulation of thixotropic flow can provide many valuable contributions to understanding and optimization of semi-solid material processing.

The financial support from the grant VEGA 1/0837/08 is gratefully acknowledged.

- [1] Flemings, M. C.: Semi-solid forming: the process and the path forward. Metallurgical Science and Technology, Vol. 18, No.2, 2000, pp. 1-4.
- [2] Kiuchi, M., Kopp, R.: Mushy/Semi-Solid Metal Forming Technology – Present and Future, CIRP Annals, Vol. 51, Issue 2, 2002, pp. 653-670.
- [3] Hallstedt, B., Balithev, E., Shimahara, H., Neuschütz, D.: Semi-solid Processing of Alloys. ISIJ International, Vol. 46, 2006, No. 12, pp. 1852–1857.
- [4] Staňková, H. e al.: Influence of Thixoforming on Structure Development of the Tool Steel. In.: 12th International Research/Expert Conference – TMT 2008, Turkey.
- [5] Atkinson, H. V.: Modelling of semi-solid processing. Aachen : Shaker, 2008. ISBN 978-3-8322-7212
- [6] Atkinson, H. V.: Modelling the semisolid processing of metallic alloys. In. Progress in Materials Science, Vol. 50, 2005, pp. 341–412.
- [7] Hirt, G., Kopp, R.: Thixoforming. WILEY-VCH Verlag GmbH & Co. KGaA, Weinheim, 2009. ISBN 978-3-527-32204.
- [8] Hufschmidt, M., Modigell M., Petera, J.: Modeling and simulation of forming processes of metallic suspensions. J. Non-Newtonian Fluid Mech., 134, (1-3) 2006, pp. 16-26.
- [9] Koke, J., Modigell, M.: Flow behaviour of semi-solid metal alloys. Journal of Non-Newtonian Fluid Mechanics, 112, (2-3), 2003, pp. 141-160.
- [10] Kumar, P., Martin, C., Brown, S.: Shear rate thickening flow behaviour of semi-solid slurries. Metall. Mater. Trans. A, 24 (5), 1993, pp. 1107–1115.

EFFECT OF THERMOMECHANICAL CYCLING ON CHARACTERISTIC OF Ni – Ti SHAPE MEMORY ALLOYS

O. Blahož⁽¹⁾, M. Kursá⁽¹⁾

- (1) Faculty of Metallurgy and Material Science, VŠB – Technical University of Ostrava, 70833, Czech Republic
otakar.blahoz@vsb.cz, miroslav.kursa@vsb.cz

Binary Ni – Ti alloys with shape memory effect are ranked among a modern materials with high qualities, so they are often applied in many branches of current industry, e.g. in electrotechnical, optical or biomedical. When we using Ni - Ti alloys in these sophisticated applications, we very often need to know how is this material going under various types of strain, in our case, under the thermomechanical cycling.

Faculty of Metallurgy and Material Science developed and designed a device for testing wire samples under thermal and mechanical cycling effect at the same time. Scheme of testing machine you can see at fig. 1. It is a lever mechanism joined with a dynamometer, combined with electric resistance heater and cooling device. Testing machine enable cycling wires in range from – 30 °C to + 200 °C and from 0 to 3000 N.

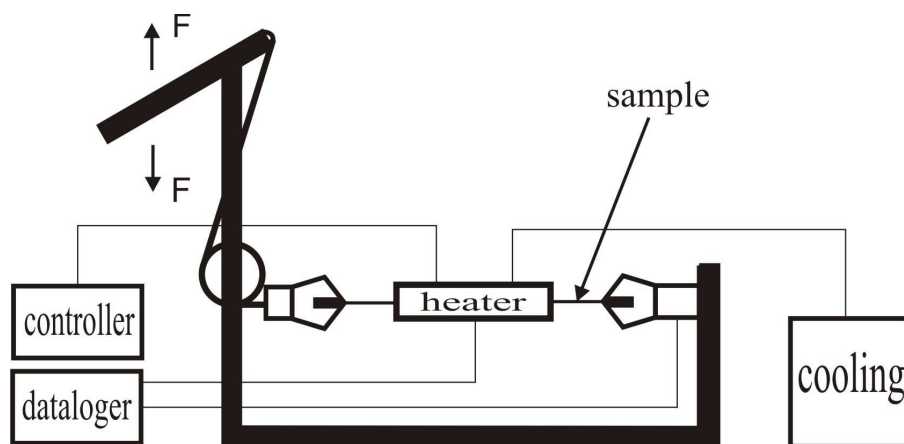


Fig. 1. Scheme of testing device for thermomechanical cycling

For verification characteristic of cycling machine was used Ni – Ti samples prepared from electrolytic Ni and Ti by plasma melting, which was homogenized in vacuum induction furnace and forged into a wire shape. A first part of initiation tests of the machine was a measuring of temperature profile of the heater during various levels of heating and there was defined area of the specimen, which is influenced by desire temperature. Example of load and thermal cycles are shown in fig. 2.

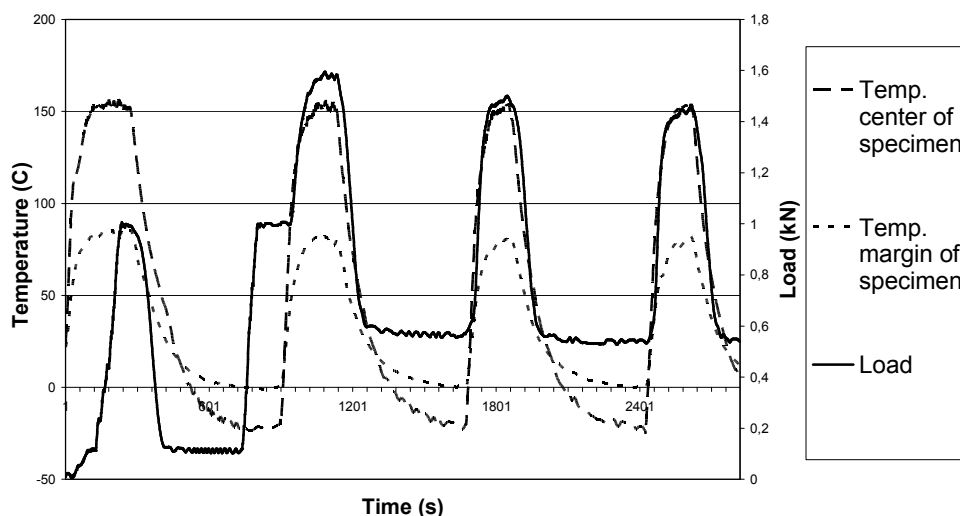


Fig. 2. Part of a testing program with curves of load and temperatures on different position on specimen. Decreasing load curve into a negative partition of the graph is causing by austenite to martensite transformation during temperature falling. In other cycles was load increased, so negative stress induced by transformation stayed in plus numbers.

For experimental research of changing transformation temperatures Ni – Ti alloys will be use 1, 10 and 100 cycles with suitable specified program of loading, heating and cooling of the material. In these cycles must be the lowest testing temperatures lower than M_f of the material and the highest testing temperature higher than its A_f [1].

Aim of this research is analyze effect of thermal and mechanical cycling on changes of transition temperatures and others material characteristics in Ni – Ti alloys with shape memory effect. Following steps in our research are preparing new types of alloys, e.g. Ni – Ti – Zr, Ni – Ti – Hf or Ni – Ti – Cu, specify their transition temperatures and recognize, how composition of these alloys can influence cycling proces and program.

The present work has been supported by the Ministry of Education of the Czech Republic under the project No. GA6379211/2201

- [1] Pacholek, P.: Návrh zařízení a řešení tepelně mechanického zpracování paměťových slitin, materiál pro vnitřní podklady VŠB – TU Ostrava v rámci grantového projektu ČR GAČR-6374041, Ostrava 2005

COMPATIBILITY OF PLASMA SPRAYED TUNGSTEN BASED MATERIALS WITH GRAPHITE SUBSTRATES

V. Brožek^(a), P. Ctibor^(b), H. Boldyryeva^(b), D.-I. Cheong^(c), S.-H. Yang^(c)

(a) Institute of Chemical Technology, 166 28 Prague, Czech Republic

(b) Institute of Plasma Physics v.v.i. Academy of Sciences of the Czech Republic, 180 00 Prague, Czech Republic

(c) IUCF Chungnam University, Daejeon, Korea

Preparation of coatings and self-standing parts from materials with the highest melting points is allowed only by limited number of techniques. Plasma torch WSP[®] with plasma temperature at an exit nozzle about 30 000 K, operating at 150 kW, enables treatment of such refractory materials with extreme melting points in amount of tens of kilograms per hour [1]. In order to further improve mechanical or physical properties of refractory-metal alloys, particle-reinforced refractory metal-matrix composites (PRMMC) [2] have been widely developed in recent years. In order to protect against tungsten oxidation, it is suggested to plasma spray tungsten powder in vacuum or lower pressure chamber with inert gas. Low-pressure plasma sprayed tungsten coating having thickness of 0.3 mm and porosity of about 6% exhibited bonding strength between tungsten coating and substrates larger than 40 MPa. The main disadvantage of graphite as a substrate is its elevated chemical activity at high temperatures. Graphite reacts not only with air oxygen but also with molten metals. It has been established that plasma spraying of refractory carbide forming metals such as W, Mo, Nb, Ta, Zr, etc. with preheating the graphite basis to 1000 °C leads to reactions of metals with graphite and formation of carbides with an adhesive force of about 3.5 MPa [3].

In our experiments a mixture of W powder was prepared with ZrC. This feedstock having an spheroidal character was fed into the plasma of the water-stabilized plasma (WSP[®]) gun by means of an inert gas carrier. Coatings of a thickness of about 1 mm were sprayed on various substrates, namely, graphite. Pure tungsten and pure ZrC were sprayed under similar conditions. Resulting coatings are well compatible with graphite and can serve as surface protection of various graphite substrates. Graphite substrates of UCAR[®] grade ATJTM and Elektrokarbon Topolcany (Slovak Rep.) type EG 621 were after chemical, phase and thermal analysis covered by plasma spray technique with tungsten and with W-ZrC cermet. Plasma spraying was carried out by means of water-stabilized plasma gun WSP[®], designed on a principle of Gerdien arc [1]. The dilatometric tests included thermal expansion measurements on samples 8 to 10 mm long, at a 5°Cmin⁻¹ rate up to 1550°C in Ar atmosphere. The measurements were performed on a Setsys 16/18 contact dilatometer (Setaram, France) with a vertical measurement chamber that enables measurements up to 1750°C in a controlled atmosphere. All here reported measurements were done in Ar.

The chemical analyses showed differences among the chemical composition of boundary layer in dependence on plasma spray setup parameters, particularly feeding distance and spray distance, as well as on feedstock chemical composition and W:ZrC ratio. The effect of substrate surface roughness and W₂C/WC thin interlayer formed on the W-C boundary was observed. Thickness of this layer increased with a coarsening of the substrate surface above $R_a = 7$, which is important for proper coating anchoring. The interlayer thickness is influenced by the substrate temperature at spraying which was maintained between 300 and 500°C to prevent oxidation. Due to mechanical properties of the graphite substrate, namely

its low hardness, R_a values were determined optically by a confocal microscopy (Olympus LEXT OLS 3000) see Fig.1.

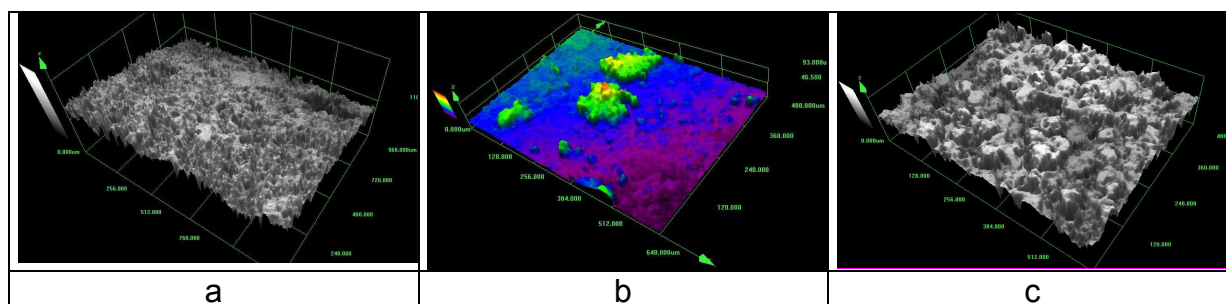


Fig. 1a – Surface of graphite substrate just before spraying; **Fig. 1b** - Surface of two single splats of W ; **Fig. 1c** - As-sprayed coating W on C ; laser confocal microscopy.

Single splats were coated on mirror-polished substrates, **Fig. 1b**. Due to high specific weight and melting point of W the character of splats is not ideally circular and their surface is uneven. Those features are present also in the coating, see **Fig. 1c**. Tungsten coatings have reached 95 % of the theoretical density; the porosity was characterized as closed. In the case of W-ZrC coatings porosity was measured by Hg-porosimetry – from Hg total intrusion volume 0.0072 ml/g and pore area 0.049 m²/g the diameters of pores were calculated as smaller than 0.148 μm to 0.630 μm respectively.

The first layer of W coating being in contact with graphite substrate reacted with them, but here the interlayer was built from WC and from W₂C. This effect could be ascertained to high temperature at the spraying from short spray distance. WC is less brittle than W₂C and its role as the interlayer is positive – CTE_W was between 4.17 and 5.15, which is closer to tabled CTE_{WC} = 5.2 than to CTE_{W₂C} = 4.0 (all values “×10⁻⁶ K⁻¹” at room temp.).

The experiments showed that powders of W and ZrC mixtures can be processed by plasma spraying with WSP[®] equipment and successfully transformed into coatings, namely on graphite substrates of various shapes. The products are slightly porous which is inherent for atmospheric plasma spray technique. Plasma spraying of a mixture of W and ZrC led to coatings with pores present predominantly inside larger particles of ZrC, which effect is probably due to incomplete melting of such particles. Due to extremely high temperatures it is necessary to have in mind the probability of creation of interlayers between substrate and coating as a consequence of chemical reactions. In our experiments these interlayers enhanced the compactness of the coating-substrate system.

- [1] Chraska P., Hrabovsky M., Proc. Int. Thermal Spray Conf. 1992, Orlando, FL, USA, Edit. C. C. Berndt, ASM Inter., Materials Park, OH, US, p.81
- [2] Zhang T., Wang Y., Zhou Y., Song G., Mat. Sci. Eng. A **512**, 19 (2009)
- [3] Obabkov N., Gorkunov V., Munter R., Beketov A., Proceedings of the Estonian Academy of Sciences, **57**, 1, 54 (2008)

STIMULATED NUCLEATION ON POLYMER NANOFIBRES

P. Demo^(a,b), Z. Kožíšek^(a), A. M. Sveshnikov^(a,b), P. Tichá^(a,b), J. Krňanský^(b)

- (a) Institute of Physics, Academy of Sciences of the Czech Republic, Cukrovarnická 10, 162 53 Prague 6, Czech Republic
- (b) Czech Technical University in Prague, Faculty of Civil Engineering, Thakurova 7, 165 29 Prague 6, Czech Republic

The sustainability based advanced industrial materials has to face more and more the problem of durability of structures. Environmental assessment shows clearly increasing volume and aggressive pollutants in air, water, and ground (“soft”) water. These chemical and biological agents permanently and effectively act on materials and structures, in particular, on their surfaces.

Recently applied, mostly chemically based protecting surfaces of materials do not fulfill sufficiently increased requirements of industry. Novel generation of protective layers need an extraordinary combination of intrinsic properties for their multiuse application. In principle, there are two ways how to protect surface of materials against impact of surrounding environment. The first one is based on surface coating by different chemical substances by traditionally used technologies (painting, spraying). Such methods are not too effective and the separation of protective coating or losing of protective properties is frequently observed.

We deal with basically new type of materials comprising all barrier and protective properties into very thin surface layers: polymer-based nonwoven nanotextiles with fibres with diameter from tens to hundreds of nanometers. These nanofibres are produced by NANOSPIDER technology, developed by research team of Prof. Jirsák (TU Liberec). Three principal ways using nanotextiles for protective layers are considered:

- ultrafine nanofibre mesh as an effective hydrophobic barrier
- nanotextile as a carrier of anticorrosive agent with incorporated nanoparticles
- nanotextile as a medium for heterogeneous nucleation and deposition of some particles, in particular, carbon for production of carbon nanotubes.

Consequently, a deeper understanding of nucleation process and subsequent growth phenomena in thin film deposition on nanofibres is required to adequately tailor the layer properties for specific application. Mechanism of the clusters formation on nonwoven nanotextiles is very poorly understood since both the wafer (substrate) and also the newly-forming clusters have to be modeled within very small, submicron scales. Hence, the energetics of this process cannot be expressed within context of classical approaches and some dialect of nanothermodynamics is developed. Moreover, within framework of kinetic description the large curvatures of individual nanofibres of the substrate must be taken into account (*e. g.*, via Tolman model [1]).

This work was supported by the Grant No. IAA100100806 of the Grant Agency of the Academy of Sciences of the Czech Republic and also by Ministry of Education and Youth of the Czech Republic, Project No. MSM 684077003.

[1] R. C. Tolman, J. Chem. Phys. 17 (1949) 333.

SPIN CROSSOVER IN Fe(II) COMPLEXES MONITORED BY DSC CALORIMETRY

L. Dlháň^a, R. Boča^a, N. Hassan^b, P. Weinberger^b, and W. Linert^b

(a) Institute of Inorganic Chemistry, Technology and Materials, FCHPT, Slovak University of Technology, 812 37 Bratislava, Slovak Republic

(b) Institute of Applied Synthetic Chemistry, Vienna University of Technology, A-1060 Vienna, Austria

Cyclohexyl-tetrazole, C_6tz , has been used in preparing iron(II) complex, $[Fe(C_6tz)_6](BF_4)_2$ (hereafter **1**), that exhibits a thermally induced spin crossover between $S = 0$ and $S = 2$ spin states [1]. In addition to a traditional monitoring based upon the magnetic susceptibility measurements, the differential scanning calorimetry has been applied. The gross heat flow has been converted to the heat capacity that after integration gave the thermodynamic parameters associated with the spin crossover: $\Delta H = 14.3 \text{ kJ mol}^{-1}$ and $\Delta S = 69 \text{ J K}^{-1} \text{ mol}^{-1}$. Based on these data the transition temperature is $T_{1/2} = \Delta H/\Delta S = 206 \text{ K}$ which matches firmly the value extracted by fitting the magnetic data.

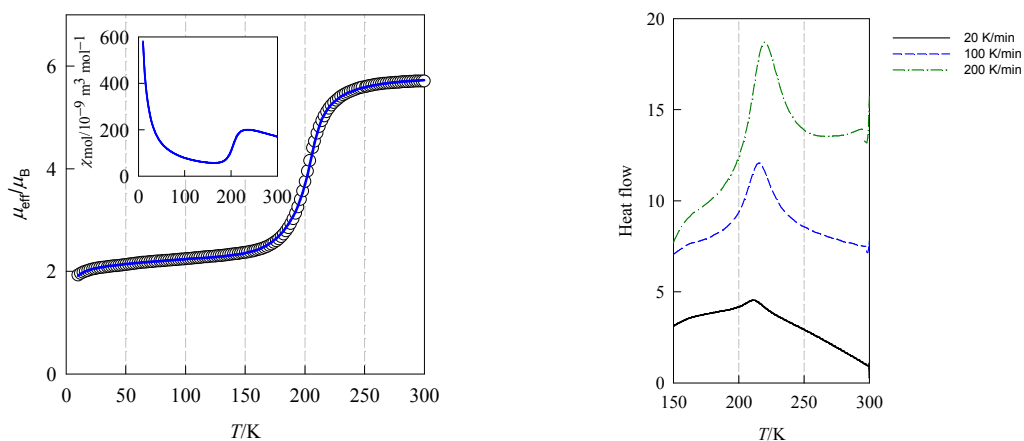
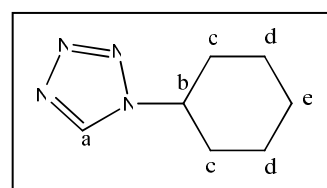
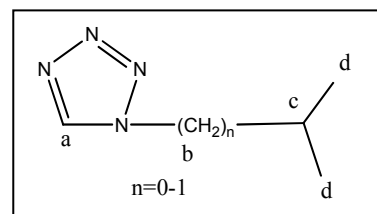


Fig. 1. Magnetic data (left) and calorimetric data (right) for **1**.

The series of $[Fe(iNtz)_6](BF_4)_2$ with $N = 3 - 5$ ($i3tz = 1$ -isopropyl-1H-tetrazole, $i4tz = 1$ -isobutyl-1H-tetrazole, $i5tz = 1$ -isopentyl-1H-tetrazole) was synthesized and characterised by X-ray powder diffraction, magnetic susceptibility measurements and DSC measurements. The $[Fe(i3tz)_6](BF_4)_2$ complex shows a spin transition at $T_c \sim 109 \text{ K}$, while the $[Fe(i4tz)_6](BF_4)_2$ features a complete but rather gradual spin transition with $T_c = 223 \text{ K}$. The DSC measurements show an endothermic peak for the $[Fe(i3tz)_6](BF_4)_2$ around $T = 260 \text{ K}$ not



corresponding to a spin transition. A well developed peak at $T_p = 225$ K matches the spin-transition temperature $T_c = 223$ K for $[\text{Fe}(i\text{Atz})_6](\text{BF}_4)_2$.

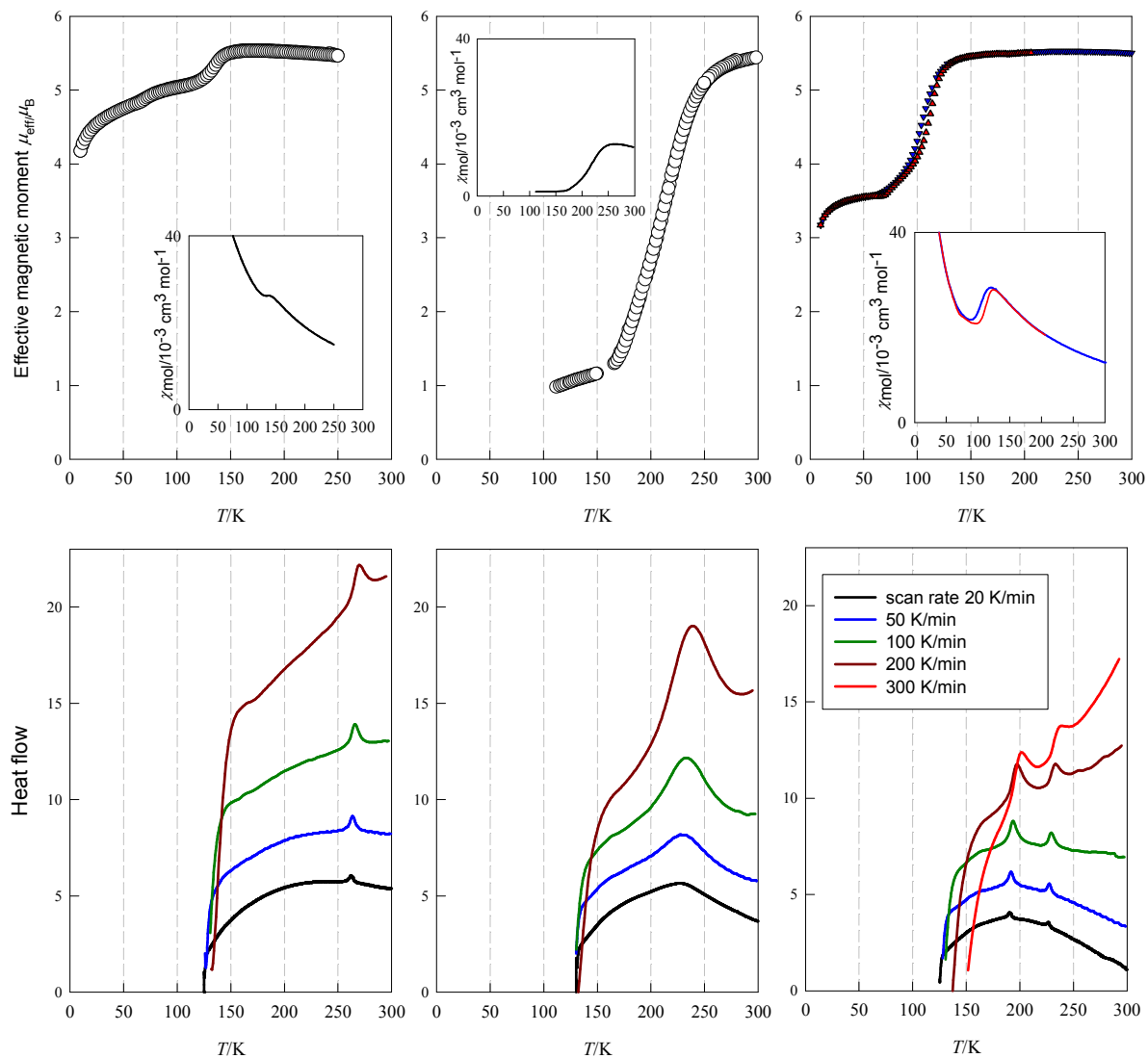


Fig. 2. Magnetic data (top) and calorimetric data (bottom) for the isopropyl-1H-tetrazole-series of $[\text{Fe}(i\text{Ntz})_6](\text{BF}_4)_2$.

Acknowledgments. Grant Agencies (VEGA 1/0213/08, APVV 0006-07, VVCE 0004-07, COST-0006-06) are acknowledged for the financial support.

[1] N. Hassan, P. Weinberger, F. Kubel, G. Molnar, A. Bousseksou, L. Dlhan, R. Boca, W. Linert: Inorg. Chim. Acta 362 (2009) 3629-3636.

LEAD-FREE SOLDERS ON THE TIN – ZINC - ALUMINIUM BASIS FOR HIGH-TEMPERATURE APPLICATIONS

J. Drápala^(a), A. Kroupa^(b), B. Smetana^(c), J. Urbánek^(d)

- (a) Vysoká škola báňská – Technical University of Ostrava, Department of Non-ferrous metals, Refining and Recycling, 15, Av. 17. listopadu, 708 33 Ostrava – Poruba, Czech Republic, e-mail: Jaromir.Drapala@vsb.cz
- (b) Institute of Physics of Materials, Academy of Sciences of the Czech Republic, 22, Av. Žižkova, Brno, Czech Republic, e-mail: kroupa@ipm.cz
- (c) Vysoká škola báňská – Technical University of Ostrava, Department of physical chemistry and theory of technological processes, 15, Av. 17. listopadu, 708 33 Ostrava – Poruba, Czech Republic, e-mail: Bedrich.Smetana@vsb.cz
- (d) Czech Technical University in Prague, Faculty of Electrical Engineering, 2. Av. Technická, 166 27 Prague 6, Czech Republic, e-mail: urbanek@fel.cvut.cz

Introduction

The production of electronics is an important phenomenon, which cannot be possible without soldering process presently. Lead-free solders of various compositions are used. They are able to substitute the lead based solders in specific applications, but the electronic industry is not satisfied because the lead-free solders often have reliability problems, usually caused by worse mechanical properties, and/or higher tendency to oxidation, higher occurrence of undesirable intermetallic phases, higher melting temperature. They are also generally more expensive (for example Sn-Ag based solders) or their usage leads to higher technology expenses. Both the basic and applied research investigate other alloy candidates for the lead-free solders but the results are not satisfactory enough yet. Systems on the Al-Zn base with another alloying element, such as Ga, Ni, Sn, seem to be promising candidates taking also into account that some of the elements represent substrate materials. Optimization of the temperature of soldering process and solder microstructure is important not only from the economical reasons but also from the technological point of view, as a higher temperature means a higher risk for the electronic components and boards.

Experiments

The results of the study of Al-Sn-Zn system which can be a possible lead-free solder candidate for high temperature-applications in electronics and for automotive industry are presented in this paper. Six binary Sn-Zn and fourteen ternary Al-Sn-Zn alloys with 0.6 to 3 wt. % Al were prepared experimentally (melting in the electrical resistance furnace and casting into a graphite mould). The alloys were studied metallographically, the micro-hardness, their overall chemical composition (ICP-AES and OES on the Spectromax device) and X-ray micro-analysis (EDAX, WDX) of the coexisting phases were measured, too. Temperatures of liquidus, solidus and other transformation reactions and latent heats of melting and solidifying were investigated applying the DTA method. Experiments were performed with Setaram SETSYS 18TM experimental laboratory system for thermal analysis. Samples of selected alloys were analysed at linear heating/cooling rate of 4°C/min in the atmosphere of high pure argon. Resulting experimental data were compared with the data of known Sn-Zn binary system and Al-Sn-Zn ternary system – see Fig. 1. MTDATA, PANDAT and THERMO-CALC programs were used for modelling of phase equilibria.

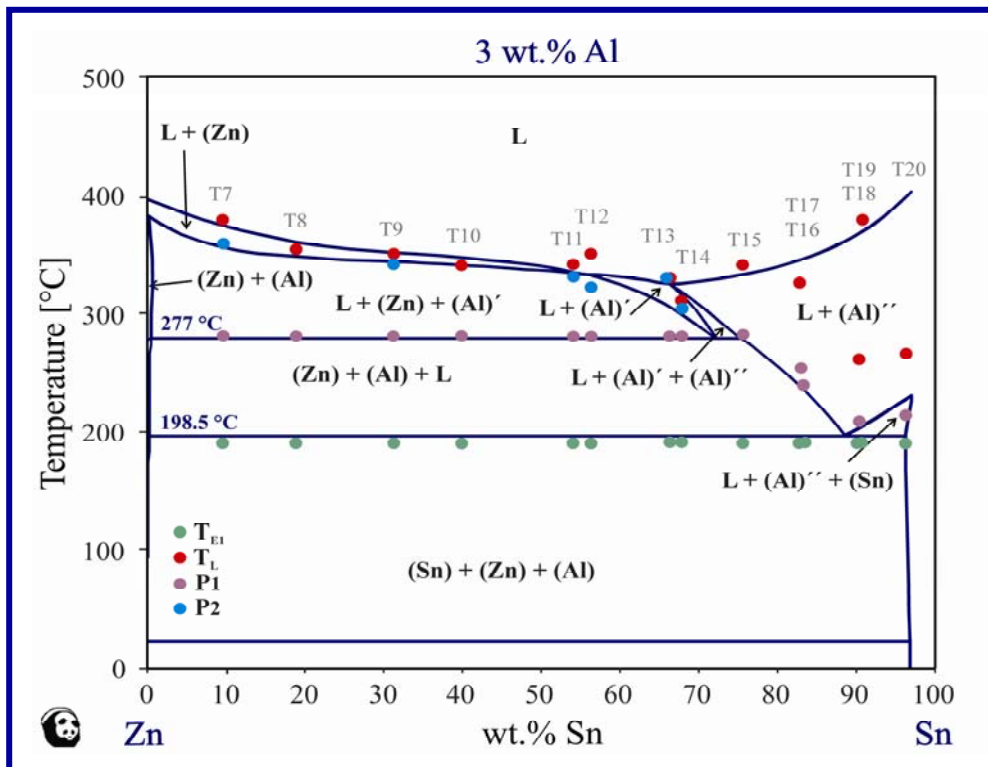


Fig. 1 Experimentally obtained values of phase transformation temperatures (DTA) compared with the values of PANDAT calculations

The X-ray analysis EDAX was performed as both the surface and point micro-analyses. The SEM analysis showed considerable heterogeneity of microstructure, which will relate to the formation of non-equilibrium phases in the course of solidification. Mostly two or three types of phases of various chemical compositions were discovered, which was also proved by the following X-ray microanalysis. Three typical phases were identified here: a phase containing a high concentration of tin without aluminium, a phase containing a high concentration of zinc without tin and small phases containing a high concentration of Al + Zn and a certain concentration of oxygen. Oxygen can originate from the preparation of samples (high affinity of aluminium to oxygen at high temperatures of remelting).

Conclusion

The study of the Al–Sn–Zn system was carried out. The results will be presented at the seminar meeting. To apply these alloys as high-temperature solders for electronics and automotive industries, it will be necessary to perform further technological tests, such as tests of resistivity, wettability, solderability, mechanical tests, which are in the state of elaboration.

Acknowledgements

This research was carried out under the project realized in the framework of European Concerted Action on COST MP0602 „Advanced Solder Materials for High-Temperature Application” and financed by the Ministry of Education, Youth and Sports of the Czech Republic (Projects No. OC 08032, OC 08053 and 6198910013).

BASIC ASPECTS AND TRENDS IN DEVELOPMENT OF NON-VOLATILE REWRITABLE PHASE-CHANGE BASED MEMORIES - OPTICAL DISCS AND PC-RAM MODULES

J. Gutwirth^(a), T. Wágner^(a, b), M. Frumar^(a)

- (a) University of Pardubice, Faculty of Chemical Technology, Department of General and Inorganic Chemistry - Research Centre LC 523, nám. Čs. legií 565, 532 10 Pardubice, Czech Republic; e-mail: Jan.Gutwirth@upce.cz
- (b) University of Pardubice, Centre for Material Science, Studentská 95, 532 10 Pardubice, Czech Republic

Several technologies for long period non-volatile rewritable data storage exist nowadays [1]. Different physical and operational principles of recording and detection were applied and thus the properties of particular memories are different. Commercially successful technologies could be divided by operational principle to magnetic data recording, magneto-optical data recording, optical recording and electrical recording. From physical point of view, effects of remanent magnetic induction, magneto-optical Kerr effect, phase change and charge retention was utilized.

The well known magnetic data recording [1], which was commercialized as a disc or tape memories (hard discs drives (HDD), floppy disc drives (FDD), streamer tapes, ...), were based on domain magnetization of active recording film (usually ferromagnetic materials as a Fe-Co-Ni) and detection of remanent magnetic induction orientation.

Currently leaved magneto-optical data recording [1] (commercialized as a magneto-optical discs) was based on laser induced heating of active recording film (usually ferromagnetic alloys of Fe-Co-Gd-Tb) over the Curie temperature and its magnetization. Principle of detection is magneto-optical Kerr effect, i.e. change of light polarization plane after reflection from magnetized material.

Nowadays widespread Flash memories could be categorized as an electric based recording. These memories denoted as EEPROM (Electrically Erasable Programmable Read Only Memory) utilize MNOS (Metal Nitride-Oxide Semiconductor) transistors. MNOS transistors are able to carry electric charge and thus able to carry the information.

Rewritable optical memories [1, 2] (commercialized as a rewritable optical discs) was based on laser induced phase change of active recording film (usually based on Sb-Te alloy) between amorphous and crystalline state. Detection consists in difference of optical reflectivity of both states.

Several new technologies were developed or approach markets now.

PC-RAM/P-RAM/C-RAM (Phase Change/Phase/Chalcogenide Random Access Memory) [3] utilizes electrically induced phase change of active material (usually Ge-Sb-Te alloy) between amorphous and crystalline state. Detection embody in electrical resistivity difference between amorphous and crystalline state.

Programmable Metallization Cells (PMC) [4] is next memory which utilizes chalcogenide materials. Principle of recording is electrically induced dissolution or separation of Ag in the chalcogenide matrix (usually Ge-S or Ge-Se alloy). Detection consists in electrical resistivity difference between Ag doped and Ag undoped material.

Technologies and principles mentioned above together with their strengths and weaknesses are summarized in Table I.

Table I. Characteristics of some rewritable non-volatile memories.

Memory type: *MOD* - Magneto-optical disc, *RWOD* - rewritable optical disc; Medium: S - stationary, R - rotating; Recording principle: EChR - electric charge retention, MI - magnetic induction, PC - phase change; Detection principle: E - electric, M - magnetic, O - optical; Risks: Mech. - mechanical, EMR - electromagnetic radiation, MF - magnetic field; Risks level: 0 - low, 0/+ - average, + - high.

Memory type	Medium	Principle of		Risks		
		Recording	Detection	Mech.	EMR	MF
EEPROM	S	EChR	E	0	+	0/+
HDD	R	MI	M	+	0	+
<i>MOD</i>	R	MI	O	+	0	0/+
<i>RWOD</i>	R	PC	O	+	0	0
PC-RAM	S	PC	E	0	0	0
PMC	S	PC	E	0	0	0

Benefits of phase change memories are visible in Table I. The main application benefit is stability against ambient, which is especially important for aerospace or military applications [5]. Next practically important benefit is cell structure as well as simple structure which allows next miniaturization and thus leads to increase of recording density and to decrease of energy consumption, heat dissipation and also to decrease of production costs.

Overview of current non-volatile rewritable data storage concepts was done [6]. Principles of particular memories were illustrated together with specification of application benefits and restrictions. Applied materials and technologies together with schemes of particular memories will be summarized. Current development to improve memory properties (especially in terms of data density, data retention, rewritability, ...) will be mentioned.

- [1] R. Waser (ed.) in: *Nanoelectronics and information technology, advanced electronic materials and novel devices*, Wiley VCH, Weinheim Germany (2003).
- [2] T. Ohta, *J. Optoelect. Adv. Mater.* **3** 3 (2001) p. 609 - 626.
- [3] G. Purvis, *III-Vs Review* **19** 8 (2006) p, 39 - 41.
- [4] M. N. Kozicki, M. Mitkova, M. Park, M. Balakrishnana, C. Gopalan, *Superlattices Microstruct.* **34** 3-6 (2003) p. 459 - 456.
- [5] T. S. Balinth, E. A. Kolawa, J. A. Cutts, C. E. Peterson, *Acta Astronaut.* **63** 1-4 (2008) p. 285 - 298.
- [6] J. Gutwirth, Disertační práce, Univerzita Pardubice (2009) (in Czech language; Available online: <https://portal.upce.cz/jetspeed/portal/prohlizeni>).

PROPOSAL OF HEAT EXCHANGER IN MICRO-COGENERATION UNIT, CONFIGURATION WITH BIOMASS COMBUSTION

J. Hužvár , P. Nemeč

Faculty of Mechanical Engineering, Department of Power, University of Žilina,
010 26 Žilina, Slovak Republic

Introduction

The EU is committed to reducing its overall emissions to at least 20% below 1990 levels by 2020, and is ready to scale up this reduction to as much as 30% under a new global climate change agreement when other developed countries make comparable efforts. It has also set itself the target of increasing the share of renewable in energy use to 20% by 2020.

One of the way how get this target is Cogeneration. Cogeneration is progressive technology of electricity and heat production, based on principle of conjugate production, what means, that electricity and heat are produced at the same time. Nowadays not only fossil fuels but also biomass began to be used.

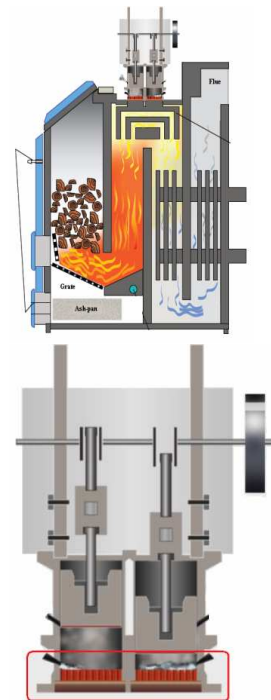
Proposal

Our target is by using analytic-experimental methods to design minimally one suitable microcogenerational process with conversion of chemically fixed energy in biomass to electricity and the low potential heat and based on the technical and economical optimization to determine functional and material requirements of optimal conversion process. Since it is experimental equipment, there is several proposals for it's construction. Device will consist of boiler for dendromass, two-cycle engine and two heat exchangers.

One of the proposals is based on the principle of heat exchange from boiler to work space by using of copper exchanger. During compress piston stroke consistent application of sprayed liquid is done by injection jet on the front area of exchanger. By liquid spraying to large area a quick heat transfer between exchanger and liquid is done (adding of heat to liquid form accumulated heat in exchanger). After the volatilization liquid is changed to high temperature steam and extends its volume. Polytrophic or simplified isothermal-adiabatic expansion follows after that and engine starts to work. After finishing of expansion up-stroke steam leaves work space of engine.

Function of injection system is to provide timed supply of conversion liquid to work space on exchanger area. Condition of successful conversion process is quality and reliability of time, volume and square parameters of injection. Very important is correct determination of injected liquid volume. It is determined based on the cylinder size, compression stroke and the temperature of injected liquid.

Important aspect of optimal heat exchange is appropriate design of exchange area between boiler and work space of two-cycle engine to reach sufficient capacity needed to warm up of liquid and its volatilization.



Heat volume for volatilization of 0.27g of water 1408W

Heat volume for warm up of water by 58°C 164W

From that can be determined necessary capacity 1572W.

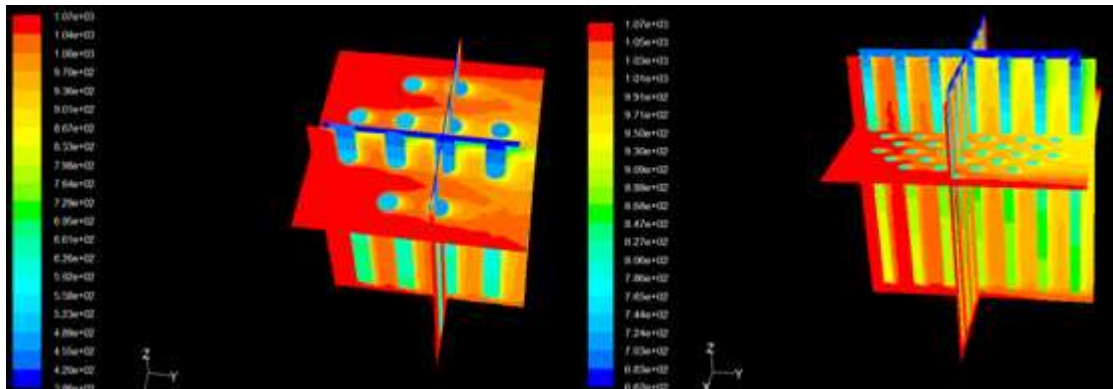
The scope of our research is to choose the most suitable design and heat transfer pipes sizes. As a heat source was suggested 23kW (P) boiler with 90% efficiency (μ). We consider with combustion of oak wood with capacity of 18.8 MJ/kg (Q). Volume of wood is calculated from equation:

$$m = \frac{P}{Q} \mu$$

From the stoichiometric equations was determined volume of combustion products and subsequently speed of flow in exchanger surroundings. Suitable material for exchanger construction is copper due to its high heat-carrying capacity.

CFD Simulation

For parameters optimizing for future experimental exchanger was mathematic model designed in Fluent software. Based on the all calculated input parameters different variants of design and sizes of pipes were defined. Calculation is applied at turbulent flow k-epsilon Standard and k-epsilon RNG with low Re number. It is necessary approximately 1.6 kW of heat for water volatilization and temperature of surface where liquid will be injected cannot drop under 450 Kelvin.



Conclusion

From mathematic model we find out that by using of heat transfer in copper pipes we are able by appropriate design reach sufficient volume of heat flow and sufficient temperature necessary for water volatilization despite of small size of volatilization area.

Acknowledgement

Proposal of solution of microgenerational unit for biomass combustion is solved by APVV program in cooperation with GoldenSun Company.

ZEOLITES AND POWDER DIFFRACTION

V. Jorik

Faculty of Chemical and Food Technology, Slovak Technical University, 812 37 Bratislava, Slovak Republic

Powder diffraction methods play in the study and characterization of zeolites an irreplaceable role. They not only providing information relatively quickly, but often present the only way to obtain the required information. Important is, however, if they are used, to understand what pitfalls lurk for of user, arising from the complex nature of zeolites. It is therefore necessary to carefully plan the experiment and be extremely careful when interpreting the results of the experiment. Interpretation of powder pattern of zeolites can be simple or complex operation, depending on the number and complexity of structural phases, which form the sample.

The interplanar spacings and intensities from measured position values and heights of diffraction lines and also line profiles (peak shape) are necessary to be calculated for this purpose. They may be then used for the following treatments:

Crystallographic analysis is focused on the processing of the basic experimental data from a powder pattern, which generates the fundamental crystallographic information about the substance under investigation. These are the interplanar spacings d , their diffraction indices, the lattice parameters, type of crystal lattice and intensity of diffractions.

Comparison of diffraction data of an unknown zeolite sample with a database of reference zeolite powder patterns permits to determine the purity of the product of synthesis of desired zeolite type (KS01 ...). It also allows distinguishing different cationic forms of a zeolite, see figure 1.

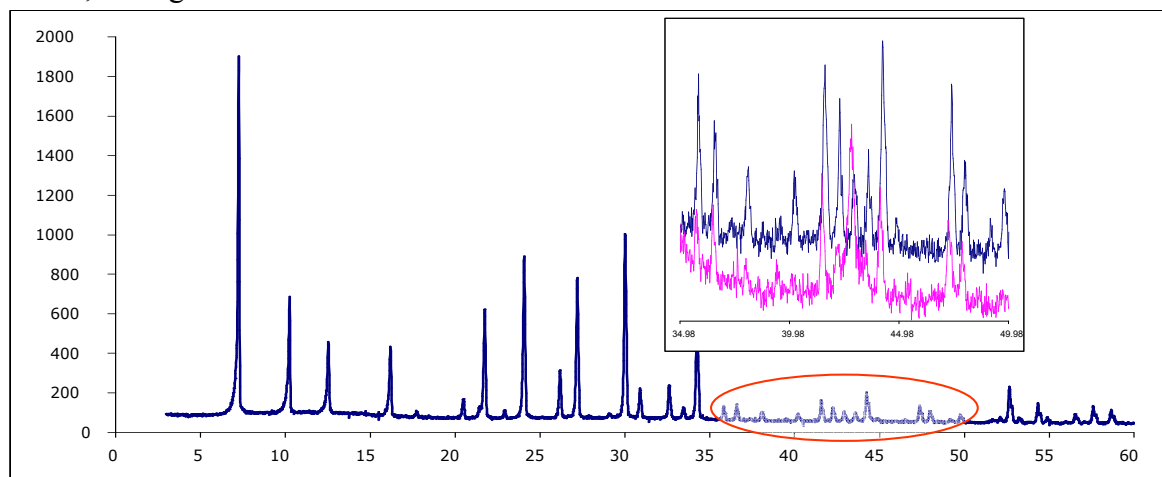


Fig. 1 Powder pattern of zeolite NaA and detailed section of powder pattern of zeolites NaA (top) and CaA (bottom) with their different cationic forms distinguished.

Precise determination of lattice parameters is not typical, universally applicable method of powder diffraction for the characterization of zeolites. However, accurate determination of lattice parameters of zeolites NaY and NaX allows us to reliably determine the molar ratio of $\text{SiO}_2/\text{Al}_2\text{O}_3$. [1-6] Moreover, the method was extended to determine the degree of decationization of both zeolites. [7]

Quantitative analysis of crystalline mixtures is a unique method for analysis of crystalline mixtures, chemical analysis of which can often be very complicated. Under diffraction of X-rays at the crystal mixture, each component produces its characteristic powder pattern independently of other components. Whole diffracted intensity of each component is proportional (after correction for absorption) to the quantity of each component presented in the mixture. Semi-quantitative analysis is often used, which is sufficient to estimate the approximate quantities of components participating in the crystal mixture or eventually an amount of crystalline phase in the bi-component mixture with an amorphous phase, see figure 2.

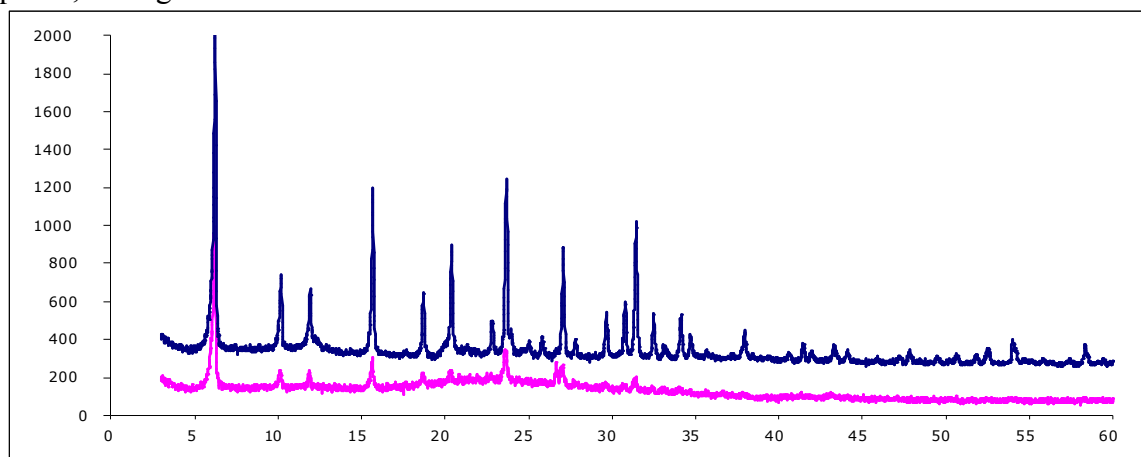


Fig. 2 Powder patterns of “balls” of NaY zeolites before activation (top) and after (incorrect) activation (bottom) with a significant amorphous background.

Determination of crystallite size by line profile analysis has a dominant position especially in the research of heterogeneous catalysts based on zeolites. Zeolites possess the crystallite size typically in the range of units to tens of micrometers. However, more interesting is the particle size of an active compound deposited on a zeolite carrier.

Structural analysis from powder data is particularly suitable for solving specific problems about the known structures of zeolites and powder pattern simulation is the most popular method for such a study. Comparison of simulated powder pattern with the experimental one directly in the Rietveld program provides an extraordinary opportunity also to simulate the effects of real structure.

- [1] Breck, D.W.: Zeolite Molecular Sieves Structure, Chemistry and Use (New York, J. Wiley, 1974).
- [2] Kubelková L., Seidl V., Barbely G., Beyer H.K.: J. Chem. Soc. Faraday Trans., 1, 84 (5) (1988) 1447.
- [3] Fichtner-Schmittler H., Lohse U., Engelhard G., Patzelová V.: Cryst. Res. Tech., 19 (1984) 1 K1-K3.
- [4] Sohn J.R., De Canio S.J., Lunsford J. H., O'Donnell D. J.: Zeolites, 6 (1986) 225.
- [5] Kerr G. T., Chester A. W., Olson D. H.: Acta Phys. Chem., 24 (1978) 169.
- [6] Jorík V.: Zeolites, 13 (1993) 187.
- [7] Jorík V.: unpublished results

MICROSTRUCTURE PROPERTIES OF TiAl-Nb ALLOY

J. Juřica, M. Losertová

VŠB-Technical University of Ostrava, faculty of Metallurgy and Material Engineering,
15 tř. 17. listopadu, CZ 708 33 Ostrava, Czech Republic
jan.jurica@vsb.cz

Intermetallic alloys based on Ti-Al offer a combination of good oxidation resistance and suitable mechanical properties, particularly high specific strength at elevated temperatures exceeding those of conventional titanium alloys. Therefore, TiAl alloys have great promising high-temperature applications [1].

Experimental Ti-45Al-10Nb alloys were prepared from the master alloy TiNb (55/45 wt. %) and Al pieces (5N) by melting in a plasma furnace with four melting passes in Ar atmosphere and feed rate of 1cm per minute.

Results of metallographic analysis and microhardness measurement of the as-cast state are presented in Figures 1 and 2. Metallographic analysis was realised by means of metallographic microscope Olympus GX51.

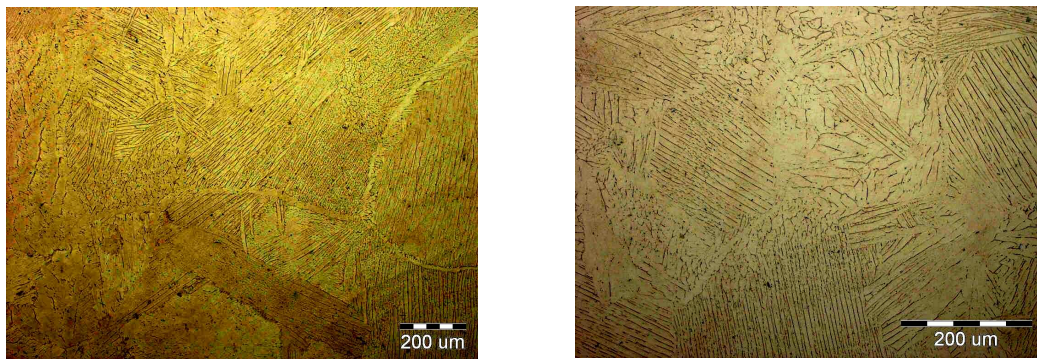


Fig. 1. Microstructure of the alloy TiAlNb after plasma melting

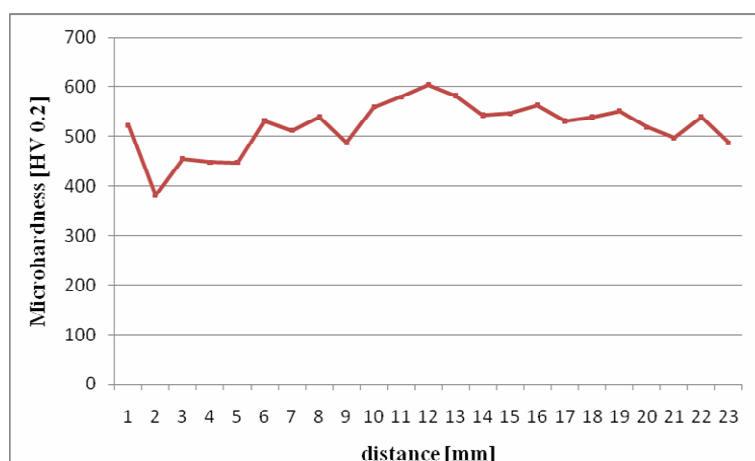


Fig. 2. Results of microhardness measurement of the TiAl-Nb sample after plasma melting

The microhardness values obtained from the measurement using the instrument LECO LM-100 with load of 0.2 kg and indentation steps of 1mm across the specimen are plotted against the distance in Figure 2.

The alloy was annealed for 12 hours at 1100°C in flowing Ar gas and quenched from 500°C in water. The samples prepared in this way were also subjected to metallographic analysis and measurement of microhardness (Figures 3 and 4).

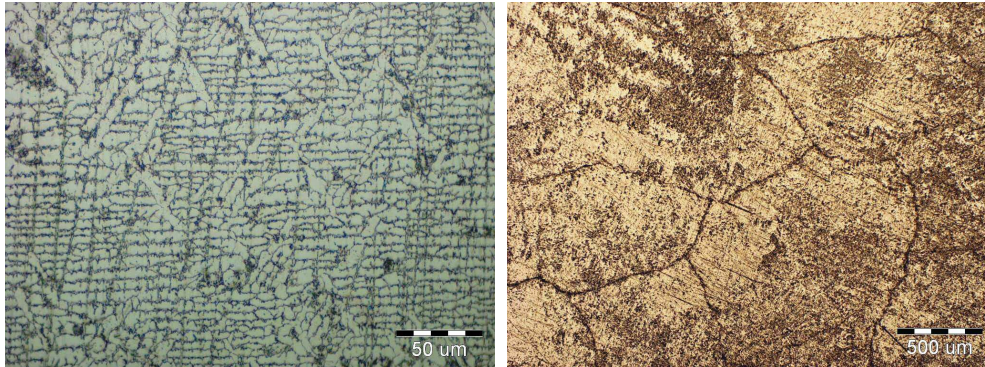


Fig. 3. Microstructure of the TiAlNb alloy after annealing

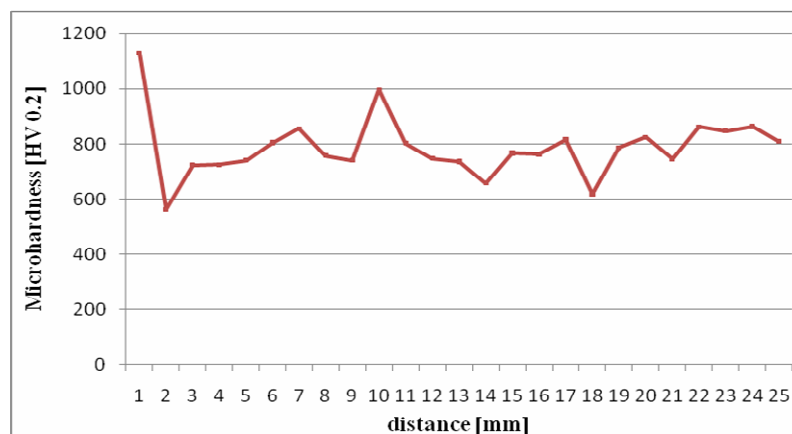


Fig. 4. Results of microhardness measurement of the TiAl-Nb sample after annealing (1100°C, 12 h, Ar)

Microhardness of plasma melted alloy showed lower values than after annealing and quenching which is related to the microstructure feature, as it can be seen in Figures 1 and 3.

The objective of this work consisted in preparation of the Ti-45Al-10Nb alloy using TiNb master alloy and Al pieces. After plasma melting and subsequent annealing a two-phase microstructure consisting of α_2 and γ phases was observed. Results of metallographic analysis and microhardness measurement show certain inhomogeneity after the plasma melting that was removed by heat treatment. The subsequent annealing and quenching in water resulted in fine lamellar structure. In the next research stage, mechanical and structural properties of the prepared alloy will be investigated.

Experimental works were solved within the frame of the project MSM 6198910013 „Processes of preparation and properties of high-purity and structurally defined special materials“.

[1] Loria, E.A. Intermetallics 9 (2001) pp. 997–1001.

NEW HALOGENCARBOXYLATES OF Cu(II) WITH NICOTINAMIDE

M. Koman and J. Moncol'

Faculty of Chemical Technology, Slovak University of Technology, 812 37 Bratislava,
Slovak Republic

The copper(II) carboxylates have been the subject of numerous investigations, especially with nitrogen donor ligands[1]. Copper(II) ions play a vital role in a number of widely differing biological processes, and their interaction with drugs administered for therapeutic reasons is of considerable interest. Some carboxylic acids and their derivatives also play an important role in biological processes[2-4]. Different coordination modes of the carboxylato groups leads to the formation of mononuclear, binuclear and polynuclear structures. Over three hundred new Cu(II) coordination compounds with bioactive ligands were prepared in our laboratory. The crystal and molecular structures of 55 these new copper(II) coordination compounds with the composition of CuX_2L and CuX_2L_2 (X = fenamates, propionates and salicylates, as well as their derivatives) and L = nicotinamide, N,N -diethylnicotinamide, 2,6-dimethanolpyridine, 2-, 3- or 4-pyridincarbinol, were studied and classified. On the basis classification the evident trends of the structural type can be predicted for the perspective new copper(II) compounds with familiar type of ligands.

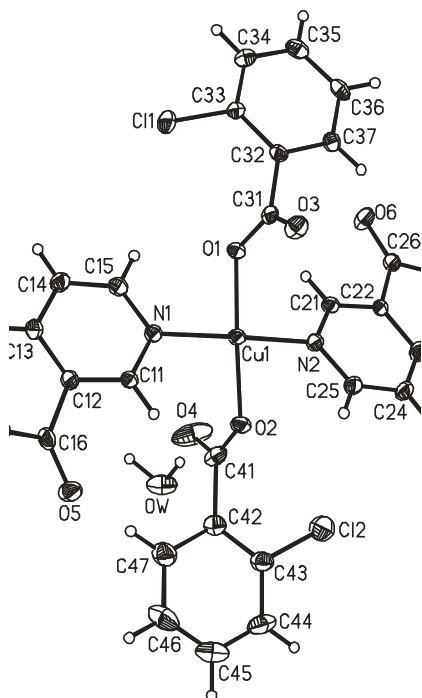


Fig. 1. Molecular structure of $[\text{Cu}(2\text{-Clbz})_2(\text{nia})_2]\cdot\text{H}_2\text{O}$

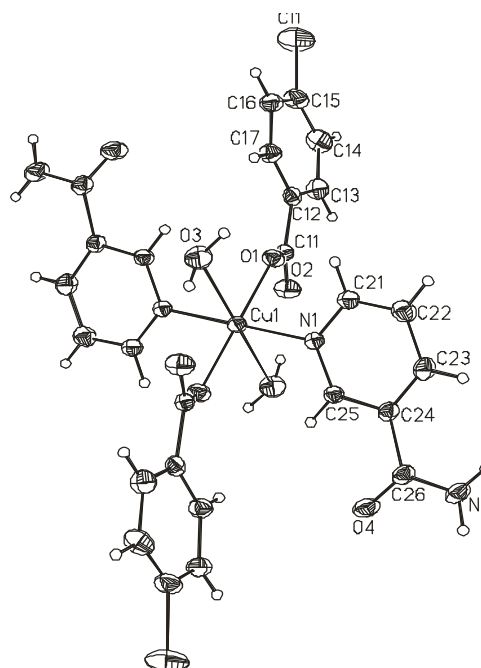


Fig. 2. Molecular structure of $[\text{Cu}(4\text{-Clbz})_2(\text{nia})_2(\text{H}_2\text{O})_2]$

The copper(II) carboxylates with nicotinamide (nia) have been prepared and characterized by X-ray structure analysis. The general molecule formulas of the Cu(II) complexes are $[\text{CuX}_2(\text{nia})_2]$ – (A – Fig.1), $[\text{CuX}_2(\text{nia})_2(\text{H}_2\text{O})_2]$ – (B – Fig.2) and $[\text{CuX}_2(\text{nia})_2(\text{H}_2\text{O})]$ – (C –

Fig. 3) (X = bz – benzoate; 2-Brbz – 2-bromobenzoate; 2-Clbz – 2-chlorobenzoate; 2-Ibz – 2-iodobenzoate; 2-NO₂bz – 2-nitrobenzoate; 3,5-(NO₂)₂bz – 3,5-dinitrobenzoate; 3-NO₂bz – 3-nitrobenzoate; 4-NO₂bz – 4-nitrobenzoate; 5-Me-2-Tpc – 5-methyl-2-tiophenate). In groups **A** and **B** the arrangement of copper(II) atoms forms an octahedron and the ligands are in *trans*-positions. In group **C**, copper(II) atoms are pentacoordinated and form a tetragonal pyramidal arrangement. The change of position of halogen atom on benzene ring benzoate anions lead to different type of monomeric coordination compounds. The X as well as some neutral ligands are active as nonsteroidal antiphlogistic drugs [5,6]. Therefore their study in the present of copper(II) is very promising.

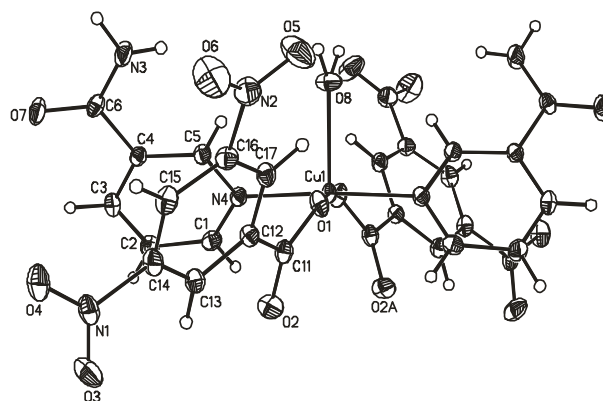


Fig. 3. Molecular structure of $[\text{Cu}(3,5\text{-(NO}_2)_2\text{-bz)}_2(\text{nia})_2(\text{H}_2\text{O})]$

Observed data are discussed and correlated with those of known Co(II), Ni(II) Mn(II) and Zn(II) complexes found in Cambridge Crystallographic Data Base. The general formula of these complexes is $[\text{MX}_2(\text{nia})_2(\text{H}_2\text{O})_2]$ (M = Co(II), Ni(II), Mn(II) and Zn(II)), the arrangement of central atoms is octahedral and ligands are coordinated in *trans*-positions, except for $[\text{Zn}(\text{bz})_2(\text{nia})_2]$ complex where Zn(II) atom is also hexacoordinated, but the ligands are coordinated in *cis*-positions.

The authors wish to thank the Slovak Ministry of Education (VEGA project 1/4454/07) for financial support.

- [1] (a)Melník M.: Coord. Chem. Rev. (1981) 36, 287. (b)Kato M., Muto Y.: Coord. Chem Rev. (1988) 92, 45.
 [2] Kozlevčar B., Lah N., Leban I. et al.: Croat. Chim. Acta (2000) 73, 733.
 [3] Melník M., Koman M., Hudecová D. et al.: Inorg. Chim. Acta (2000) 308, 1.
 [4] Koman M., Melník M., Moncol' J. et al.: Inorg. Chem. Comm. (2000) 3, 489.
 [5] Moncol' J., Múdra M., Lönnecke P. , et al.: Inorg. Chim. Acta (2007) 360, 3213.
 [6] Moncol' J., Maroszová J., Koman M. et al.: J. Coord. Chem. (2008) 61, 3740.

NUCLEATION BARRIER IN SMALL VOLUMES

Z. Kožíšek^(a), P. Demo^(a, b), A. M. Sveshnikov^(a, b), P. Tichá^(a, b)

- (a) Institute of Physics, Academy of Sciences of the Czech Republic, Cukrovarnická 10, 162 53 Prague 6, Czech Republic
- (b) Czech Technical University in Prague, Faculty of Civil Engineering, Thakurova 7, 165 29 Prague 6, Czech Republic

At phase transition the small clusters are formed from supersaturated melt or supersaturation solution first of all and then continue to grow to macroscopic sizes. During this process it is necessary to overcome some energy barrier called nucleation barrier. Small clusters (sub-critical nuclei) appear due to fluctuations and they have tendency to disappear. Supercritical clusters (called nuclei of a new phase) grow to macroscopic sizes, which correspond to lower energy state. Critical cluster is in metastable equilibrium with the mother phase.

It is known that in small systems (such as microemulsions) one needs to set higher supercooling (or supersaturation) to form nuclei of a new phase. What is the volumic influence to nucleation process? Certainly the kinetic equation describing nucleation process does not change, only the number of molecules with volume decreases.

We have solved the kinetic equations for nucleation from the melt at various supercoolings. We have determined the critical supersaturation at certain volume, which corresponds to the condition, when one nucleus of given size will appear within the considered system. In that case one gets the critical supersaturation as a function of volume.

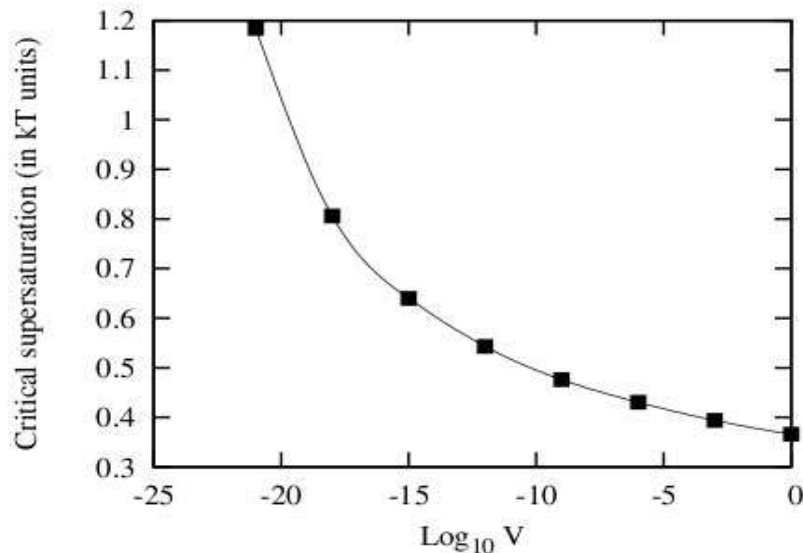


Fig. 1: Critical supersaturation needed to form one nucleus formed by 1000 molecules as a function of volume.

Thus it is possible to predict how it is necessary change the supercooling of the melt to be formed one nucleus of chosen size in given volume. For model system critical supercooling (difference in chemical potentials of both phases) is depicted in Fig. 1 for cluster size 1000

molecules, *i. e.* at critical supersaturation only one nucleus of 1000 molecules in size will be formed.

It is seen that the critical supersaturation increases with decreasing volume of the melt. Knowing the critical supersaturation, one can easily determine the nucleation barrier. It was shown that in the small volumes due to higher supersaturation the kinetics of formation of nuclei is changed as the depletion of the mother phase plays important role (for details see [1, 2]).

This work was supported by the Grant No. IAA100100806 of the Grant Agency of the Academy of Sciences of the Czech Republic. Scientific activities in the Institute of Physics AS CR are supported by the Institutional Research Plan No. AV0Z10100521.

- [1] Z. Kožíšek and P. Demo, *Size distribution of nuclei formed by homogeneous nucleation in closed systems*, J. Aerosol, Sci, 40 (2009) 44 - 54.
- [2] Z. Kožíšek and P. Demo, *Homogeneous nucleation rate at various supersaturations in a closed system*, J. Aerosol Sci. (2009) - accepted for publication.
Doi: 10.1016/j.jaerosci.2009.05.004.

STUDY ON GROWTH OF LEAD HALIDES SINGLE CRYSTALS FOR SOLID-STATE LASERS IN MID-IR

R. Král and A. Cihlár

Institute of Physics AS CR v.v.i., Cukrovarnická 10, 160 00 Prague 6, Czech Republic
kral@fzu.cz

Very recently it has been found that single crystals of rare-earth elements doped ternary alkali lead halides such as KPb_2Cl_5 (KPC), RbPb_2Cl_5 (RPC) and RbPb_2Br_5 (RPB) are promising laser host materials for mid-infrared solid-state lasers [1, 2]. Single crystals of these compounds are prepared from the melt by the vertical Bridgman method [3-5]. However, crystal growth remains a challenge, due to serious complications in the preparation of pure starting materials. Lead halides always undergo hydrolysis and as result hydroxy- and oxyhalides form. If these impurities are not removed, the melt sticks to the quartz ampoule. This leads to its cracking as well as of the crystal being grown. Moreover, other phases could arise in the crystals prepared.

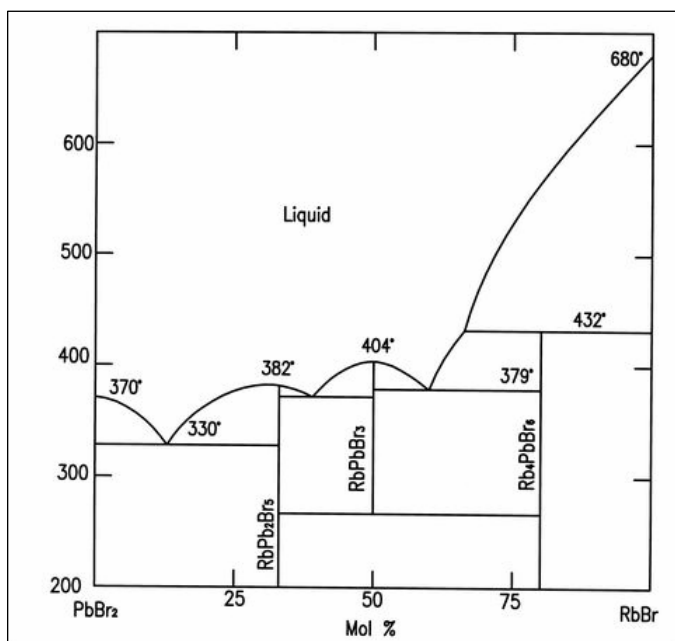


Fig. 1: The phase diagram of the $\text{PbBr}_2 - \text{RbBr}$ system.

This communication deals with the purification of starting materials and growth of pure and doped ternary rubidium lead bromide RbPb_2Br_5 single crystals. RPB crystallized with tetragonal structure and its cell parameters are as follows $a=8.41 \text{ \AA}$; $c=14.5 \text{ \AA}$. Its melting point is at 382°C . The phase diagram of the RbBr-PbBr_2 system is shown in Fig. 1. Besides RPB another congruently melting compound RbPbBr_3 with melting at 404°C and an incongruent one - Rb_2PbBr_4 , with a peritectic temperature of 432°C are formed. DTA measurements show a heat effect at 267°C , which belongs to the disproportionation reaction of RbPbBr_3 [6].

The purification procedure is based on the removal of the above mentioned oxidic compounds by halogenation of molten bromide and its subsequent horizontal zone refining under protective atmosphere.

To optimize the growth process it was necessary to select a proper temperature regime in the furnace and a growth rate. To achieve this goal the growth process was studied by the direct observation of the interface position and its shape when pulling out the growth ampoule

from the furnace (Fig. 2) and by an analysis of induced striations. To induce the striations the pulling rate was deliberately changed between 0.26 mm/h and 3.65 mm/h .

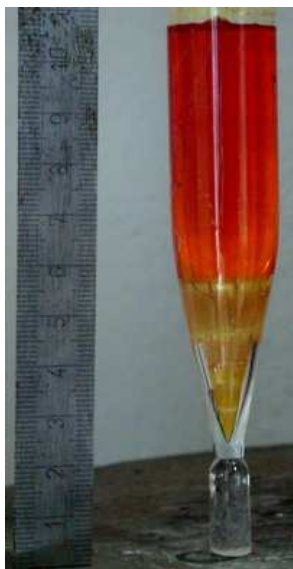


Fig. 2: The direct observation of RbPb_2Br_5 crystal during the growth process.

From such a purified material single crystals were prepared by the vertical Bridgman method. The growing rate was 0.49 mm/h . The diameter of the grown crystal was 16 mm and the length between 40 and 50 mm . Their purity and optical quality were confirmed.

This work at the Institute of Physics of the AS CR is supported from the Grant Agency of AS CR by the Junior research grant project No. KJB200100901.

- [1] P. Page, K. Shaffer, S. Payne, W. Krupke, J. Lightwave Technology 15 (1997) 786.
- [2] K. Rademaker, W.F. Krupke, R.H. Page, S.A. Payne, K. Petermann, G. Huber, A.P. Yelisseyev, L.I. Isaenko, U.N. Roy, A. Burger, K. C. Mandal, K. Nitsch, J. Opt. Soc. Am. B 21 (2004) 2117.
- [3] K. Nitsch, A. Cihlár, Z. Málková, M. Rodová and M. Vaněček, J. Crystal Growth 131 (1993) 612.
- [4] K. Nitsch, M. Dušek, M. Nikl, K. Polák, M. Rodová, Prog. Cryst. Growth Charact. 30 (1995) 1.
- [5] K. Nitsch, V. Hamplová, M. Nikl, K. Polák, M. Rodová, Chem Phys. Lett. 258 (1996) 518.
- [6] M. Cola, V. Massarotti, R. Riccardi and C. Sinitri, Z. Naturforsch. 126 (1971) 1328.

THE PROPERTIES OF NATURAL RUBBER/CLAY COMPOUNDS

S. Lálíková, M. Pajtášová, D. Ondrušová, T. Bazyláková, M. Olšovský^(a)

(a) Faculty of Industrial Technologies, Alexander Dubček University of Trenčín, Púchov, Slovak Republic, contact author: lalikova@fpt.tnuni.sk

Clays and clay minerals such as montmorillonite, saponite, hectorite are widely used as fillers for rubbers and plastics for many years, for saving polymer consumption and reducing the cost [1]. Their addition into polymer matrix leads to significant improvements in physical-mechanical properties. It is caused by their nanometric dimensions and high aspect ratio. The nanoscopic phase distribution as well as synergism between polymer and the layered silicate result in additional properties, such as flame retardation, enhanced barrier properties and ablation resistance, which are not observed in either component [2, 3].

The present work investigates the properties of model rubber compounds, which were prepared with the addition of natural bentonite in function of reinforcement filler. The influence of the used type and quantity of filler was evaluated from results of thermal analysis (DTA, TG), cure characteristics (M_L , M_H , t_S , t_{90} , R_V) and physical-mechanical properties (tensile strength, modulus 300, tensibility, hardness). The obtained values at the model rubber compounds were compared with the values of standard rubber compound.

The model rubber compounds were prepared by the scheme displayed in Fig. 1 and with the prescriptions mentioned in Tab. 1.

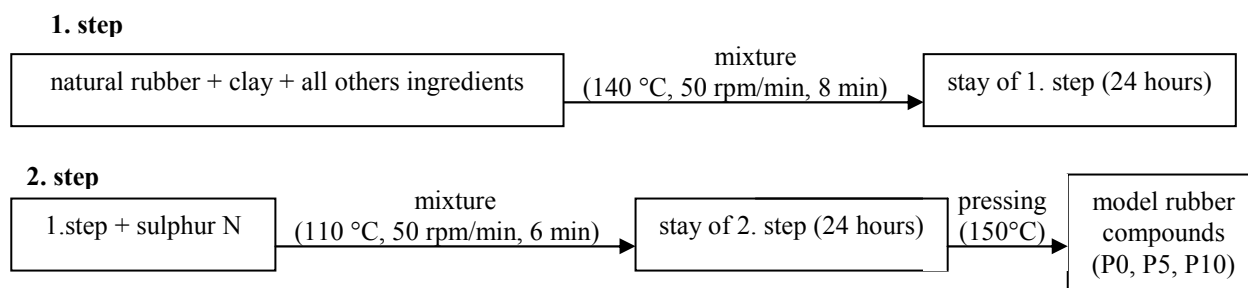


Fig.1: The scheme of preparation of the model rubber compounds

Tab.1: The prescriptions of the prepared compounds

Compounds	P0 [phr]	P5 [phr]	P10[phr]
SMR-20		100	
ZnO	4,6	4,6	4,6
Sulfenax CBS*	1,5	1,5	1,5
Carbon black N660	10	5	-
Bentonite	-	5	10
Sulphur N		1,8	

*N-cyclohexyl-2-benzothiazolsulfenamid

Samples of prepared model rubber compounds were investigated by methods of thermal analysis (DTA, TG), which were simultaneously measured in the temperature range of 40 °C - 900 °C at a heating rate of 10 °C/min (Fig. 2 and 3).

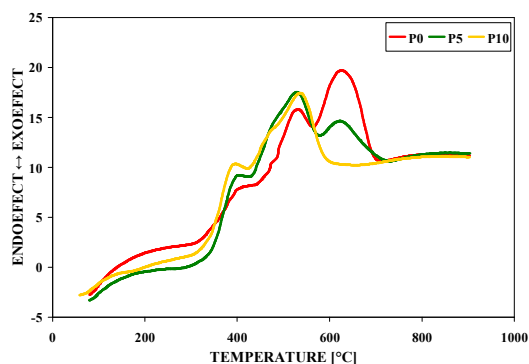


Fig. 2: DTA of model rubber compounds

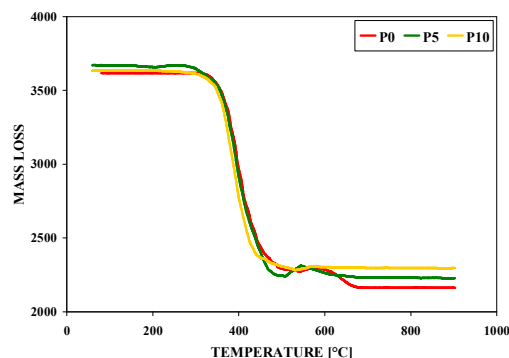


Fig. 3: TG of model rubber compounds

The curing behavior (M_L , M_H , t_s , t_{90} , R_v) was investigated by using of vulcameter Monsanto 100 at the temperature 150 °C during 60 min. and the results of measurements are present in Table 2.

Tab.2: Cure characteristics of model rubber compounds

	Measure	P0	P5	P10
M_L	N.m	5,0	2,7	1,8
M_H	N.m	45,0	43,8	38,5
t_s	min	1,5	1,5	4
t_{90}	min	3,5	4,6	8,2
R_v	min ⁻¹	50,00	32,26	23,81

Physical-mechanical properties (tensile strength, modulus at 300 elongation - M_{300} , tensibility) were measured at room temperature by using of instrument Instron at deformation rate 50 mm/min. Hardness was determined at the same temperature by hardness tester IRHD. The measured values are mentioned in Table 3.

Tab. 3: Physical - mechanical properties of model rubber compounds

Type of test	Measure	P0	P5	P10
Tensile strength	MPa	13,17	14,90	20,10
Modulus 300	MPa	5,77	8,29	7,58
Tensibility	%	685	539	796
Hardness	IRHD	47,6	46,2	43,3

The obtained results in present study confirm, that the addition of filler on the base of natural clay, bentonite has a positive effect on studied properties, because its presence in NR matrix improves the strength, elasticity et al. of final vulcanizates.

The authors sincerely thank the Slovak Grant AV 4/2014/08 for the financial support.

- [1] R.A. Vaia, K.D. Jandt, E.J. Kramer, E.P. Giannelis, *Macromolecules* 28 (24) (1995) 8080-5.
- [2] L.A. Utracki, *Clay-Containing Polymeric Nanocomposites*, Rapra, Shawbury 2004.
- [3] J. Njuguna, K. Pielichowski, *Adv. Eng. Mater.* 5 (2003) 769.

STRUCTURE AND ELECTRICAL PROPERTIES OF COMPOSITES OF POLYSTYRENE WITH MODIFIED CARBON BLACK

J. Lipták

Faculty of Electrical Engineering, Czech Technical University of Prague, 166 27 Prague, Czech Republic

When the carbon black (CB) is used as filler in polymer composite, the composite properties can change from insulator to conductive ones. It is widely used for heating cables or screening desks and so on. The composites of conductive polymers with fullerenes are intensively studied for solar cells applications¹.

When the concentration of the filler in the composite reaches the percolation value the continuous electrically conductive network is formed. Dependence of conductivity on CB concentration shows the sharp rise² (percolation threshold). Also, the network in the bulk increases the viscosity³ of the composite. The primary problems of the CB network formation are interactions between CB agglomerates. The interactions can be effected by many parameters.

In summary, it can be pointed out that there are four principal ways to influence the resulting structure of CB in the composite. 1. Effect of polymer² (solubility, thermoplastics, gels ...). 2. Effect of external field (electrical^{5, 6}, centrifugal, gravitational ...) and conditions (temperature, humidity). 3. Effect of sample preparation technique (the speed and time of dispersion, concentration of added salt, ultrasound acting ...) and 4. Effect of carbon black⁴ (density, surface area, composition ...).

The carbon black agglomeration without external field takes place due to Van der Waals forces which are reasonably affected by added or extracted ions. There are a small amount of different ions inside CB particles. From this point of view it seems to be possible to modify CB surface. This work deals with the structure and consequently electrical properties of carbon black – polystyrene (PS) composites with CB soaked with different substances with ion interactions before dispersing in polystyrene solution.

Sample preparation: Plate composites CB – PS with the diameter 40 mm and the thickness from 0,05 mm to 0,2 mm with the CB loading 0,5%w to 10%w were prepared from the solutions by the method of spin coating and simple coating into Petri dishes. Four series of the samples were prepared. 1. Dry CB was soaked in water vapour up to approx. 30%w of water. 2. Dry CB was soaked in ethanol vapour up to approx. 30%w of ethanol. 3. CB with lower concentration of ions which were extracted in water. 4. Dry CB without any modification was used for comparison. Secondly, the CB was mixed with the solution of 5 g of polystyrene in toluene and dispersed and pulverized by IKA rotational homogenizer at speed 20000 rpm for the 2 minutes. After that, the ultrasonic homogenizer Sonopuls UW 3200 (Bandelin) with the power 40 W for the time 3 x 1 minutes was used.

Electrical measurements: The impedance analysis in the frequency region 100 Hz to 1 MHz was carried out with the PM 6306 RLC meter FLUKE with 1 V measurement voltage. In normal direction the plate condenser with micro shift was used. In planar direction the dot contacts by silver paste were prepared and the conductance G and the capacity C were

measured. From analogy with dielectric measurements the new quantities were defined as follows:

$$e_2 = \frac{G}{f} \quad \text{and} \quad tg = \frac{G}{Cf}, \quad (1)$$

where f is the measuring frequency.

From our sample preparation it can be sad that CB evolves ions when it is soaked in distilled water. After several days of soaking the original water conductivity 0,12 mS/m was increased approximately 100 times. CB was dried up to constant weight and used for composite samples. On the other hand, increasing of the conductivity of toluene or ethanol at the same experiment was not observed.

From optical observation we can pointed out two results. The final structure of the composite depends on the time (speed) of evaporation. When the evaporation time is short agglomeration takes place quickly into large agglomerates. Increasing the time (for example by covering the Petri dish or by increasing of toluene content) we observed more fine structure.

The impedance measurements show the typical results for partially conductive materials with space charge polarization. Both real and imaginary part of complex permittivity (or modified quantities Eq.1) for the most samples monotonically decrease with frequency. But there are a few differences between our samples with modified CB (Fig.1). When the plot $\log(e_2)$ versus $\log(f)$ is linear with the slope minus one the d.c. conductivity takes place. From Fig.1 it can be seen that the highest conductivity is observed for the de-ionized CB with practically linear function. The similar linearity is observed for the sample with dry CB, but the conductivity is approx. 10 times lower. The samples with CB saturated by water and ethanol show non-linear curves indicating dielectric losses connected probably with water or ethanol clusters bonded on CB. These results are supported by the tg versus $\log(f)$ dependences.

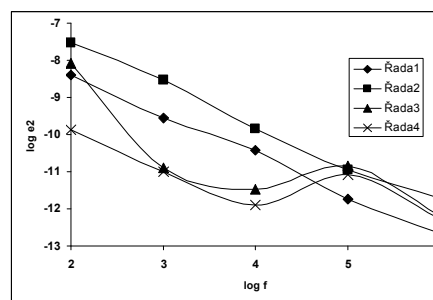


Fig.1: Dependence of $\log(e_2)$ on $\log(f)$ for the sample with 1w% CB: 1. Dry. 2. De-ionized. 3. with water. 4. with ethanol.

In this work it was shown that both CB structure and electrical properties of the composites can be changed using the modified CB. Good substances seem to be water and ethanol with their water bridges. Also, for CB modification can be used the change of ions concentration inside the CB or in CB ion atmosphere.

- 1) Bjorklund, G. S., Baer, T. M.: Photonics Spectra (2007) 70
- 2) Miyasaka, K. at all: Journal of Materials Science 17 (1982) 1610
- 3) Lakdawala, K., Salovey, R.: Polymer Engineering and Science, 27 (1987), 1043
- 4) Ezquerro, T. A. at all.: J. Mater. Sci. Lett, 5, 1065 (1986)
- 5) Prasse, T. at all: Appl. Phys. Lett., 72, 290-3 (1998)
- 6) Lipták, J.: The 18th joint seminar DMSRE 2.-5. 9. 2008, Hnanice

MORPHOLOGY ANALYSIS OF SILICON NANOPARTICLES PREPARED BY CAVITATION DISINTEGRATION

R. Dvorský^(a), J. Luňáček^(a), A. Slíva^(b), K. Piksová^(c),

- (a) Department of Physics, VŠB - Technical University of Ostrava, 17. listopadu 15, 708 33 Ostrava - Poruba, Czech Republic
- (b) Laboratory of Bulk Materials, VŠB - Technical University of Ostrava, 17. listopadu 15, 708 33 Ostrava - Poruba, Czech Republic
- (c) Department of Physical Electronics, ČVUT - Faculty of Nuclear Sciences and Physical Engineering, Czech Republic, Trojanova 13, 120 00 Praha 2, Czech Republic

The first part this work deals with the physical mechanism analysis of the cavitation disintegration of the solid particles in the device called WJM (Water Jet Mill) [1]. The attention is paid to the detail parameters of the cavitation bubble implosions. In the several ten microns range, the dominant driving force of the disintegration is bubble implosions, while the capillary pressure plays the crucial role in the submicron range. Fig. 1 demonstrates the estimate of the lowest impact pressure values providing total condensation of all vapors to the centre core.

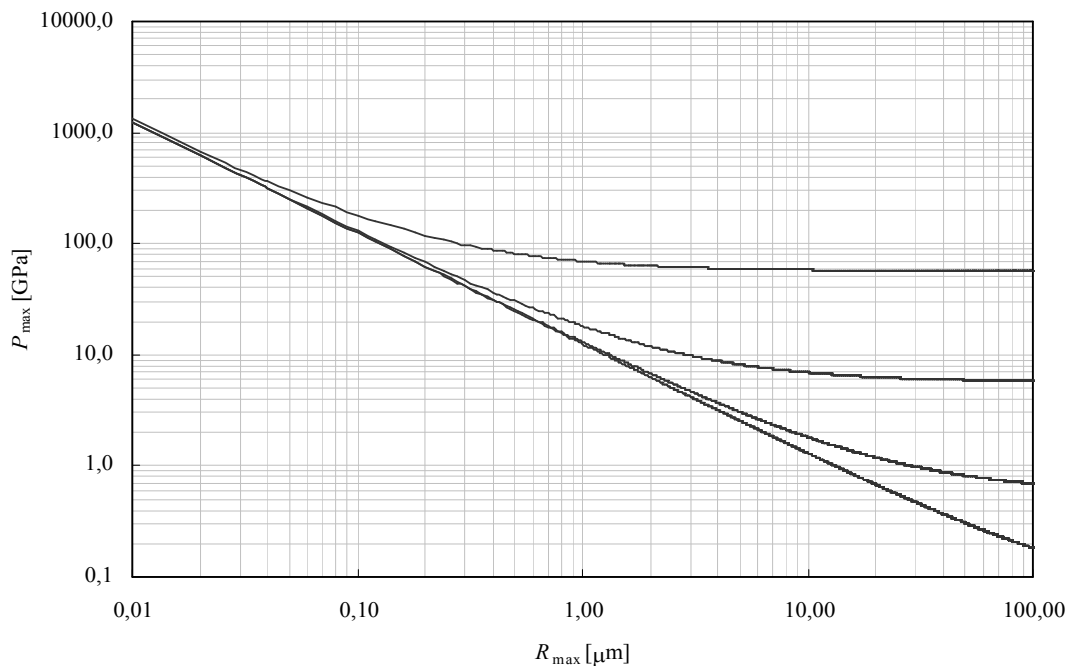


Fig. 1 Impact pressure p_{\max} of the collapse at the boundary between liquid and the particle as a function of the initial maximal size R_{\max} of the cavitation bubble. Top-down for the surrounding pressure $p = \{1, 10^{-1}, 10^{-2}, 10^{-3}\}$ MPa.

During the cavitation bubble implosion, when the pressure in the surrounding is 1 MPa, the impact pressure reaches cca 57 GPa. This value is much greater than compressive strength for majority disintegrated materials ($\sigma_p \leq \sigma_p(\text{Al}_2\text{O}_3) \approx 3 \text{ GPa} \ll 57 \text{ GPa}$).

The disintegration mechanism in WJM is caused by cavitating water-jet whose velocity is about $660 \text{ m}\cdot\text{s}^{-1}$. The smallest size of the particles of disintegrated material was approximately 100 nm, but the mechanical damage of the impact target on the bottom of the

WJM was relatively small. Therefore we suppose that the disintegration of particles was mainly caused by the cavitation bubble implosions taking part on their surface.

Through the use of experimental milling and separation tests the water suspensions of the disintegrated nanoparticulate silicon were obtained. The study and morphological analysis of these nanoparticles is described in the next part of the paper. The suspension was thickened by the turbulent ultra-filtration. Water evaporation was realized either on the wafer or by lyophilisation sublimation. The samples were studied by electron microscopy. It can be seen that the silicon nanoparticle aggregates (Fig. 2) or long nanostrings (Fig. 3) were created.

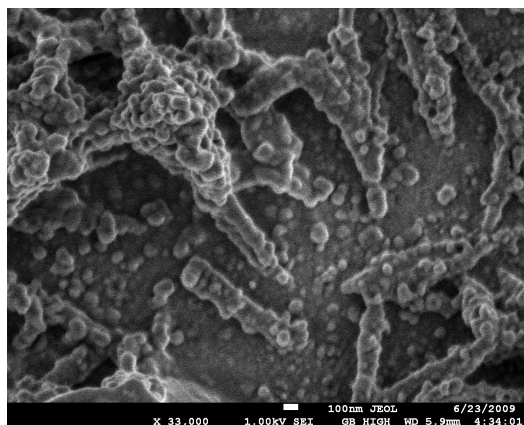


Fig. 2 Nanoparticle aggregates of the silicon obtained by WJM disintegration. High Resolution Field Emission Scanning Electron Microscopy (JSM 7500F)

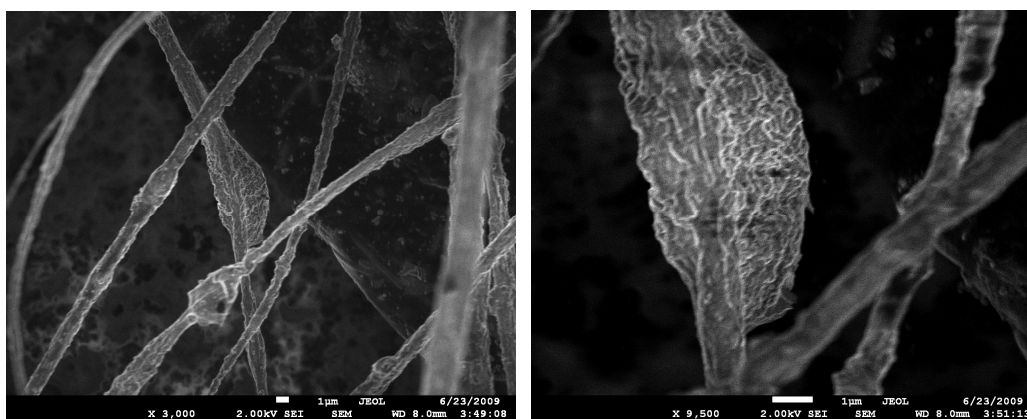


Fig. 3 Nanostrings of the silicon obtained by WJM disintegration and by the following lyophilisation sublimation. High Resolution Field Emission Scanning Electron Microscopy (JSM 7500F)

For comparison, the morphology analysis of the samples was studied by the following methods: Atomic Force Microscopy (AFM), High Resolution Field Emission Scanning Electron Microscopy (FE SEM), confocal optical microscopy and laser diffraction.

This research was partially supported by the Grant Agency of the Czech Republic (project No. 106/08/1092) and by the grant MSM 6198910016.

- [1] Dvorský, R., Slíva, A., Luňáček, J.: Preparation of Nanoparticle Materials in New Device WJM (Water Jet Mill), Book of abstracts of 1st Nanomaterials and Nanotechnology Meeting NANO OSTRAVA 2008 (1. – 4.9.2008).

THERMAL STABILITY OF UNDOPED POLYSILICON LAYERS

D. Lysáček, L. Válek

ON Semiconductor, 756 61 Rožnov pod Radhoštěm, Czech Republic

Abstract

The grain size of as-deposited and annealed polysilicon layers has been investigated by scanning electron microscopy. Intentionally undoped layers were prepared by low pressure chemical vapor deposition (LPCVD) at temperature of 640 °C. Primary recrystallization of the layers has been observed during annealing at temperatures in range from 900 °C to 1150 °C. The activation energy of the silicon self interstitials diffusion along the grain boundaries was calculated as 2.2 eV. The difference in the grain-growth process was observed for the undoped layers grown either on (i) lightly boron doped substrate or (ii) on the substrate heavily doped with antimony.

Introduction and experimental

Grain boundaries in the polysilicon layer are energetically favorable sites for the metal impurities and act as metal traps. Hence, the gettering ability of the polysilicon strongly depends on the size of the grains. The thermal cycles during subsequent steps of a device fabrication induce the recrystallization of the layer.

The silicon wafers were sliced from two Czochralski-grown ingots, one lightly doped with boron ($7 \cdot 10^{13}$ atoms/cm³) and another heavily doped with antimony ($5 \cdot 10^{19}$ atoms/cm³). The 150 mm wafers have the crystallographic orientation (100) and thickness 525 μm. The polysilicon layers were grown using the LPCVD technique. The layers thickness was 1.1 μm. The wafers were annealed under the ambient atmosphere for 0.5 hr at temperatures from 650 °C to 1150 °C. The non-annealed wafers were used as the reference samples. Layers cross-sections were studied using a Scanning Electron Microscope (SEM) with an electron beam acceleration voltage of 10 kV.

Results and discussion

It was shown that while the boron (p-type) doping has a negligible effect on the recrystallization process, the presence of the n-type dopant in the layer enhances the recrystallization process [1]. Wada and Nishimatsu [2] reported the primary recrystallization of the polysilicon layers proceeds via the grain boundary-induced growth. The elementary process behind the primary recrystallization is the diffusion of silicon self-interstitials along the grain boundary region. In this case, the grain size d increases as the square-root of the annealing time t [1] following the equation:

$$d^2 = d_0^2 + \frac{2ab^2\lambda D_1\gamma}{k_B T} \cdot \exp\left(\frac{-\Delta G}{k_B T}\right) \cdot t, \quad (1)$$

where d_0 is the initial grain size, a is the geometric factor, b is the lattice constant, λ is the grain boundary energy, k_B is the Boltzmann constant, T is the annealing temperature, D_1 is the diffusivity of silicon self interstitials in bulk, ΔG is the difference in the diffusion activation energy between the grain boundary and bulk and γ is the constant equal to $1.0 \cdot 10^{-11}$ [1].

The grain size was estimated from SEM images. The dependences of the grain size on the annealing temperature are shown in Fig. 1. The grain size does not change significantly

for annealing temperatures up to 900 °C for both layers deposited on (i) the lightly boron doped substrates and (ii) the heavily antimony doped substrates. The primary recrystallization was observed between annealing at 900 °C and 1150 °C. At 1050 °C and above the grain size is significantly higher for the layers deposited on the heavily antimony doped substrates. We attribute this to the enhancement of the grain growth by the antimony dopant diffused from the substrate into the layer. At temperatures above 1000 °C the time necessary for the dopant diffusion through the whole polycrystalline layer is much shorter than the annealing time and layer behaves as the doped layer during the recrystallization.

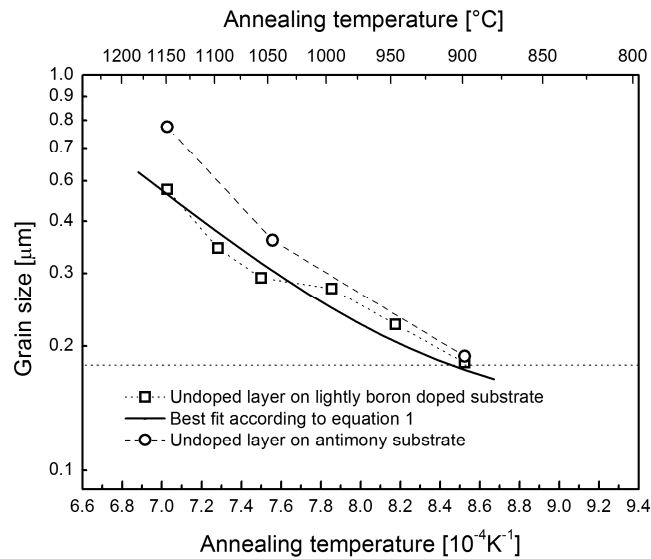


Fig. 1 The grain size of layers annealed for 0.5 hr at various temperatures. The dashed lines are to guide the eye only. The grain size measured on the reference sample and after annealing at 650 °C does not differ significantly from the size measured at 900 °C. This fact is represented by the horizontal dotted line.

The measured grain sizes for the undoped layer on the lightly boron doped substrate (open squares) and their best fit according to equation 1 (solid line) are plotted in Fig. 1. The ΔG value obtained from this simulation is 1.7 eV. The uncertainty in ΔG determination estimated from the variance of the measured grain size is approximately ± 0.2 eV. The activation energy of diffusion along the grain boundaries calculated from the ΔG value is approximately 2.2 eV. To get this, we used the value of the activation energy for the silicon atoms self-diffusion in silicon bulk as 3.9 eV [3].

Conclusions

Our results demonstrate that the undoped polysilicon films show negligible changes in the structure and the grain size after the annealing at temperatures below 900 °C. The primary recrystallization was observed between annealing at 900 °C and 1150 °C.

The activation energy of the silicon self interstitials diffusion along the grain boundaries was calculated to be approximately 2.2 eV. The different grain-growth mechanism was found to be a consequence of antimony diffusion into the polysilicon layer.

1. L. Mei, M. Rivier, Y. Kwark, and R. W. Dutton, J. Electrochem. Soc. 129 (1982) 1791.
2. Y. Wada, S. Nishimatsu, J. Electrochem. Soc. 125 (1978) 1499.
3. S. W. Jones, Diffusion in Silicon, ICKnowledge LCC, Georgetown, MA, 2006.

SCINTILLATION PROPERTIES OF Ce³⁺-DOPED (Y-Lu) ALUMINUM GARNETS GROWN BY LPE METHOD IN DIFFERENT FLUXES

J.A. Mareš^(a), P. Průša^(b), M. Nikl^(a), M. Kučera^(c), K. Nitsch^(a), A. Beitlerová^(a)

- (a) Institute of Physics, Academy of Sciences of Czech Republic, Cukrovarnická 10, 162 53 Prague 6, Czech Republic
- (b) Faculty of Nuclear Sciences and Physical Engineering, Czech Technical University in Prague, Břehova 7, 115 19 Prague 1, Czech Republic
- (c) Faculty of Mathematics and Physics, Charles University, Ke Karlovu 5, 121 16 Prague 2, Czech Republic

Ce³⁺-doped yttrium Y₃Al₅O₁₂ (YAG) or lutetium Lu₃Al₅O₁₂ (LuAG) aluminum garnets belong to efficient scintillating crystals also with other good properties as mechanical and chemical stability. Ce³⁺-doped YAG and LuAG single crystals are grown by the Czochralski method but very thin single crystalline layers or films (SCF) can be prepared by a liquid phase epitaxy method (LPE) [1,2]. During last years we have investigated SCF of YAG:Ce and LuAG:Ce grown by LPE in different fluxes (using those containing PbO, BaO and MoO₃) [1-4]. Generally, LPE method allows to prepare this SCF of thickness from a few μm up to 60 μm [1,2]. Besides Ce³⁺ dopant also other ones are tested as e.g. Bi³⁺ which is described in paper [5]. The aim of this talk is to present short summary of scintillation response studies of various Ce³⁺-doped YAG or LuAG SCF grown under different condition of growths.

Scintillation properties of thin SCF of Ce³⁺-doped YAG or LuAG garnets were measured under α-ray particle excitation, e.g. under 5.4856 MeV energy of ²⁴¹Am. It is not possible to use γ-ray excitation because very weak linear absorption in thin SCF while α-ray

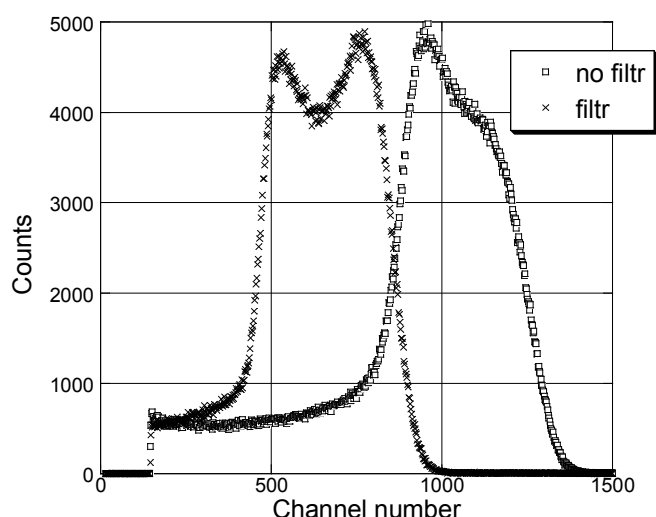


Fig. 1. ²⁴¹Am pulsed height spectra of LuAG:Ce SCF of ~ 5 μm thickness

particles have stopping range in these crystals around 10 μm [4]. Pulsed height spectra of one of the measured samples (with or without filtr) are presented in Fig. 1 while Fig. 2 shows N_{phels} yields dependence of various LuAG:Ce SCF on Ce content. As was described above we will discuss and summarize N_{phels} yield of YAG:Ce and LuAG:Ce SCF prepared by LPE from different fluxes: (i) PbO-B₂O₃, (ii) BaO-B₂O₃ and (iii) MoO₃-Li₂MoO₄. Generally, the (i) flux allows to prepare thick films up to 60 μm but it has disadvantage that contaminates the films by Pb²⁺ which decreases the yield of the films [6].

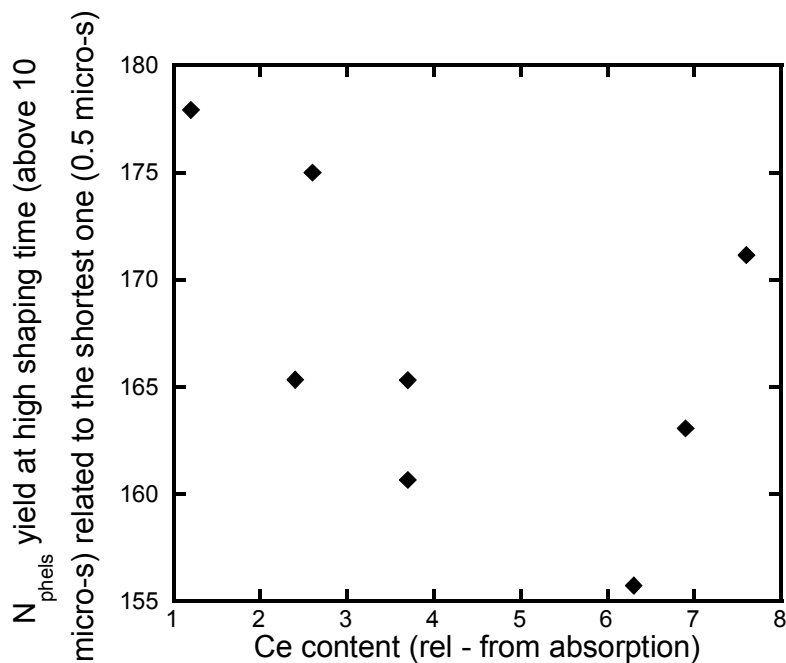


Fig. 2 Dependence of N_{phels} yield on Ce content for different LuAG:Ce SCF

Generally, the other fluxes (ii) and (iii) show higher N_{phels} yields but their SCF thicknesses are less compared with those prepared from flux (i). Detailed results of LuAG:Ce SCF were published in paper [2] while that obtained on YAG:Ce in [4].

Besides Ce^{3+} doping ion also other are investigated as Bi^{3+} , Pr^{3+} or even Sc^{3+} [7]. Possibilities of these dopants will be shortly discussed at the end of this talk.

Acknowledgements Financial support of the Czech Science Foundation project no. 202/08/0893 is gratefully acknowledged.

References

- [1] J. A. Mares, A. Beitlerova, M. Nikl, N. Solovieva, K. Nitsch, M. Kucera, M. Kubova, V. Gorbenko and Y. Zorenko, *Rad. Measur.* 42 (2007), 533-536.
- [2] P. Prusa, T. Cechak, J.A. Mares, M. Nikl, A. Beitlerova, N. Solovieva, Yu.V. Zorenko, V.I. Gorbenko, J. Tous and K. Blazek, *Appl. Phys. Lett.* 92 (2008), 041903-1-3.
- [3] M. Kucera, K. Nitsch, M. Kubova, N. Solovieva, M. Nikl and J.A. Mares, *IEEE Trans. Nucl. Sci.* 55 (2008), 1201-05.
- [4] P. Prusa, M. Nikl, J.A. Mares, M. Kucera, K. Nitsch, and A. Beitlerova, *phys. stat. sol. A* 206 (2009), 1494-1500.
- [5] Y. Zorenko, J.A. Mares, R. Kucerkova, V. Gorbenko, V. Savchyn, T. Voznyak, M. Nikl, A. Beitlerova and K. Jurek, *J. Phys. D: Appl. Phys.* 42 (2009), 075501 (7 pp).
- [6] V.A. Babin, V. Gorbenko, A. Makhov, J.A. Mares, M. Nikl, S. Zazubovich and Yu. Zorenko, *J. Lumin.* 127 (2007), 384-390.
- [7] Private information from some of the authors of this paper – M. Kucera, M. Nikl and K. Nitsch.

COMPARISON OF PLASTIC DEFORMATION AND GRAIN BOUNDARIES ORIENTATION OF STEEL

M. Martinkovič

Slovak University of Technology Bratislava, Faculty of Materials Science and Technology in Trnava, Institute of Materials , J. Bottu 25, 917 24 Trnava

Introduction

Final properties of forming steel or another alloys pieces are affected by production, at first conditions of mechanical working. For all that it is needful to know detail structure changes of plastic deformed material caused by bulk forming. Bulk forming leads to grain boundaries deformation. To obtain value of strain is possible by measurement of degree grain boundaries deformation. On metallographic cut it is possible to observed grain boundaries orientation which was cased by grain boundaries deformation. Stereological measured of degree of grain boundaries orientation is relatively simple, but orientation is not the same as deformation. It is necessary to build up conversion of grain boundary orientation degree to deformation.

Measurement of grain boundary orientation

Two basic types of grain boundaries orientation it is possible to measure: planar on orthogonal section of deformed parts and linear on parallel section. The method of oriented test lines is used [1]. Test lines are placed perpendicular and parallel to the grain boundaries orientation direction effected by straining [2]. From the relative number (number to unit of length) of parallel test lines intersections with grain boundaries $(P_L)_P$ and perpendicular lines ones $(P_L)_O$ on orthogonal section was total relative surface area (area to unit test volume) $(S_V)_{TOT}$ of grains estimated according equation (1) and planar oriented part of relative surface area $(S_V)_{OR}$ of grains estimated according equation (2). Degree of grain boundaries orientation was estimated as $(S_V)_{OR}$ to $(S_V)_{TOT}$ ratio.

$$(S_V)_{TOT} = (P_L)_O + (P_L)_P \quad (1)$$

$$(S_V)_{OR} = (P_L)_O - (P_L)_P \quad (2)$$

From the relative number (number to unit of length) of parallel test lines intersections with grain boundaries $(P_L)_P$ and perpendicular lines ones $(P_L)_O$ on parallel section was total relative surface area (area to unit test volume) $(S_V)_{TOT}$ of grains estimated according equation (3) and linear oriented part of relative surface area $(S_V)_{OR}$ of grains estimated according equation (4). Degree of grain boundaries orientation was estimated as $(S_V)_{OR}$ to $(S_V)_{TOT}$ ratio.

$$(S_V)_{TOT} = \pi/2 (P_L)_O + (2-\pi/2) (P_L)_P \quad (3)$$

$$(S_V)_{OR} = \pi/2 ((P_L)_O - (P_L)_P) \quad (4)$$

Conversion of orientation to deformation

Conversion of grain boundary orientation degree to deformation was based on similar comparison orientation – deformation of idealized grain shape. Four types of ideal grain shape was used – globe, cube, isometric cylinder and isometric double cone. From three basic equations – definition of deformation, definition of degree of orientation and invariability of volume the dependence of deformation to orientation was solved. Two types of deformations /orientations were analysed – linear and planar. Results with initial orientation were normalized to star to origin. Dependences of strain D to orientation O for globe G, cube K and cylinder C are on fig. 1 (a- linear, b- planar orientation/deformation).

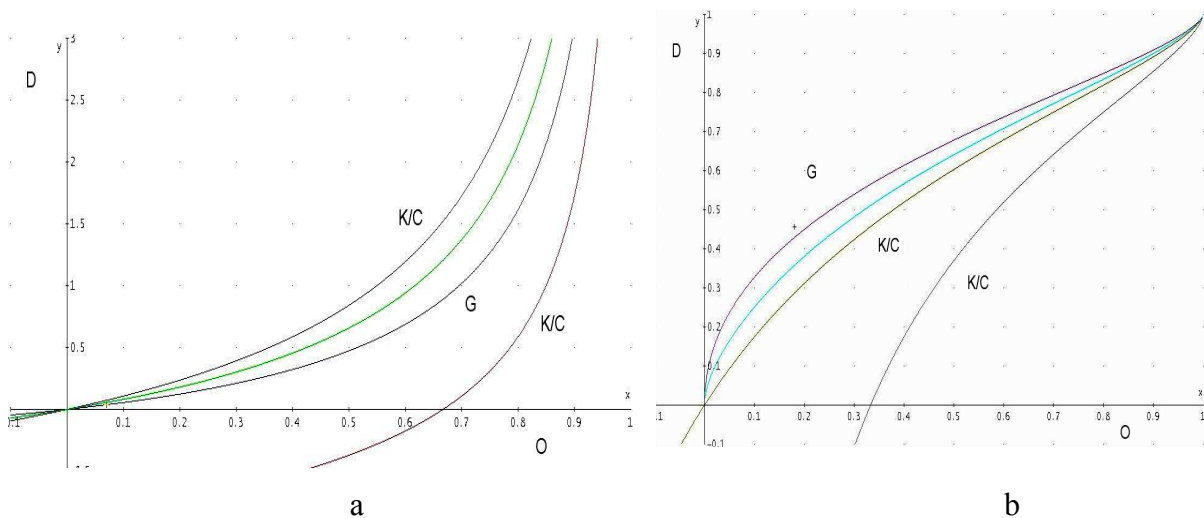


Fig. 1. Dependences of strain D to orientation O for globe G, cube K and cylinder C (a- linear, b- planar orientation/deformation)

Conclusion

The results of these models have some differences. It is necessary to fit them using comparison with experimental results. The utilization of stereology metallography allow very simple and effective experimental estimation of plastic deformation degree by measure of grain boundaries orientation in various places of bulk formed parts. Such results are very needful not only for effective technology application, but for instance for verification of bulk forming numerical model by comparing this results with numeric simulated ones

This work was supported by VEGA Grants No. 1/0837/08, 1/0126/08 and was created within VEGA Grant project No. 1/0218/09 which is not supported by Slovak Republic Ministry of Education

Literature

- [1] Saltykov, S., A. Stereometričeskaja metallografia, Stereometric metallography, Moskva: Metallurgia 1970, 3-11-1 88-70.
- [2] Russ, J., C., Dehoff, R., T.: Practical stereology, New York: Plenum Press 2000, 0-306-46476-4.

MATHEMATICAL CALCULATION OF TOTAL HEAT POWER OF THE SODIUM HEAT PIPE

P. Nemeč, J. Hužvár

Department of Power Engineering, Faculty of Mechanical Engineering, University of Žilina, 010 26 Žilina, Slovak Republic

Abstract: Article deal about heat pipe, their basic principles and operating limits. High temperature heat pipes are being evaluated for use in energy conversion applications such as fuel cells, gas turbine re-combustors, and Stirling cycle heat sources, with the resurgence of space nuclear power, additional applications include reactor heat removal elements and radiator elements. In the temperature range between 500 and 1000 °C, heat pipes can offer the favourable features of passive, reliable operation, effective thermal coupling between non-contacting fluid streams, and modest cost. Long operating life and reliable performance are critical requirements for these applications.

Introduction

Heat pipes are passive devices that transport heat over relatively long distances via the latent heat of vaporization of a working fluid. Capillary-driven two-phase systems offer significant advantages over traditional single-phase systems. Heat pipe generally has three sections: an evaporator section, an adiabatic section, and a condenser section.

Due to the two-phase characteristic, the heat pipe is deal for transferring heat over long distances with a very small temperature drop and for creating a nearly isothermal surface for temperature stabilization. The amount of heat that can be transported through the use of latent heat is typically several orders of magnitude greater than transported by sensible heat for a geometrically equivalent system. Additionally, no mechanical pumping systems are required due to the capillary-driven working fluids. Given the wide range of operating temperatures for working fluids, the high efficiencies, and the absence of external pumps in heat pipes, these systems are seen as attractive options in a wide range of heat transfer applications.

Heat pipe construction

The major components of a heat pipe are a sealed container, a wick structure, and a working fluid. The material and geometry of the heat pipe container also must have a high burst strength, low weight, high thermal conductivity, and low porosity. The most commonly constructional materials of heat pipes are steels, copper and glass. The wick structure is placed on the inner surface of the heat pipe wall and is saturated with the liquid working and provides the structure to develop the capillary action for liquid returning from the condenser to the evaporator. The working fluid must have good thermal stability properties at the specified operational temperature and pressure. Working fluid must have high wettability, surface tension and other desirable thermo-physical properties include a high liquid thermal conductivity, high latent heat of vaporization, low liquid viscosity, and a low vapor viscosity.

Heat transfer limitations

Heat pipes undergo various heat transfer limitations depending on the working fluid, the wick structure, the dimensions of the heat pipe, and the heat pipe operational temperature. Heat transfer limitations determine the region of total power heat pipe for operation temperature range. There are equations for solution heat transfer limitations:

$$\begin{aligned} \text{Vapor-pressure limitation} \quad Q_{vp} &= \frac{\pi \cdot r_v^4 \cdot h_{fg} \cdot \rho_{v,e} \cdot P_{v,e}}{12 \cdot \mu_{v,e} \cdot l_{eff}} \\ \text{Sonic limitation} \quad Q_s &= 0,474 \cdot A_v \cdot h_{fg} \cdot (\rho_v \cdot P_v)^{0,5} \\ \text{Entrainment limitation} \quad Q_e &= A_v \cdot h_{fg} \cdot \left(\frac{\rho_v \cdot \delta_l}{2 \cdot r_{c,ave}} \right)^{0,5} \\ \text{Capillary limitation} \quad \dot{Q}_c &= \frac{\sigma_l \cdot \rho_l \cdot h_{fg}}{\mu_l} \cdot \frac{K \cdot A_v}{l_{eff}} \cdot \left(\frac{2}{r_{c,e}} - \frac{\rho_l \cdot g \cdot l_l \cdot \cos \Psi}{\sigma_l} \right) \\ \text{Boiling limitation} \quad \dot{Q}_b &= \frac{4\pi \cdot l_{eff} \cdot \lambda_{ef} \cdot T_v \cdot \sigma_v}{h_{fg} \cdot \rho_v \cdot \ln \frac{r_i}{r_e}} \cdot \left(\frac{1}{r_n} - \frac{1}{r_{c,e}} \right) \end{aligned}$$

Conclusion

Liquid-metal heat pipes operate above 500 °C. Very high heat fluxes can be obtained using liquid metals due to the characteristics of the fluid: namely, very large surface tensions and high latent heats of vaporization. Heat pipe operation is depending on heat transfer limitations. There are five known transport limits (Vapor-pressure limitation, Sonic limitation, Entrainment limitation, Capillary limitation, Boiling limitation), that are influenced by hydrodynamic and thermo physical process. Solution of these 5 limits we can find and determine mathematical or theoretical total heat power, which can be able to transfer by heat pipe. With sodium heat pipes are easily reachable heat flows of 10^8 W/m²,

This article was created within the solution of project APVV - 0517 – 07.

References

- [1] Reay, D., Kew, P.: Heat Pipes Theory, Design and Applications, Fifth Edition 2006 UK, ISBN – 13: 978 – 0 – 7506 – 6754 -
- [2] Ochterbeck, Jay M.: Heat pipes, In Heat Transfer Handbook, 1. Edition - July 2003, ISBN-10: 0-471-39015-1.
- [3] Nemeč, P.: Influence heat transfer limitations of heat pipes on their cooling power; Zborník prednášok Transcom 2009, ISBN 978-80-554-0031-0.

GROWTH OF RARE EARTH GARNET LAYERS BY LIQUID PHASE EPITAXY

K. Nitsch, A. Cihlář, M. Rodová, R. Král

Institute of Physics AS CR, Cukrovarnicka 10, 162 00 Prague 6, Czech Republic
e-mail: nitsch@fzu.cz

Liquid phase epitaxy - LPE - is an important technological process in which a thin layer of crystalline material is deposited from solution onto a substrate of the same structure and orientation. A distinction is made between homoepitaxy in which the film has the same composition as the substrate and heteroepitaxy where the film and substrate differ in composition.

Epitaxial growth of garnet films was connected with magnetic rare earth iron garnets and their application in bubble memories in the 1970's [1], while nowadays the magnetic LPE films can be used in producing the microwave solitons [2] or and in testing steel valves of diesel engines using the magneto-optical effects [3]. Ce:YAG and Ce:LuAG films are promising candidates for 2D scintillation imaging screens with submicrometer resolution and they can replace polished thin plates of aluminum garnets single crystals in this application [4].

There are three variations of LPE, namely tipping, sliding and dipping. Tipping was first used by Nelson [5] in 1963 to grow semiconductor layers for Ge tunnel diodes and GaAs laser diodes. A form of slider used so far was developed by Blum and Shih [6] in 1972. The dipping and tipping techniques were used for the first time by Linares in 1965 [7] and 1968 [8], respectively, to grow iron garnet films on YAG and GGG substrates.

A typical dipping apparatus consists of a Pt crucible in a furnace with access from the top. The substrate horizontally attached in the Pt holder is suspended above a surface of garnet-flux solution until it reaches thermal equilibrium with the melt. Then it is dipped into the flux for a predetermined period of time and rotates during growth at 30 - 200 rpm. The supersaturation needed is reached either by programmed flux cooling after the substrate immersion or the substrate is dipped into beforehand supercooled flux. Transfer from a nutrient source in a temperature gradient was also used.

As fluxes the mixtures of the following compounds such as PbO-B₂O₃ (PB), BaO-BaF₂-B₂O₃ (BBB) and MoO₃-Li₂MoO₄ (ML) have been used.

The PB flux, the most often used solvent system for growth of garnet films, can be supercooled considerably with a high stability against spontaneous nucleation and high quality garnet films can be grown under isothermal conditions at constant supercooling [9]. Nevertheless, this flux has also some disadvantages: (i) the considerable volatility of PbO, which influences the saturation temperature of the garnet-flux melt, (ii) high toxicity, and so exhausts must be filtered to prevent environmental contamination, (iii) reactivity with the platinum crucible and following embedding of Pt⁴⁺ ions in the garnet lattice. The divalent and tetravalent lead ions, Pb²⁺ and Pb⁴⁺, also enter the crystal lattice in concentration from 0.1 up to 8 wt% depending on the solution composition and supercooling. In iron garnets these 'charged' impurities are not mutually compensated and they may change the valency of iron ions leading to the increased microwave losses, which restrict some applications of iron garnet.

The Ce-doped aluminum garnet films for scintillators prepared from the PB flux exhibit good optical, emission, structural and surface properties. However, the presence of Pb^{4+} , Pb^{2+} and Pt^{4+} ions initiate formation of a variety of point defects, which result in electron traps [10]. These evoke a loss of energy due to nonradiative transitions as well as appearance of a slow component in the luminescence/scintillation decay of Ce^{3+} centers and in the decrease of related luminescence intensity [11].

The BBB ternary solvent system has negligible volatility, negligible toxicity unless ingested, only very low Ba^{2+} incorporation in the film and negligible chemical reactivity with platinum [12]. On the other hand, higher viscosity and higher surface tension compared to the PB flux cause that the BBB solvent adheres easily on the sample surface and this makes it difficult to remove completely all the solvent rests from the substrate surface after the growth. The adhering solidified flux layer often results during the cooling in defect formation in the layer, which makes worse its quality and surface morphology. The Ce-doped aluminum garnet films prepared from the BBB flux exhibit excellent optical and emission properties [13], but defect density in the films is higher than that grown from the PB flux.

Another flux used for growing the garnet films is the mixture of $MoO_3-Li_2MoO_4$ [14]. This system is characterized by low volatility, low viscosity and low toxicity. Neither the lithium nor the molybdenum are significantly incorporated into the LPE film, which is important for Nd:YAG laser films. The garnet solubility is only of the order of 0.5 mole % and layers are grown in temperature gradient with growth rates as low as $0.05 \mu m/min$.

This work was supported from the Grant Agency of the Academy of Sciences of the Czech Republic (Grant No. KAN300100802).

- [1] A.H. Bobeck, E.G. Spencer, L.G. van Uitert, S.C. Abrahams, R.L. Barns, W.H. Grodkiewicz, R.C. Sherwood, P.M. Smith et al., Appl. Phys. Lett. 17 (1970) 131.
- [2] M. Chen, M.A. Tsankov, J. M. Nash, C. E. Patton, Phys. Rev. Lett. 70 (1993) 1707.
- [3] P. Novotný, P. Macháč, M. Kučera, K. Nitsch, B. Skrbek, NDT&E Int.40 (2007) 203.
- [4] T. Martin and A. Koch, J. Synchrotron Rad. 13 (2006) 180.
- [5] H. Nelson, RCA Rev. 24 (1963) 603.
- [6] J.M. Blum and K.K. Shih, J. Appl. Phys. 43 (1972) 1394.
- [7] R.C. Linares, R.B. McGraw, J.B. Schroeder, J. Appl. Phys. 36 (1965) 2884.
- [8] R.C. Linares, J. Crystal Growth 3-4 (1968) 443.
- [9] H.J. Levinstein, J. Licht, R.W. Landorf, S:L. Blank, Appl. Phys. Lett. 19 (1971) 486.
- [10] V. Babin, V. Gorbenko, A. Makhov, J.A. Mareš, M. Nikl, S. Zazubovich, Y. Zorenko J. Lumin. 127 (2007) 384.
- [11] M. Kučera, K. Nitsch, M. Kubová, N. Solovieva, M. Nikl, J. A. Mareš, IEEE Trans. Nucl. Sci. 55 (2008) 1201.
- [12] R. Hiskes, J. Crystal Growth 27 (1974) 287.
- [13] M. Kučera, K. Nitsch, M. Nikl, S. Daniš, M. Hanuš, ICDIM 2008, Aracaju, 2008.
- [1] W.A. Bonner, Mat. Res. Bull. 12 (1977) 289.

COMPREHENSIVE TESTING OF STRUCTURAL POWDER MASS WATER REPELLENTS BASED ON SILICONE

J. Nováček, S. Štátník

Brno University of Technology, Faculty of Civil Engineering, Technology Institute of Building Materials and Components, Veveří 95, Brno 602 00,
novacek.j@fce.vutbr.cz , stastnik.s@fce.vutbr.cz

Abstract

Silicon structural powder mass water repellents become a functional component of a whole variety of modern building materials. The largest application of these admixtures is in a wide range of dry mortar mixtures. The current technical standards do not provide a methodology for reliable measurement of their hydrophobic effect. Methodology for determination of durability and effect of these admixtures to materials where they are applied, has not been assessed, either. Thus, this work is devoted to compilation a methodology for a comprehensive testing of structural powder mass water repellents by means of both load and application way with the help of laboratory-simulated and real climatic conditions. The attention in this paper was particularly paid on water repellents based on silicon. However, the all research has been also focused on their comparison with waterproof metallic soaps and substances based on hydrofobised polyvinyl acetates.

Introduction

Hydrofobic additives (powder mass water repellents) are the mostly used in following applications: jointing fillers, coating isolations, sanitation mortars, wide variety of mineral polymer/silicate plasters, and purely polymer plaster pastes. Mass powder water repellents for dry mortar applications have following chemical bases:

- Oleate
- Stearate
- Mixed products (Oleate + Stearate)
- Silicone based (Silane/Siloxane)
- Hydrofobized polyvinylacetate based binders

Current test standards do not include procedures for obtaining information on the effectiveness and durability of structural powder mass water repellents, we can only use current basic test methods for testing mortars and concretes. But real load acting on hydrophobised products is a synergy of all weather conditions (frost/defrost cycles , rain, condensation, presence of salts, temperature changes, solar UV radiation, mechanical water erosion, and cyclic soaking with water and drying).

Therefore, our effort is to establish a test procedure exposing hydrophobised mortars to all of these effects and thus give a quality overview of individual powder structural water repellents. A new comprehensive method of testing durability consists of two parts:

1. Application test

Water repellents are applied to a mixture of a real product where they interact with additives and polymers. Testing begins already 3 to 4 days after batching. Three sets of samples are made (a Q-UV test set, a reference set, and a set exposed to an actual climate).

The implementation of application test consists in an application of mortars on the test plates which are subsequently placed in the Q-UV apparatus. The device is able to simulate cyclic exposure to solar UV radiation, condensation of air humidity, and simulation of wind-driven rain by water nozzle washing.

Application test has 2 main outputs:

- a) Visual comparison of the Q-UV tested samples, the samples subjected to a climate, and reference samples (range of salt efflorescence and change of mortar colour).
- b) Mutual comparison of the samples by measuring the surface absorptivity.

2. Comprehensive loading test (CLT)

The comprehensive loading test consists in cycling extreme climatic conditions. Samples of hydrophobised mortars are immersed in water for 4 hours, then frozen at $-20\text{ }^{\circ}\text{C}$ for 4 hours, and then dried at a temperature of $65\text{ }^{\circ}\text{C}$. A simple silicate system, in which there is no reaction with the additives, is used for the production of samples. A dose of water repellents is chosen unified for all compared types.

The following physico-mechanical characteristics of mortars are tested after 0, 20, 40, and 80 cycles of a comprehensive load test:

- Whole cubature water up-take after 24hours
- Surface water up-take (UNI 10859)
- Compressive strength
- Tensile strength

The current experiment focuses on the comparison of mono-functional water repellents on basis of silane / siloxane. The attention in the next step will be devoted to testing of metallic soaps.

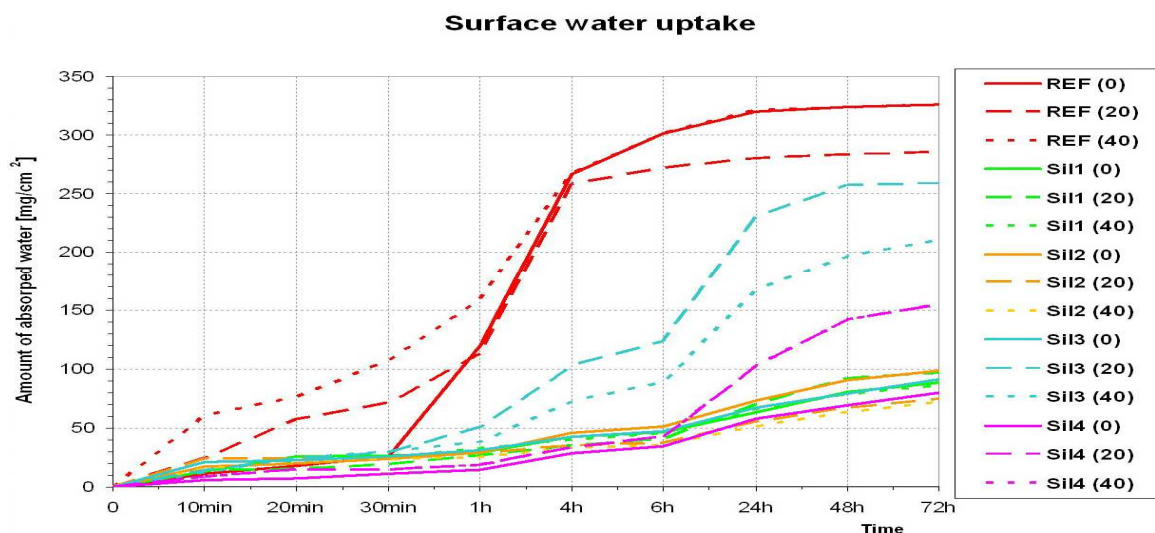


Fig. 1. Surface water up-take (UNI 10859) of compared monofunctional silicone based hydrofobizers after 0, 20, 40 cycles of CLT.

This outcome has been achieved with the financial support of the CIDEAS project No. IM0579.

THE ZERO FIELD SPLITTING OF PARAMAGNETIC TRANSITION METAL COMPLEXES

B. Papánková^(a), R. Boča^(a), L. Dlháň^(a), J. Titiš^(b) and I. Svoboda^(c)

- (a) Faculty of Chemical Technology, Slovak University of Technology, 812 37 Bratislava, Slovak Republic
- (b) Department of Chemistry, University of SS Cyril and Methodius, Trnava, Slovak Republic
- (c) Material Science, Darmstadt University of Technology, D-64287 Darmstadt, Germany

Paramagnetic transition metal complexes have long been studied for their many interesting and useful properties. The key properties of transition metal complexes arise from the details of their electronic structure. The intricacies of the electronic structure in transition metal complexes with stable states in which the spin angular momentum has $S > 1/2$, are governed by the zero field splitting (ZFS). ZFS is a very subtle effect that has important and determining consequences for the properties of transition metal complexes. The ZFS also influences molecules other than transition metal complexes, such as organic and organometallic molecular magnets. ZFS is usually characterized by two parameters, termed the axial (D) and rhombic (E) zero field splitting constants. These parameters can be measured by a variety of techniques.

The magnetism of metal complexes is determined by the crystal-field multiplets that exhibit a further splitting under the influence of an applied magnetic field (Zeeman splitting) [1]. Just the Co(II) complexes represent an interesting case where several important factors tune the overall magnetic behavior. Therefore we prepared a mononuclear hexacoordinate Co(II) complexes that exhibit an effectively compressed tetragonal bipyramid. These complexes have been structurally characterized and subjected to magnetochemical studies.

Subject - a series of Co(II) complexes:

- $[\text{Co}(\text{CCl}_3\text{COO})_2] \cdot 4\text{H}_2\text{O}$, $M = 455.75 \text{ g mol}^{-1}$, dinuclear units
- $[\text{Co}(\text{C}_2\text{O}_4)(\text{bpy})_2] \cdot 5\text{H}_2\text{O}$, $M = 539.32 \text{ g mol}^{-1}$, interacting mononuclear units
- $[\text{Co}(\text{MeIz})_2(\text{ac})_2(\text{H}_2\text{O})_2]$, $M = 377.27 \text{ g mol}^{-1}$, mononuclear
- $[\text{Co}(\text{pic})_2(\text{H}_2\text{O})_2] \cdot 2\text{H}_2\text{O}$, $M = 375.7 \text{ g mol}^{-1}$, mononuclear

...in comparison with related Co(II) complexes

- $[\text{CoL}_2(\text{H}_2\text{O})_2]$
- $[\text{Co}(2\text{-MeSnic})_2(\text{H}_2\text{O})_2(\text{Me}_2\text{fupy})_2]$
- $[\text{Co}(\text{poxbim})_2(\text{H}_2\text{O})_2](\text{ClO}_4)_2$
- $[\text{Co}(\text{Iz})_6](\text{HCOO})_2$

These complexes exhibit a rather different magnetic behaviour evidencing a sizable magnetic anisotropy and a diverse field development of the magnetization differing from the Brillouin function.

Fig. 1. Magnetic functions (SQUID data):

- Effective magnetic moment vs T
- Magnetization vs B

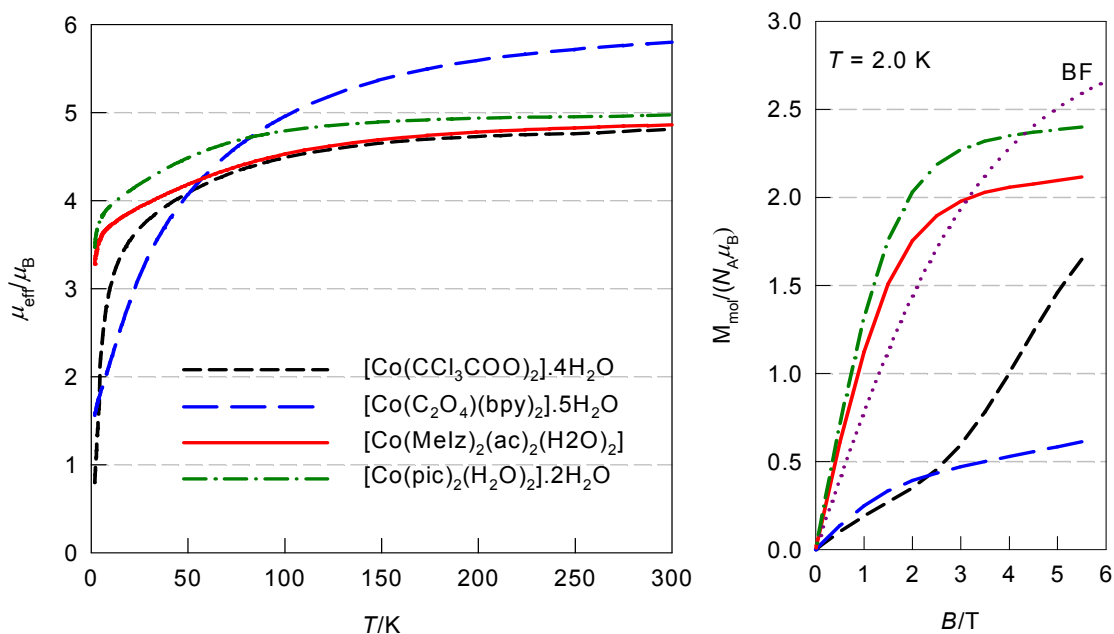


Fig. 2. Search for a magnetostructural D-correlation in Co(II) complexes: D_{mag} vs D_{str} (analogous to that for Ni(II) complexes) [2].

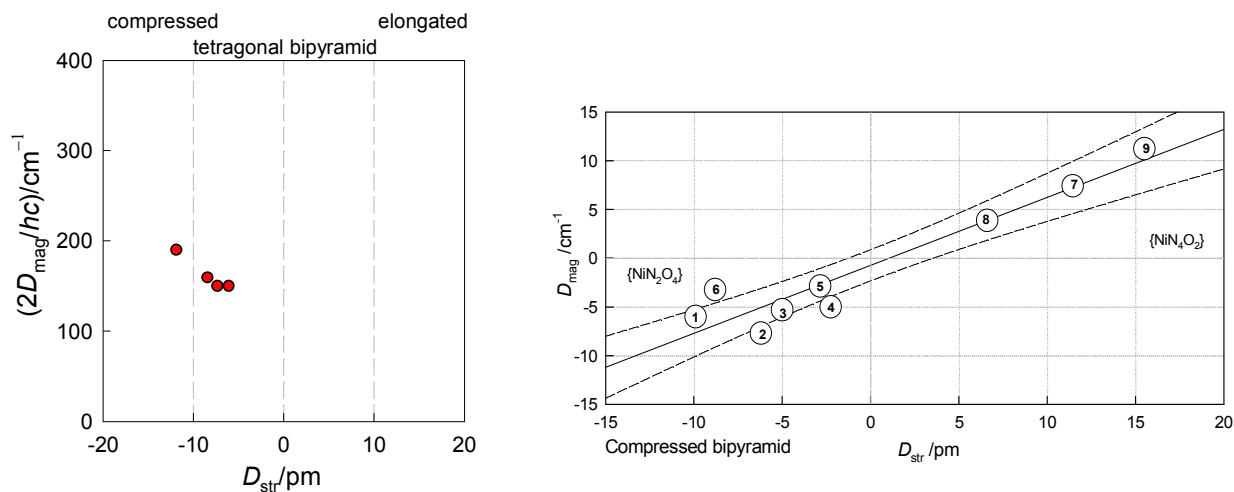


Fig. 3. The magnetostructural D – correlation for Ni(II) complexes. Broken lines - confidence interval; dotted – prediction interval.

Grant agencies are acknowledged for the financial support: COST 0006-06, APVV 0006-07, VVCE 0004-07 VEGA 1/0213/08

[1] R. Boča, Struct. Bonding 117 (2006) 1.

[2] R. Boča, J. Titiš: in Coordination Chemistry Research Progress, Nova Science Publishers, New York, 2007, pp. 247-304.

COMPLEXES OF Ni(II) WITH 2,2'-DIPYRIDYLAMINE

A. Pavlová^(a), N. Pavlišáková^(a), J. Černák^(a)

(a) Department of Inorganic Chemistry, Institute of Chemistry, P. J. Šafárik University, Moyzesova 11, 041 54 Košice, Slovakia

Low-dimensional magnetic systems are an attractive group of materials as they exhibit particular magnetic phenomena with respect to three-dimensional (3d) systems [1]. Low-dimensional magnetic materials based on coordination compounds can be chemically realized using the methods of crystal engineering, i.e. by the use of an appropriate combination of magnetic central atom, blocking ligand(s) (with the aim to tune the dimensionality of the formed system) and suitable bridging species which link the magnetic building blocks [2, 3].

As a part of our studies on low-dimensional systems based on Ni(II) we decided to use 2,2'-dipyridylamine (*dpya*) as a blocking ligand and fumarato or maleato (*mal*) anions as bridging ones. The use of nickel nitrate as a starting salt in the aqueous-ethanolic system Ni(II) – *dpya* – *mal* led unexpectedly to formation of $[\text{Ni}(\textit{dpya})_2\text{NO}_3]\text{NO}_3$ (**1**), which, however, was possible to prepare also by direct syntheses [4]. The formed ionic compound consists of $[\text{Ni}(\textit{dpya})_2\text{NO}_3]^+$ complex cation in which nickel atom is hexa-coordinated by one chelate bonded nitrate ligand and two chelate bonded *dpya* ligands. The second nitrate group acts as a counterion [4].

As a continuation of this study we have examined the possibility to replace the nitrate anions in **1** by nitrite ones starting from a mixture of nickel chloride and sodium nitrite. From this reaction system we have isolated two novel complexes $[\text{Ni}(\textit{dpya})_2\text{NO}_2]\text{Cl}$ (**2**) and $[\text{NiCl}(\textit{dpya})(\text{H}_2\text{O})(\text{NO}_2)]$ (**3**). The prepared complexes were characterized by chemical analyses, infrared spectroscopy and X-ray single crystal structure analyses.

The crystal structure of violet **2** ($R_1 = 0.0313$) is ionic and is built up of $[\text{Ni}(\textit{dpya})_2\text{NO}_2]^+$ cations containing hexacoordinated Ni(II) central atom and not coordinated chloride anions. Four coordination sites around Ni(II) atom are occupied by two chelate bonded *dpya* ligands via both pyridine nitrogen atoms while the remaining two coordination sites are occupied by oxygen atoms from chelate bonded nitrite ligand. This coordination mode is similar to that found in the violet nitrate complex **1**.

The crystal structure of green **3** ($R_1 = 0.0689$) is molecular; the $[\text{NiCl}(\textit{dpya})(\text{H}_2\text{O})(\text{NO}_2)]$ molecule exhibits internal mirror symmetry. The Ni(II) central atom is hexa-coordinated in the form NiClO_3N_2 ; in the equatorial plane are placed one chelate *N*-bonded *dpya* ligand and one chelate *O*-bonded nitrite ligand, while the axial positions are occupied by one aqua and one chloro ligands.

Acknowledgement

This work was supported by the Slovak grant agency APVV under contracts Nos. APVV-VVCE-0058-07 and APVV-0006-07, and by grant agency VEGA (grant 1/0089/09). Partial

support from P. J. Šafárik University (VVGS 37/09-10) and VVGS PF 19/2009/CH are acknowledged, too.

References

- [1] D. Gatteschi, R. Sessoli, J. Villain, *Molecular Nanomagnets*, Oxford University Press Inc., New York, 2006.
- [2] R.G. Wilett, Z. Wang, S. Molnar, K. Brewer, C.P. Landee, M.M. Turnbull, W. Zhang, *Mol. Cryst. Liq. Cryst.* 233 (1993) 277.
- [3] F.A.A. Paz, J. Klinowski, *Pure Appl. Chem.* 79 (2007) 1097.
- [4] J. Černák, A. Pavlová, M. Dušek, K. Fejfarová, *Acta Crystallogr. C* 65 (2009) m260.

MODELLING OF CONSTRICTION PHENOMENON IN COMPOSITE CONTAINING CONDUCTIVE CARBON PARTICLES

I. Pilarčíková, J. Hampl, S. Jirků

Czech Technical University, Faculty of Electrotechnical Engineering, Technická 2,
166 27 Praha 6, Czech Republic

Introduction:

Solution of constriction phenomenon in polymer composites filled with conductive carbon particles is based on theory of contacts transient resistance.

A **contact** represents two electrical conductors being in common contact. Through these conductors, electric current is flowing at contact points. Since surface of no contact is absolutely flat, electric current flows from one contact to another only at certain points (see Fig 1). This effect (called constriction phenomenon) represents one of main causes of contacts transient resistance.

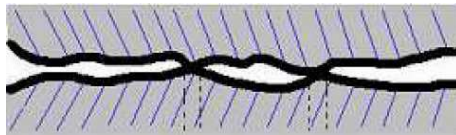


Fig. 1. Contact points of conductors

Proper contact points of printed contacts represent only a minor part of total contact surface. Inputting into the so called constriction point, current lines narrow themselves and the current flows only through a small contact surface. A constriction space is of certain active resistance. Its amount is determined for fine metals in vacuum. If some electric current flows through the constriction space, the following voltage within the so called R_U constriction resistance originates: $U = R_U \cdot I$

Solving:

Constriction phenomenon in polymer composites filled with conductive carbon particles is solved in plane at use of two models.

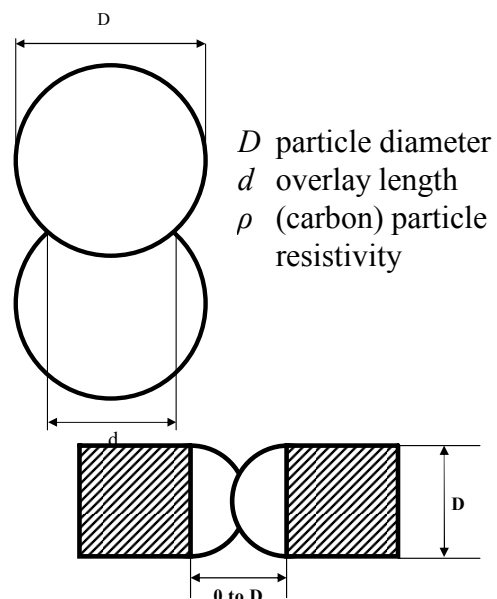
1st Model: Contact of spherical particles

It is assumed that carbon particles in composites can not only contact each other (as metals) but also grow through each other.

Cross-hatched surface is of high-conductive varnish and $\rho^{lak} = 10^{-4}\rho$, semicircular segment of conductive paper is of ρ resistivity. Lower contact is of D width while upper one of d width.

D and d widths match with overlay of both particles.

By measuring on the model, distribution of current field within the semicircular segment as well as shape resistance arisen from field deformation are detected.



2nd Model: Connecting of two spherical particles by means of conductive bridge

D particle diameter, W bridge width, l bridge length.

Bridge surface is the same as spherical particle surface:

$$l \cdot w = \pi \frac{D^2}{4}$$

Particles and bridge resistivity is of ρ again.



Cross-hatched surface is of high-conductive varnish and $\rho^{lak} = 10^{-4}\rho$, semicircular segment and bridge are of conductive paper and ρ resistivity. Semicircular segment is of D diameter.

Graphite bridge is of $w \times l$ sizes and ρ resistivity.

By measuring on the model, distribution of current field within the semicircular segment as well as shape resistance arisen from field deformation are detected. Bridge slenderness changes during measuring.

For realization of planar field analogous model, it is used direct current field in a layer of graphite paper of constant h thickness.

One-sided graphite paper ($R_{\square} = 1,58 \cdot 10^3 \Omega$) was used for building of analogous models for our analogous facility. Silver varnish Degussa 200 ($R_{\square} = 0,4 \Omega$) proved as the best for building of conductive parts of models edges (electrodes).

The electrical field on Figs 2 and 3 is mapped by means of dimensionless equipotential lines frameworks $V^* = const$ and electrical streamline $W^* = const$ where W is so called current function. Dimensionless potential is standardized by $U_0 = V_2 - V_1$ difference of E_2 and E_1 electrodes. Then, a dimensionless potential value matches with $V = const$ equipotential line.

$$V^* = \frac{V - V_1}{V_2 - V_1}$$

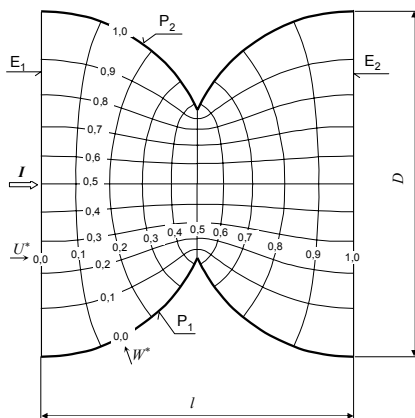


Fig. 2. Electrical fields on Model 1 sample

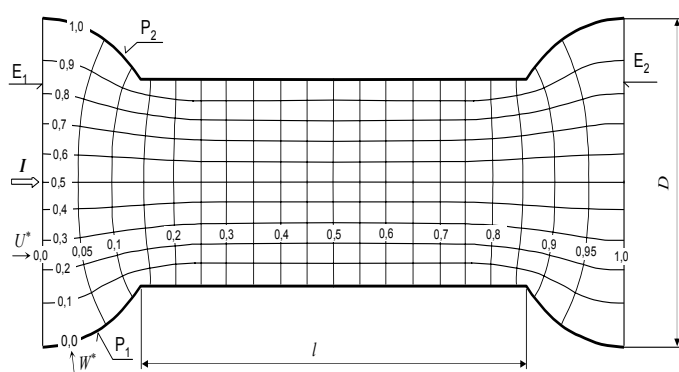


Fig. 3. Electrical fields on Model 2 sample

PREPARATION AND PROPERTIES OF LITHIUM YTTRIUM PHOSPHATE - $\text{LiY}(\text{PO}_3)_4$ GLASS

M. Rodová, A. Cihlár, R. Král and K. Nitsch

Institute of Physics AS CR, Cukrovarnicka 10, 162 00 Prague 6, Czech Republic
e-mail: rodova@fzu.cz

In search of new scintillating materials to be used in the detection of x-rays, gamma-rays and neutrons the attention was paid to glasses because of their low cost, ability to host emission centers in high concentration, good mechanical properties, thermal and chemical stability and easy shaping. As a result of our recent activity in this field we present a newly developed glass, cerium doped sodium gadolinium phosphate - $\text{Ce:Na}_{1-x}\text{Gd}_x(\text{PO}_3)_4$, for effective detection of γ - and X-rays [1]. By adding gadolinium ions into sodium phosphate the energy guiding sublattice arises, which supports nearly-resonant energy migration towards Ce^{3+} ions and increases luminescence efficiency. It was found that the radioluminescence intensity of these glasses increased with Gd concentration. For glass of stoichiometric composition $\text{NaGd}(\text{PO}_3)_4$ doped with 1 mol% of Ce^{3+} the intensity is almost threefold in comparison to standard BGO scintillator [2].

This contribution deals with glassy lithium yttrium phosphate $\text{LiY}(\text{PO}_3)_4$, enriched by boron and doped by some rare earth ions such as Ce^{3+} , Pr^{3+} and Nd^{3+} and its aim is to inform about the results achieved when testing this glass for neutron detection. This compound is supposed to meet the main requirements for an efficient neutron scintillator such as high cross section for neutron capture, fast scintillation response and low density ensuring relative insensitivity to background gamma radiation. While the high cross section for neutron capture is based on the presence of isotopes ^6Li and ^{10}B in the glass, fast scintillation response in the range of tens of nanoseconds can be reached by doping the scintillator material by rare earth ions with fast 5d-4f emission transitions (Ce^{3+} , Pr^{3+}).

Glassy $\text{LiY}(\text{PO}_3)_4$ samples were prepared by a rapid quenching of a mixture of LiPO_3 and YPO_4 in molar relation 1:1 and small amount of P_2O_5 and CePO_4 . The mixture was heated up to 1200°C in a quartz crucible, cooled by pouring into a graphite mould, short tempered at 280°C and in the end cooled down to the room temperature. Prepared glass samples $10\times 10\times 25$ mm were colorless and transparent [3].

The glass-forming ability of prepared glass was evaluated according to the relation $K_{gl} = (T_c - T_g)/(T_m - T_c)$ where K_{gl} is the numerical measure of glass forming tendency, T_g , T_c and T_m are the temperatures of glass transition, crystallization and melting [4]. If the K_{gl} is greater than 0.5 the glassforming tendency of glass is high. For studied $\text{LiY}(\text{PO}_3)_4$ glass the K_{gl} was determined as 2.14 what means that its glassforming tendency is high.

As thermal stability of glasses is important in their application, crystallization processes, their kinetics and mechanism are subject of considerable theoretical and practical interest. The glass crystallization kinetics is experimentally studied by methods of thermal analysis under both isothermal and non-isothermal conditions and experimental basis are thermal data collected by DTA or DSC at continuous heating rate (non-isothermal conditions) and isothermal annealing of glass.

Crystallization kinetics in supercooled melts under isothermal conditions is described by the standard nucleation-growth model as the time dependence of the crystallized volume

fraction $\alpha(\tau)$. The relation is usually written in the form $\alpha(\tau) = 1 - \exp[-k(t)^n]$ and it is well-known as the Johnson, Mehl and Avrami equation (JMA) [5]. In this relation t is the time, n the Avrami exponent and k is the temperature dependent reaction rate constant given by $k = A \exp\left(-\frac{E_C}{RT}\right)$, where E_C is the apparent activation energy for crystallization, A the frequency factor and T the temperature.

For crystallization under non-isothermal conditions a number of models were developed and the most employed ones are presented as follows:

To analyze non-isothermal data Kissinger proposed the following relation $\ln \frac{\beta}{T_p^2} = -\frac{E_C}{RT_p} + \ln \frac{AR}{E_C}$, where T_p is the crystallization peak temperature. Overall activation energy for crystallization E_C and the frequency factor A can be determined by plotting $\ln(\beta/T_p^2)$ vs. $1/T_p$. However, this dependence often yields two parts with different slopes for lower and higher heating rates. Two values of the energy E_C and two values of the frequency factor A can be calculated from the slopes (E_C/R) and intercepts $\ln(AR/E_C)$, respectively.

Ozawa devised another procedure, which is given by $\ln \beta = -1.0516 \frac{E_C}{RT_p} - const.$ and E_C can be calculated from the slope of the dependence of $\ln \beta$ on $1/T_p$.

Another method for non-isothermal conditions was suggested by Matusita et al. in the form $\ln[-\ln(1-\alpha)] = -n \ln \beta - 1.052 \left(\frac{mE_C}{RT}\right) + const.$, where n and m are numerical factors. If below the transformation temperature the tested glass contains no nuclei, $n = m + 1$ and if some nuclei are present, $n = m$. When plotting $\ln[-\ln(1-\alpha)]$ against $1/T$ energy E_C can be calculated from the dependence slope and the value of n is determined from the slope of the dependence of $\ln[-\ln(1-\alpha)]$ on $\ln \beta$ at a temperature T_p .

The research work at the Institute of Physics AS CR is supported by Institutional Research Plan No. AV0Z10100521.

- [1] M. Nikl, K. Nitsch, E. Mihóková, N. Solovieva, J.A. Mareš, P. Fabeni, G.P. Pazzi, M. Martini, A. Vedda, S. Baccaro, Appl. Phys. Lett. 77 (2000) 2159.
- [2] K. Nitsch, A. Cihlář, D. Klimm, M. Nikl, and M. Rodová, J. Therm. Anal. Calorim. 80 (2005) 735.
- [3] K. Nitsch, M. Rodová, J. Therm. Anal. Calor. 91 (2008) 137.
- [1] A. Hrubý, Czech. J. Phys., B 22 (1972) 1187.

HETEROBIMETALLIC COORDINATION COMPOUNDS BASED ON COPPER AND NICKEL

I. Sabová, J. Černák

Department of Inorganic Chemistry, P. J. Šafárik University, Moyzesova 11,
041 54 Košice, Slovakia

Study of magnetic properties remains a major challenge in inorganic chemistry for the last decades. The study of correlation crystal structure – magnetic properties is motivated by theoretical as well as practical reasons [1]. Potentially interesting type of materials is represented by coordination compounds containing two metallic central atoms exhibiting different spins arranged in one-dimensional geometry – the alternate chains. If one central atom in the alternate chains is bearing spin $S = 1/2$ and the second $S = 1$, then such materials, at sufficiently low temperature ($T \ll J$, where J is the magnetic exchange parameter), will behave as a ferromagnetic chain despite antiferromagnetic interactions between the respective atoms. Theoretical prediction of the variation of magnetic susceptibility versus temperature was outlined by Furusaki et al. [2].

Search in the CSD (Cambridge Structural Database) [3] has shown 253 entries for Cu-Ni hetero-bimetallic compounds with known crystal structures. As both nickel and copper central atoms can be dia- or paramagnetic, four possible combinations can arise: (1) both central atoms are diamagnetic (d-d type); (2) Cu(II) atom is paramagnetic and the Ni(II) is diamagnetic (p-d); (3) diamagnetic Cu(I) atom associated with paramagnetic Ni(II) atom (d-p); and (4) both central atoms are paramagnetic (p-p). For the last group two further possibilities may arise. Firstly, both central atoms occupy crystallographically and stereochemically distinct sites in the unit cell, and secondly, the same crystallographic site is statistically occupied by both central atoms (substitution). Previously we have prepared and characterized the Cu(II)-Ni(II) complex $[\text{Cu}_{0.05}\text{Ni}_{0.95}(\text{bpy})_2(\text{ox})] \cdot 4\text{H}_2\text{O}$ ($\text{bpy} = 2,2'$ -bipyridine, $\text{ox} = \text{oxalato}$) [4] which belongs to the second type.

As a continuation of our studies we have explored the aqueous-ethanolic system Cu(II) – bpy – $[\text{Ni}(\text{CN})_4]^{2-}$ and as a result of our synthetic effort we have isolated two new complexes $[\text{Cu}(\text{bpy})_2(\text{CN})]_2[\text{Ni}(\text{CN})_4] \cdot 2\text{H}_2\text{O}$ (**1**) and $[\text{Ni}(\text{bpy})_3][\text{Cu}(\text{CN})_3] \cdot n\text{H}_2\text{O}$ (**2**). The results of chemical analyses, FT-IR spectroscopy and single crystal X-ray analyses indicate that **1** belongs to p-d type and **2** to d-p type of Cu-Ni heterobimetallic compounds, respectively. The formation of both complexes exhibit ionic structures. The results are discussed.

Acknowledgement

This work was supported by the Grant Agencies VVGS UPJŠ (Grant No. 37/09-10) and VVGS PF (Grant No. 19/2009/CH). We thank Dr. J. Kuchár from University of P. J. Šafárik for X-ray data collection.

References

- [1] E. Dagotto, Phys. World (1996) 22.
- [2] A. Furusaki, M. Sigrist, P. A. Lee, K. Tanaka, N. Nagaosa, Phys. Rev. Lett. 73 (1994) 2622.
- [3] F.H. Allen, S. Bellard, M. D. Brice, B. A. Cartwright, A. Doubleday, H. Higgs, T. Hummelink, B. G. Hummelink-Peters, O. Kennard, W. D. S. Motherwell, J.R. Rodgers, D. G. Watson, Cambridge Structural Database System (CSDS), Cambridge, UK, 1994 (Version January 2005).
- [4] J. Kuchár, J. Černák, I. Sabová, Ch. Kappenstein, M. Kajňaková, M. Orendáč, R. Boča: Solid State Sciences, 11 (2009) 950.

STRUCTURE AND ELECTRIC RESISTIVITY OF SINTERED AND PLASMA SPRAYED TUNGSTEN – BASED CERMETS

V. Brožek ^(a), P. Ctibor ^(b), D.-I. Cheong ^(c), S.-H. Yang, ^(c), J. Sedláček ^(d)

- (a) Institute of Chemical Technology, Prague, Czech Republic
- (b) Institute of Plasma Physics AS CR, Prague, Czech Republic
- (c) IUCF – Chungnam National University, Daejeon, South Korea
- (d) Czech Technical University in Prague, Faculty of Electrical Engineering, Department of Electrotechnology, Technická 2, 166 27 Prague 6, Czech Republic

Presented work is concentrated on electric conductivity of plasma sprayed tungsten-based cermets and their comparison with their analogs made pressure-assisted sintering. These materials exhibit excellent mechanical properties [1], low thermal expansion and high resistance to heat. They have many applications in chemical industry, aerospace, nuclear and military equipments and electronic industry whereas the further improvements in production processes and their economic as well as ecological aspect is a permanent challenge.

Spraying was carried out by a water-stabilized plasma gun WSP[®]500 at IPP, Prague, Czech Republic. Powder was fed into the plasma jet by two injectors and forced in by Ar gas with a flow rate 3.2 slpm. Substrates were preheated to over 180°C in all cases. Graphite substrate surfaces with their original very low roughness R_a 1.1±0.1μm and $R_{y\ max}$ 14.5±2.0μm were covered by the coating and detached after spraying. Substrates were during the spray process enveloped by a steam of protective and cooling gas (Ar+7%H₂) oriented in opposite direction towards the plasma jet of WSP[®].

Commercial tungsten feedstock (GPT, Bruntal, Czech Republic) with a nominal size from 32 to 63μm was sprayed. The agglomerated powder containing 20 vol. % of ZrC (8.02 wt.%) in W-matrix was prepared as a laboratory product (IUCF, Daejeon, South Korea). The size of this powder was from 30 to 60μm. This composite feedstock was prepared via sintering of the spray dried composite powder prepared by mixing of W and ZrC within a ball mill.

For comparison and because of targeting of the plasma spray to highest accessible density, sintered samples were prepared by means of powder metallurgy. The conditions of pressure sintering were extreme – temperature 2000°C and pressure 5.5 GPa in the apparatus of “belt” type, used originally for preparation of synthetic diamonds. Homogenized powder mixture with 30 vol. % of ZrC, the balance being W, were sintered for 15 min of the delay on maximum temperature and pressure.

Sprayed as well as sintered samples were discs with diameter 20 mm and thickness between 1 and 3 mm. They were grinded before electrical measurement with SiC papers and then cleaned ultrasonically in ethanol.

Owing to the small electric resistance values of measured samples, the modified method according to standard DIN/ IEC 468 [2,3] was used for the resistivity determination of all reported samples. Measurement set-up consist of DC programmable power supply Agilent N5742A (80A), 7 1/2 digit nano-voltmeter Agilent 34420A, 6 1/2 digit voltmeter Agilent 34401, electrometer Keithley 6517, reference resistance standard Metra 0,001Ω and measuring fixture. All samples were measured at the same DC current value of 10A. Reference resistance standard was placed in the temperature-stabilized oil bath. To reduce the spurious thermoelectric effects on the sense voltage contacts, commutation of the measuring

current was applied during the measurement. To eliminate the spurious influence of time dependent fluctuation of power supply, it was necessary to execute synchronous voltage measurement on the resistance standard and the sample. Whole measuring procedure was controlled by a PC via GPIB bus. Time of measurement was minimized (5 measurements during time frame 12s) to reduce the warming of metallic sample. The sample temperature was monitored by thermocouple type K on the sample surface, the temperature change do not exceeded 1°C during the measurement time.

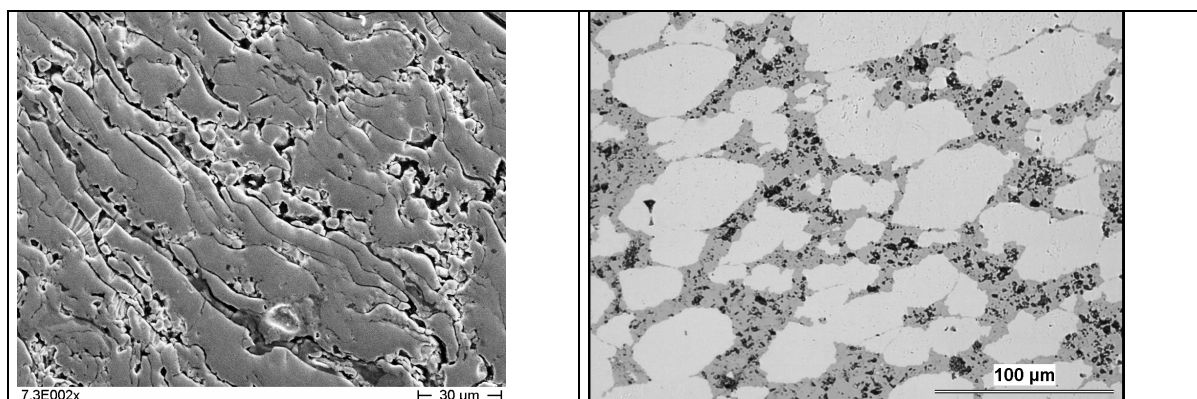


Fig. 1 - Cross section of the W90-ZrC10 coating (left; SEM-SE image) and W70-ZrC30 sintered (optical image).

Table 1 – Electric resistivity of cermet samples

Sample	W-10ZrC (WSP)	W-20ZrC (WSP)	W-30ZrC (belt)
Resistivity [nΩm]	89	587	139
<i>Calculated</i>	<i>74</i>	<i>92</i>	<i>113</i>

Electric resistivity results in Table 1 show that the coatings imply higher resistivity for the same quantity of the carbide admixture (in approximation; direct comparison was not available). This tendency is associated with the microstructure – from Fig. 1 we see the layered character of the coating and the isotropic nature of the sintered sample. In the case of the coating all pores (black in Fig.1) and defects in interlamellar contact contribute to the resistivity whereas in the sintered cermet the pores are present only within the carbide and tungsten (light in Fig.1) is itself nearly defect-free. The higher content of the carbide means higher resistivity. It is expectable because according on-line resources (e.g. matweb.com) the resistivity of pure W is about 60-70 nΩm and of pure ZrC is it about 500 nΩm. The electrical characterization of pure tungsten coatings is not in scope of this paper because of the shapes of samples not suitable for the measurement.

The strong disagreement of measured and calculated (after Lichtenecker mixing rule) value for 20% of ZrC addition in the coating is probably due to more defects in this coating.

- [1] Ctibor, P., Brožek, V., Cheong, D.-I., Yang S.-H., Chráska P., Plasma Spraying of refractory cermets by water-stabilized spray system, Acta Technica, in print, 2009.
- [2] DIN / IEC Standard 768 - Method of Measurement of Resisitvity of Metallic Materials.
- [3] Czichozs, H., Saito, T., Smith L. (Eds.), Handbook of Materials Measurement Methods, Springer Science&Bussines Media Inc. (2006) 442, ISBN 3-540-20785-6.

PARAMETERS OF SPENT RADIOACTIVE SOURCE

J.Sitek ^(a), J. Lipka ^(a)

(a) Faculty of Electrical Engineering and Information Technology, Slovak University of Technology, 812 19 Bratislava, Slovak Republic

The phenomenon of resonant emission or absorption of gamma rays in a solid matrix degradation by recoil or thermal broadening and giving an energy distribution dictated by the Heisenberg uncertainty principle is known as the Mössbauer effect. A direct application of the Mössbauer effect arises from its ability to detect slight variation in energy of interaction between a nucleus and extra nuclear electrons, variations which were previously considered negligible. In Mössbauer experiment, the emitting and absorbing nuclei are embedded in solid lattice and as a result is the recoil momentum being taken up by the crystal as whole. The gamma transition energy is then shared between the gamma photons and lattice vibration phonons. Because of quantization conditions, a fraction of events f , occur with no change in the lattice vibrations. This fraction is known as recoilless fraction. In Mössbauer experiment the source and absorber are in relative motion and must contain the same isotope. A Mössbauer spectrum is a record of the intensity of transmitted resonant gamma ray beam through an absorber as a function of the velocity moving absorber with respect of the source. In Mössbauer spectroscopy was recorded about 100 transitions of 83 isotopes in 44 elements. However, the most popular is the 14,41 keV gamma transition in isotope Fe^{57} , because its energies give reasonable spectra at the room temperature. During whole period of Mössbauer spectroscopy majority of works (more than 85 %) was done with this isotope .

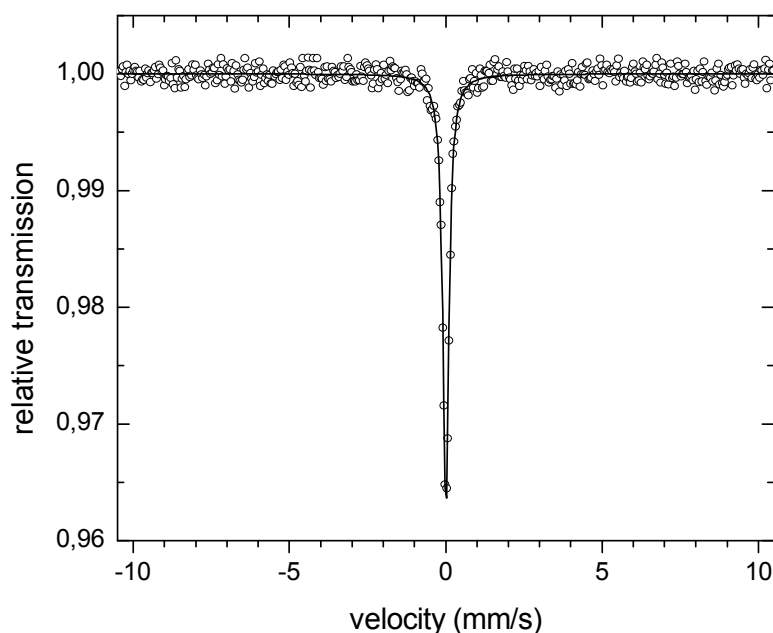
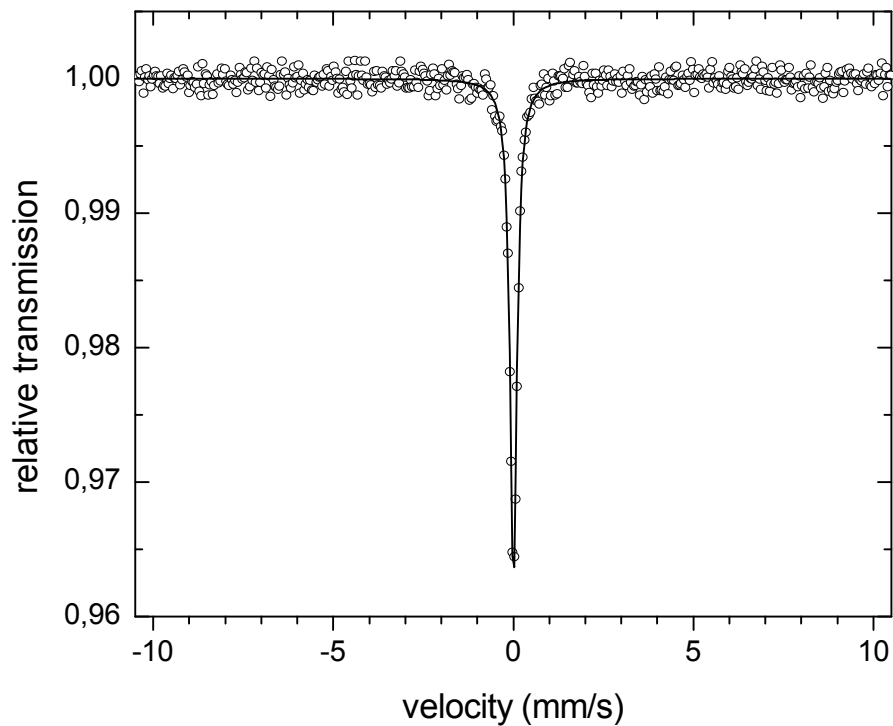


Fig.1. Mössbauer spectrum of spent source

One of the most important experimental aspects is the choice of a source matrix. Isotope Fe^{57} is daughter product of isotope Co^{57} , therefore we must choice the suitable host matrix. To

have a high recoilless fraction and single narrow emission line the Rh matrix is most suitable. Experimental application such a source is given not only by its activity but also by half time, which is in the case of Co^{57} (Rh) Mössbauer source 270 days.

We stored Mössbauer source a few years till it lost activity at the value a few Becquerel. Such a source was removed from the holder and we used it as a absorber .We supposed that this spent source as a special kind of absorber contain sufficient amount of isotope Fe^{57} nuclei for record of Mössbauer spectrum. Measurement was done at the standard spectrometer and the Mössbauer spectrum is shown in Fig.1. From fitted parameter of the spectrum we can determine the exact value of zero velocity which indicated at the very pure isotopes. From the line width we can find the broadening due to real thickness of the sample. From the area of the spectrum the value of recoilless fraction f was calculated and consequently the concentration of Fe^{57} nuclei was determined.



BOND AND ETCH-BACK SOI

J. Šik, M. Lorenc, P. Kostelník

ON Semiconductor, 756 61 Rožnov pod Radhoštěm, Czech Republic

Silicon-On-Insulator (SOI) replaces traditional silicon wafers used for many semiconductor applications with a substrate consisting of:

- Top layer of monocrystalline silicon, where active circuits are formed (device layer),
- Buried layer of insulating silicon oxide (BOX),
- Substrate providing a mechanical support for the two layers above (handle wafer).

Basic technique of bonding, mechanical grinding and polishing is usually used for thick SOI manufacturing, i.e., for SOI with the device layer thicker than $\sim 2 \mu\text{m}$. Applications of thick SOI are mainly bipolar, power IC's, and MEMS. On the other hand, thin SOI technology offers a largest set of benefits to the traditional CMOS process. Specific applications can profit from device speed improvement, significant reduction in power consumption, device area reduction, and others [1].

Homogeneity of thin device layer is extremely critical in case of thin SOI fabrication. Many techniques like SMART CUT[®] (the hydrogen implantation and exfoliation method defining device film), ELTRAN[®] (epitaxial layer transfer; employs selective etching of porous Si and water jet splitting), SIMOX (separation by implantation of oxygen below the surface) were developed and patented [2].

Bond and etch-back SOI (BESOI) is a method of fabrication thin SOI where the thickness of final device layer is determined by etching to a predefined etch-stop layer. It is usually preceded by a coarse material removal step such as grinding. The etched surface needs to be treated to recover surface roughness by either chemical-mechanical polishing (CMP) or annealing [2].

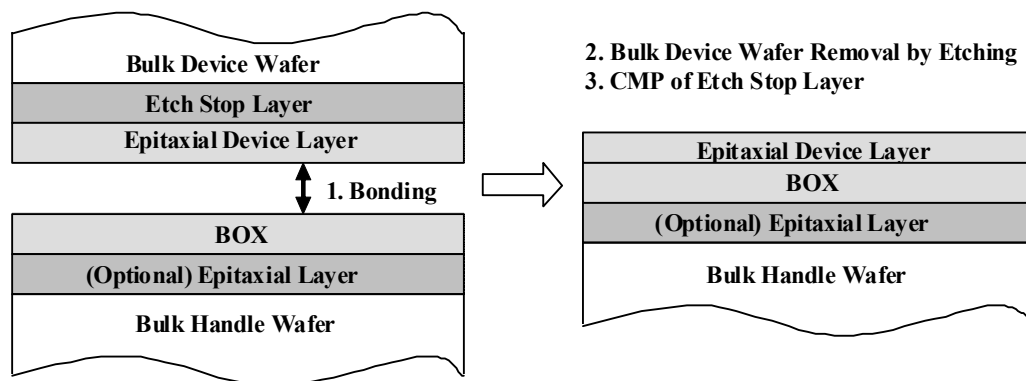


Fig. 1 Schematic procedure of thin BESOI wafer production.

In this work we will focus on development of BESOI wafer with thin device layer (of thickness $\sim 1 \mu\text{m}$) manufactured by direct bonding, back grinding, etching and CMP according the scheme shown in Fig. 1.

Device and handle wafers were produced with excellent geometrical parameters. Total thickness variation (TTV) of 150 mm wafers was $\sim 0.6 \mu\text{m}$. Wafers site flatness (SBIR) $< 0.2 \mu\text{m}$ was achieved for all sites $15 \times 15 \text{ mm}^2$ on the wafer. As wafers bonding requires excellent topography of bonded surface, RMS values of $\sim 0.15 \text{ nm}$ on the area of $1 \times 1 \mu\text{m}^2$ for (100) surface were achieved with single wafer grinding by diamond wheel and single wafer polishing. We used thermal oxidation of handle wafer for BOX layer growth with target thickness of $\sim 0.5 \mu\text{m}$. The epitaxial p++ etch stop layer [3] grown on device wafer was used. To avoid misfit dislocations in slightly doped device layer, Ge co-doping is usually utilized.

Although quality of device and handle wafers is fully suitable for spontaneous bonding by SÜSS bonder [4] we added plasma activation of bonded surfaces to reduce hydro-carbons and consequent voids on the bonded interface. Out-diffusion of boron in etch-stop layer during post-bonding annealing was modeled. Tetra methyl ammonium hydroxide (TMAH) was chosen as a selective etchant [5] after coarse grinding. For SOI structure characterization spreading resistance profiling (SRP) and Fourier transform infrared spectroscopy (FTIR) were used.

We acknowledge Markus Gabriel and his team from SÜSS MicroTec for their assistance with wafer bonding.

- [1] J. Wasselin, SOI to Replace Bulk Silicon, www.euroasiasemiconductor.com, October 2007, p. 84.
- [2] Silicon wafer bonding technology for VLSI and MEMS applications, ed. by S. S. Iyer, A. J. Auberton-Hervé, INSPEC, The Institution of Electrical Engineers, London 2002.
- [3] H. Baumgart, T. J. Letavic, and R. Egloff, Evaluation of wafer bonding and etch back for SOI technology, Philips J. Re. 49 (1995) 91-124.
- [4] www.suss.com
- [5] S. Tatic-Luic, Wen-Yue Zhang, N. Navneet, Etch-stop characteristics of heavily B/Ge-doped silicon epilayer in KOH and TMAH, Sensors and Actuators A 123-124 (2005) 640-645.

SHAPE MEMORY ALLOYS ON THE BASE OF TiNb

P.Štěpán, M. Losertová

VŠB-Technical University of Ostrava, Faculty of Metallurgy and Material Engineering,
15 Av. 17. listopad, 708 33 Ostrava, Czech Republic
petr.stepan@vsb.cz

Binary TiNb-based alloys with shape memory effect are investigated as Ni-free suitable substitution of TiNi-based alloys in biocompatible applications. It has been confirmed [1,2,3] that TiNb alloys exhibited shape memory effect and superelastic behavior at room temperature in wide range of Nb content (16.7 - 50 wt.% Nb).

Experimental alloys with nominal composition of Ti-25at.% Nb and Ti-22at.% Nb were prepared using Ti-45 wt.% Nb master alloy and Ti pieces (3N8) by means of plasma furnace melting with four passes (two passes in Ar and last two passes in Ar-5% H₂).

Heat treatment of prepared samples was realised for 12 hour at 1100°C in flowing Ar gas in high temperature furnace Linn HT1800 and quenched from 500°C in water.

The samples for metallographic observation were electrolytically polished and etched. Two phase microstructure with coarse grains of the as-cast sample observed using metallographic microscope OLYMPUS DP12 is shown in Figure 1.

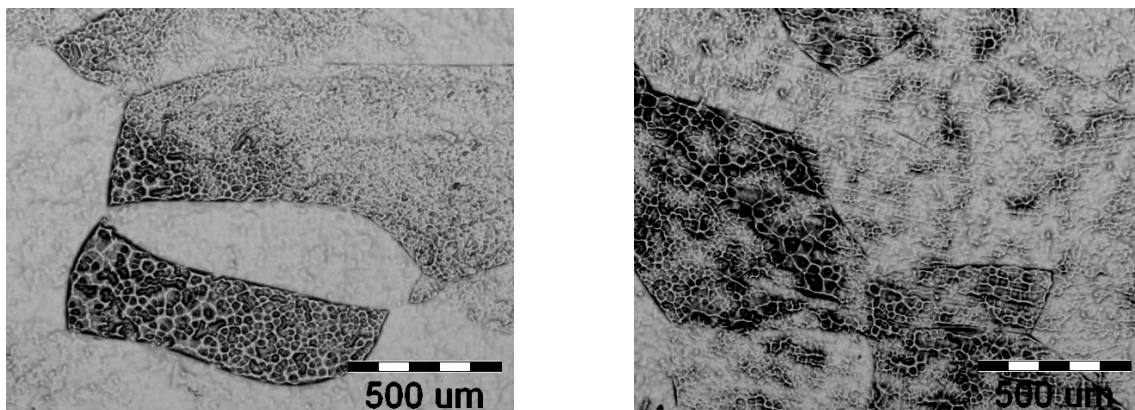


Fig.1 – Microstructure of the Ti-25at.%Nb alloy plasma melted.

Microhardness measurement across as-cast (plasma melted) and annealed samples was performed by means the LECO LM-100 instrument with load of 0.2 kg and indentation step of 1 mm. The results for the sample after annealing and quenching has shown the significant increase in values for both alloy compositions (Figure 2 and 3).

Conclusion

The TiNb alloys with nominal compositions Ti-22 at. % Nb and Ti-25 at. % Nb were prepared using plasma melting. Metallographic observation together with microhardness measurement of both alloy compositions confirmed the great influence of the heat treatment on the microstructure and mechanical properties. Further research will be focused on phase transformations and mechanical properties.

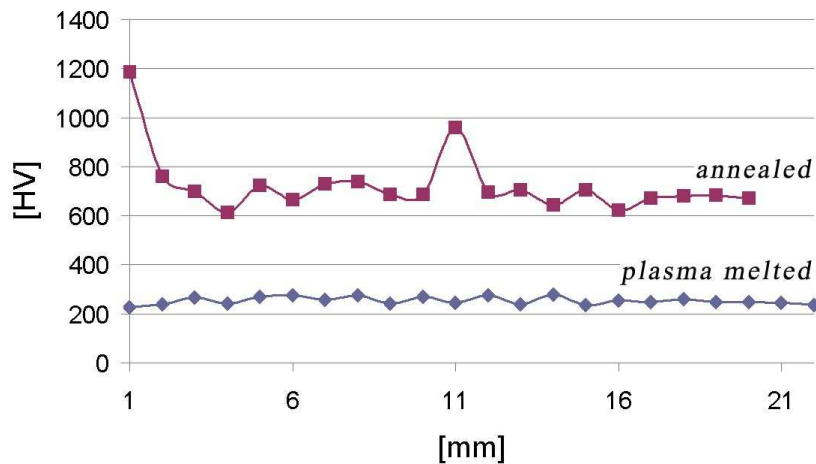


Fig. 2. Microhardness profiles across the Ti-22 at. % Nb sample plasma melted and annealed

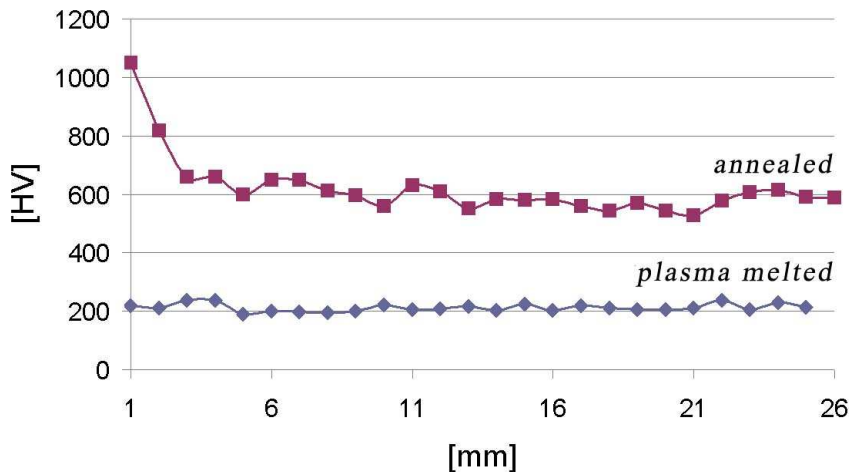


Fig. 3. Microhardness profiles across the Ti-25 at.% Nb sample plasma melted and annealed

- [1] Y.B. Wang, Y.F. Zheng, The microstructure and shape memory effect of Ti-16 at. % Nb alloy, *Materials Letters* 62 (2008) 269–272.
- [2] H.Y. Kim, J.I. Kim, T. Inamura, H. Hosoda, S. Miyazaki, Effect of thermo-mechanical treatment on mechanical properties and shape memory behavior of Ti-(26–28) at. % Nb alloys *Materials Science and Engineering A* 438–440 (2006) 839–843.
- [3] S. J. Li, R. Yang, M. Niinomi, Y. L. Hao, Y. Y. Cui and Z. X. Guo Phase transformation during aging and resulting mechanical properties of two Ti-Nb-Ta-Zr alloys, *Materials Science and Technology* 2005 vol. 21 NO 6.

Acknowledgement: *Experimental works were realised within the frame of the project MSM 6198910013 „Processes of preparation and properties of high-purity and structurally defined special materials“.*

ENGINEERING OF DEFECTS IN HEAVILY BORON-DOPED SILICON

L. Válek, D. Lysáček, J. Šik

ON Semiconductor, 756 61 Rožnov pod Radhoštěm, Czech Republic

Polished silicon wafers experience huge thermal budget during the fabrication of electronic devices. Long annealing at high temperatures may induce formation of defects which may harmfully affect the device performance. The predisposition to defect formation can be often traced back up to the process of the silicon crystal growth. In this work we show how the crystal growth process can be optimized with respect to the process of device fabrication.

Silicon wafers heavily doped with boron are required as the substrate for the fabrication of specific Zener diodes. It was found that a significant portion of the diodes show unacceptably high reverse current. Data analyses revealed the correlation to the position of the substrate wafer in the crystal (Fig. 1). Consequently, wafers from the crystal portion related to the reverse currents issues could not be used, which resulted in the financial loss of tenths of thousand dollars per year.

Detailed analyses revealed a number of bulk crystal defects in the substrate wafers. The defects were identified as the oxide precipitates, which nucleated and grew in the crystal during its growth [1]. The size and volume density of the oxide precipitates correlates well with the occurrence of the reverse currents. This reveals oxygen precipitation as the root cause of the device issues. Obviously, small oxide precipitates form in most of the crystal and they dissolve at the high temperatures of device fabrication. In the beginning of the crystal, on the other hand, oxide precipitates grow up to the supercritical size, survive, and cause issues during the device fabrication process.

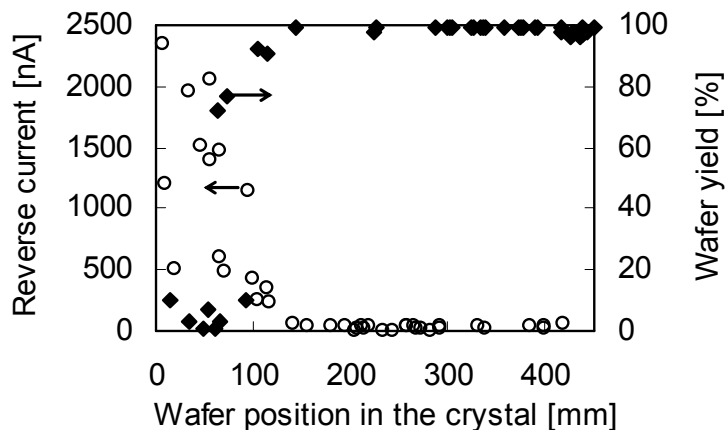


Fig. 1. Values of the diode reverse current (left axis) and wafer yield (right axis) vs. position of the substrate wafer in the crystal. The yield-to-current anticorrelation is obvious. Wafers from (0-150) mm of the crystal are unacceptable for device manufacturing.

Formation of oxide precipitates in silicon crystals is driven [2] by (a) oxygen concentration, (b) presence of vacancies and (c) thermal history of the crystal. Higher oxygen concentration yields a higher level of supersaturation and the faster precipitation. Vacancies can consume silicon interstitials emitted during the precipitate growth, which enables further

interstitial emission and promotes the growth of the precipitate. Thermal history of the crystal affects the size of grown-in oxide precipitates through the time available for their growth.

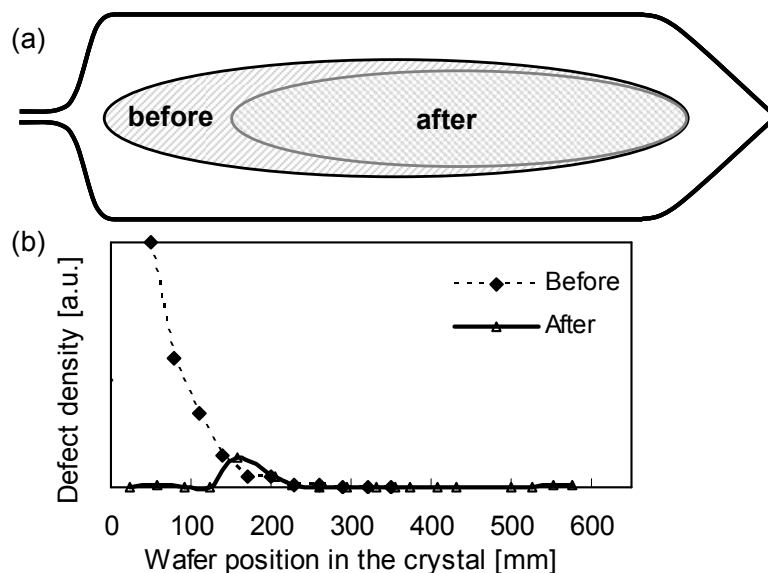


Fig. 2. (a) Distribution of point defects in studied silicon crystals before and after the optimization of the crystal growth process. Vacancy-containing core is drawn with hatches; crystal rim is interstitial-dominated. (b) Number of oxidation induced defects detected on the wafers revealing the extent of oxygen precipitation in the crystal.

While suppression of oxygen precipitation through decreasing oxygen concentration in the crystal is technologically and economically demanding, and the possibilities to influence the crystal thermal history are very limited, we found that oxygen precipitation in our crystals can be effectively suppressed through engineering of point defects.

Defect analyses revealed the presence of vacancy- and interstitials-dominated regions in the crystals. The distribution of these regions is shown in Fig. 2. It is known that the growth of oxide precipitates is enhanced in silicon matrix containing vacancies, while it is suppressed in material containing silicon interstitials. The crystal growth process was therefore optimized in such a way that the vacancy-containing core was shrunk in a portion of the crystal. This part of the crystal became fully dominated by silicon interstitials, which lead to effective suppression of oxygen precipitation, as it is demonstrated in Fig. 2(b).

The wafers sliced from the optimized crystals passed successfully the device manufacturing process. Significant material- and cost-saving in the crystal growth process was achieved through engineering of crystal defects during the growth of silicon single crystals.

- [1] L. Válek, J. Šik, D. Lysáček, Sol. Stat. Phenom. 131-132 (2008) 167.
- [2] L. Válek, D. Lysáček, J. Šik, J. Electrochem. Soc. 154 (2007) 904.

SPECTRAL-STRUCTURAL CORRELATIONS IN COPPER(II) TETRACYANIDOPLATINATE COMPLEXES WITH BI- AND TRIDENTATE N- DONOR LIGANDS

M. Vavra, I. Potočňák

Department of Inorganic Chemistry, Institute of Chemistry, P.J. Šafárik University,
Moyzesova 11, SK-041 01 Košice, Slovak Republic

Coordination compounds of the general formulae $\{[\text{Cu}(\text{L}2)_2][\text{Pt}(\text{CN})_4]\}_n$ (where $\text{L}2$ are bidentate 1,2-diaminoethane (*en*) and its *N*-monomethyl (*men*), *N,N'*-dimethyl (*bmen*) and *N,N*-dimethyl (*dmen*) derivatives, and 2,2'-bipyridine (*bpy*)), $\{[\text{Cu}(\text{L}3)][\text{Pt}(\text{CN})_4]\}_n$ (where $\text{L}3$ are tridentate bis-(2-aminoethyl)amine (*dien*) and bis-(3-aminopropyl)-amine (*bapa*)) and $\{[\text{Cu}(\text{aepn})(\text{NH}_3)][\text{Pt}(\text{CN})_4]\cdot\text{H}_2\text{O}\}_n$ (*aepn* = tridentate 3-(2-aminoethylamine)-propylamine) were prepared. These compounds were characterized by single X-ray crystal structure analysis and IR spectroscopy and these results were correlated.

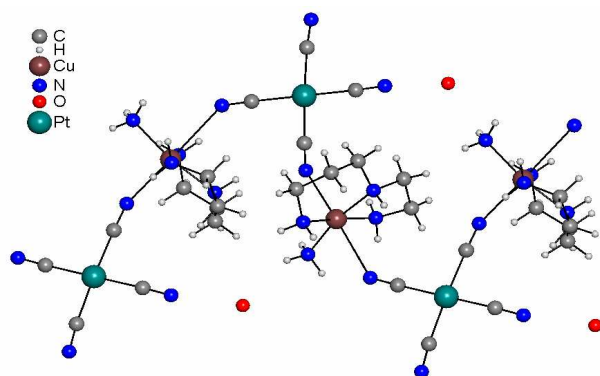


Fig. 1: 2,2-TC chain in $\{[\text{Cu}(\text{aepn})(\text{NH}_3)][\text{Pt}(\text{CN})_4]\cdot\text{H}_2\text{O}\}_n$

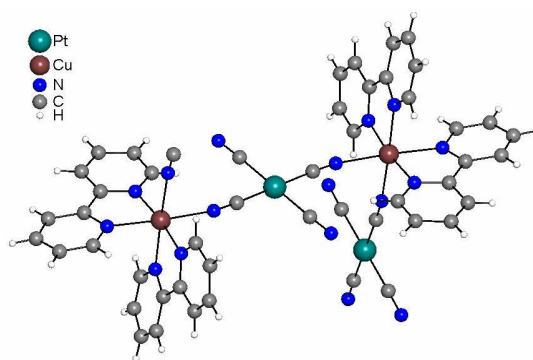


Fig. 2: 2,2-CT chain in $\{[\text{Cu}(\text{bpy})_2][\text{Pt}(\text{CN})_4]\}_n$

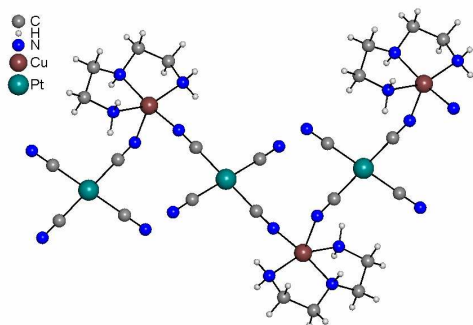


Fig. 3: 2,2-CT chain in $\{[\text{Cu}(\text{dien})][\text{Pt}(\text{CN})_4]\}_n$

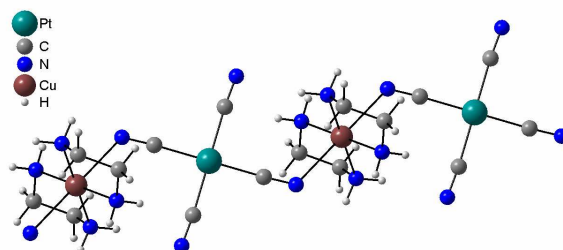


Fig. 4: 2,2-TT chain in $\{[\text{Cu}(\text{en})_2][\text{Pt}(\text{CN})_4]\}_n$

Crystal structures of the presented compounds are formed by 1D zig-zag chains with two bridging cyanido groups connecting copper and platinum atoms, nevertheless the

individual *zig-zag* chains differ from each other in the position of the breaks. The breaks of the chains are either on the Pt(II) or Cu(II) atoms, with a very unusual *cis*-coordination of bridging CN groups on Pt(II) (2,2-*TC*) (Fig. 1) and Cu(II) atoms (2,2-*CT*) (Figs. 2 and 3), or most frequently on the nitrogen atoms of the bridging cyanido groups (2,2-*TT*), with a rather small value of the Cu–N≡C angle (Fig. 4).

Not only the shape of the chains but also the coordination numbers of Cu(II) atoms are different. While Pt(II) atoms are square-planarly coordinated by four C-bonded cyanido groups in all compounds, coordination numbers of Cu(II) atoms in the $\{[\text{Cu}(\text{L}2)_2][\text{Pt}(\text{CN})_4]\}_n$ and $\{[\text{Cu}(\text{aepn})(\text{NH}_3)][\text{Pt}(\text{CN})_4]\cdot\text{H}_2\text{O}\}_n$ compounds are 6 and in the $\{[\text{Cu}(\text{L}3)][\text{Pt}(\text{CN})_4]\}_n$ compounds are 5.

The number and the position of $\nu(\text{C}\equiv\text{N})$ absorption bands in the IR spectra of 1D complexes may help to predict the number and type (terminal or bridging) of cyanido groups in these complexes (spectral-structural correlations, Fig. 5). With the presumption of a spectral equality of the terminal cyanido groups, three $\nu(\text{C}\equiv\text{N})$ absorption bands may indicate two different bridging CN groups, usually in 2,2-*CT* chains with penta-coordinated Cu(II) atoms or in 2,2-*TC* chains with hexa-coordinated Cu(II) atoms (the band at the lowest wavenumber belongs to the terminal groups). Two $\nu(\text{C}\equiv\text{N})$ absorption bands may signify that not only the two terminal cyanido groups but also the two bridging cyanido groups are spectrally equal, usually in 2,2-*TT* chains with hexa-coordinated Cu(II) atoms. Lower number of $\nu(\text{C}\equiv\text{N})$ absorption bands than expected indicates an overlap of the bands corresponding to the bridging and terminal CN groups. This overlap is observed if the Cu–N(cyanido) bond length is too long, above 2.5 Å, when the bridging cyanido groups behave spectrally as terminal ones.

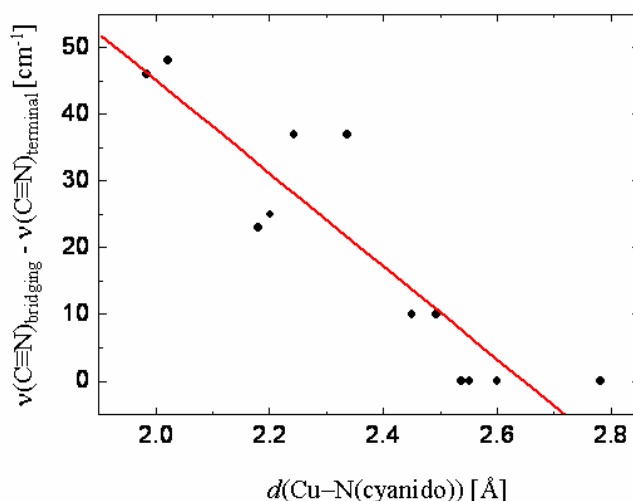


Fig. 5: $\nu(\text{C}\equiv\text{N})_{\text{bridging}} - \nu(\text{C}\equiv\text{N})_{\text{terminal}}$ dependence on $d(\text{Cu-N(cyanido)})$

This work was supported by the Slovak Grant Agency VEGA, Grant No. 1/0079/08; by the grants of Slovak Research and Development Agency No. APVV-VVCE-0058-07 and No. APVV-0006-07 and by the Faculty of Science and P.J. Šafárik University Internal Grant System, Grants Nos. VVGS PF 19/2009/CH and VVGS 37/09-10.

INFLUENCE OF RARE-EARTH ELEMENTS ON THE ELECTRICAL AND OPTICAL PROPERTIES OF INP BULK CRYSTALS

R. Yatskiv ^(a), J. Zavadil ^(a) and L. Pekarek ^(a,b)

- (a) Institute of Photonics and Electronics Academy of Sciences of the Czech Republic
 (b) Institute of Physics Academy of Sciences of the Czech Republic Prague, Czech Republic

Using rare earth (RE) elements can be one of the most promising ways for further improvement of substrate materials [1,2]. Strong motivation to study REs in the InP is connected with their high chemical reactivity and reduction capability. A number of elements (for example Si, O, S and C), which act as dopants in InP form stable compounds with REs. Since these compounds are insoluble in In, REs can be used to remove these impurities from the growth melts and reduce the background electron concentration of the grown crystals.

In this paper, we report on the growth of Pr, Dy, and Er treated InP crystals by a modified vertical Bridgman method, and on the investigation of their electrical and optical properties.

The initial polycrystalline InP was synthesized and grown from 6N purity In and P by a modified vertical Bridgman method using conical quartz crucibles placed inside a sealed evacuated quartz ampoule. The growth temperature was kept at 960 °C and the temperature gradient was 25 °C/cm. The phosphorus temperature was 450 °C, corresponding to the phosphorus vapor pressure of about 0.1 MPa. The crystals were grown conventionally as well as with Pr, Er, and Dy admixture to the growth melt. 1 mm thick wafers of 8 mm in diameter were cut from the bottom and from the top of the conical crystal ingot and characterized by the measurements of resistivity and Hall coefficient in van der Pauw configuration in the temperature range from the room temperature (RT) to 10 K. PL spectra were taken at various temperatures and various levels of excitation by Ne and Ar ion lasers in an optical He closed cycle cryostat enabling measurements in the range 3.5-300 K.

Table 1 Electrical properties of InP crystals

Sample	RE	RE Content (wt.%)	Electron concentration n, (cm ⁻³)		Electron mobility μ, (cm ² V ⁻¹ s ⁻¹)	
			300K	77K	300K	77K
InP	-	0	2.9E15	2.7E15	4524	2587
InP	Pr	0,057	1.9E15	2.1E15	3875	27770
InP	Er	0,133	1.8E15	1.7E15	3767	13120
InP	Dy	0,089	4.6E15	4.4E15	3326	4332

Electrical characteristics of bulk InP crystals are shown in Table 1. In the case of conventionally prepared crystals, the electron concentration and mobility at room temperature was $2.9 \times 10^{15} \text{ cm}^{-3}$ and $4524 \text{ cm}^2 \text{ V}^{-1} \text{ s}^{-1}$, respectively. Pr or Er admixture reduced the concentration of residual donors in the samples (Table 1). It may be explained by a strong interaction of REs with the background impurities in the melt. REs act as getters and purify crystals during growth. The best results were observed in the case of Pr and Er admixtures. At the temperature of liquid nitrogen the electron mobility was up to five times higher compared to the conventionally prepared material. It indicates effective binding of shallow donors to RE elements forming neutral complexes. In the case of Dy admixture, no purification effect was

observed. Samples prepared with the admixture of Dy are characterized by smaller electron mobility and higher concentration of free electrons compared to the undoped ones.

Low-temperature PL spectra of the samples prepared with and without REs are presented in Figure 1(I,II). Transitions due to free exciton (F.E.) and excitons bound to the neutral donor (D^0, X) or the neutral acceptor (A^0, X) are well resolved for all samples. The excitonic peak is very sharp for all samples (FWHM < 1 meV), which corresponds well with the high purity of the prepared crystals ($n = 1.8-4.6 \times 10^{15} \text{ cm}^{-3}$). Transitions described as B-A and D-A are related with shallow acceptors and correspond to conduction band-acceptor and donor-acceptor pair transitions, respectively. The spectra distinguish three subbands for conventionally prepared and REs treated InP samples. The two B-A subbands are tentatively assigned to Zn and C. The observed increase of electron concentration in samples grown with the addition of Dy is confirmed by low-temperature PL. It follows from Figs. 1(I) that the relative intensity of transitions due to donor-acceptor pairs recombination (D-A sub-band) is by far the strongest in case of Dy admixture.

The long-wavelength part is usually dominated by Mn related band consisting of three partly resolved peaks at 1.191 eV ($n=0$), 1.149 eV ($n=1$) and 1.109 eV ($n=2$), which are interpreted as zero photon line (NP), and one (-LO), and two (-2LO) photon replicas (fig. 1 (II)). A band due to Mn was evidently observed only in the case undoped InP (curve (a)). In the case of REEs doped crystals was observed reduce (curve (c)) or disappearance (curves (b), and (d)) concentration of Mn.

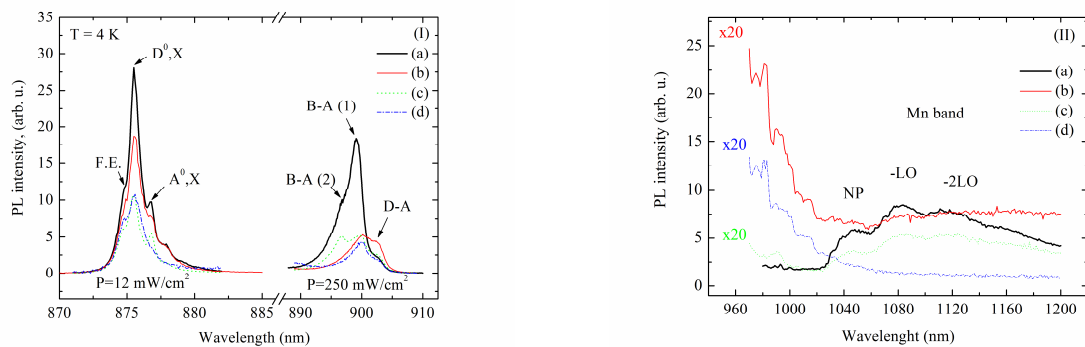


Figure 1. Low temperature PL spectra of InP samples prepared with and without RE elements. (a) –InP, (b) – InP:(Dy), (c) – InP:(Er), (d) – InP:(Pr).

Series of polycrystalline InP samples have been prepared by a modified vertical Bridgman method with RE admixtures. Low temperature PL and Hall effect measurements indicate that (i) Er, Dy, and Pr are not incorporated into the crystal lattice in the form of electrically active centers, (ii) its presence in the growth process leads to pronounced gettering of shallow donor and acceptors impurities, (iii) the increased electron mobility of InP prepared with Er and Pr admixture is caused by the formation of neutral complexes due to the effective binding of shallow donors and REs. The work has been financially supported by the Academy of Sciences of the Czech Republic with grant KJB200670901.

- [1] R. Yatskiv at. all, Growth of InP crystal with rare-earth elements, in: International conference on InP (2009) p. 1-3
- [2] L. F. Zakharenkov at. all, On the influence of lanthanides on the electrical properties of InP bulk crystals, Sov. Phys. Semicond. 21 (1987) 347-349.

Anamet s.r.o. instruments for material testing

I. Čulák

Anamet s.r.o., 1. Maja 29, 900 01 Modra, Slovak Republic

Anamet s.r.o. (see www.anamet.sk) is distributor of analytical, measuring and testing instruments in Czech and Slovak republic. Wide range of suppliers allows Anamet to fulfill requirements of most of the laboratories in industry as well as in research and development area.

Malvern Instruments is leader in particles distribution equipment and rheology, both for laboratories and production.

Netzsch Geratebau offers complete range of thermoanalytical instruments, dilatometers, DSC, DTA, LFA as well as refractories testing instruments for temperature range from -170°C to $+2800^{\circ}\text{C}$.

Tinius Olsen is the oldest universal testing machines supplier, from 19th century offers wide range of tensile testers, torsion testers, extensometers, instruments for testing plastic materials – MFI, Vicat, HDT and many others.

Angelantoni climatic, vibration, calorimetric chambers are used round the world.

Konica Minolta has the widest range of spectrometers, colorimeters, radiometers, spectroradiometers, glossmeters.

A.m. instruments and some others will be briefly presented.

Meranie veľkosti a distribúcie častíc



Termoanalýza

NETZSCH

Univerzálne skúšobné stroje, plastometre

TINIUS OLSEN LIMITED

(formerly Hounsfield Test Equipment Ltd)

Tinius  Olsen

TENSILE, COMPRESSION, IMPACT, MELT FLOW, BRINELL, SHEAR, STRETCH RECOVERY, PUNCTURE, HEAT DISTORTION (VICAT), BEND/FLEXURE, SEAM STRENGTH, TORSION

Tel.: +420 - 257 328 175
Fax.: +420 - 257 323 278

IČ: 256 52 150
DIČ: CZ256 52 150

Bankovní spojení: KB Praha,
č.ú.: 35-8062660297/0100,
IBAN CZ9601000000358062660297

e-mail: sales@anamet.cz
www.anamet.cz

Zastúpenie pre Slovensko: Igor Čulák tcl.: +421905249664

e-mail: igor_culak@nextra.sk



EN ISO 9001:2000
12 100 22058 TMS

ITES Vranov, s. r. o.

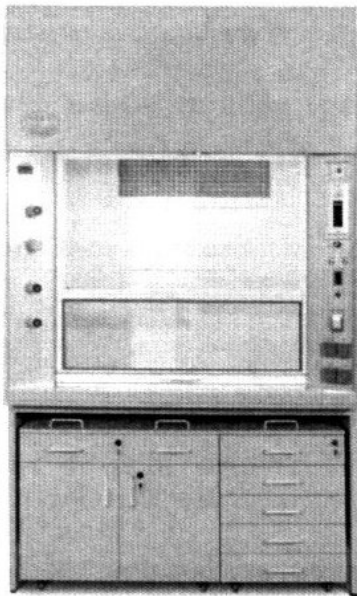
Čemernianska 137

093 03 Vranov nad Topľou, Slovenská republika

... nábytok a digestory pre laboratórium

V spoločnosti ITES Vranov s.r.o. nás zaujímajú predstavy našich zákazníkov. Na Vaše želanie pre Vás vytvoríme laboratórium presne na mieru.

Odlíšte sa od iných laboratórií nielen profesionálnym prevedením laboratórneho nábytku, ale aj napríklad jeho dizajnom a úrovňou bezpečnosti obsluhy. S použitím materiálov špičkovej kvality zároveň zvyšujeme úžitkovú hodnotu nábytku.



ITES partner vo Vašom laboratóriu

KONTAKT

tel: +421-57-4461961, 4431139

fax: +421-57-4422097

e-mail: ites@ites.sk

<http://www.ites.sk>

PRELIMINARY PROGRAM DMS-RE
Závažná Poruba 2009

Monday, August 31, 2009

REGISTRATION..... 10:00 – 13:30
LUNCH..... 13:00
OPENING..... 14:00 – 14:10

LECTURES

14:10 – 14:30	<i>J. Drápala</i> LEAD-FREE SOLDERS ON THE TIN – ZINC - ALUMINIUM BASIS FOR HIGH-TEMPERATURE APPLICATIONS
14:30 – 14:50	<i>D. Lysáček</i> THERMAL STABILITY OF UNDOPED POLYSILICON LAYERS
14:50 – 15:10	<i>J. Lipták</i> STRUCTURE AND ELECTRICAL PROPERTIES OF COMPOSITES OF POLYSTYRENE WITH MODIFIED CARBON BLACK
15:10 – 15:30	<i>R. Dvorský</i> MORPHOLOGY ANALYSIS OF SILICON NANOPARTICLES PREPARED BY CAVITATION DISINTEGRATION
15:30 – 16:00	COFFEE BREAK
16:00 – 16:20	<i>J. Gutwirth</i> BASIC ASPECTS AND TRENDS IN DEVELOPMENT OF NON-VOLATILE REWRITABLE PHASE-CHANGE BASED MEMORIES - OPTICAL DISCS AND PC-RAM MODULES
16:20 – 16:40	<i>J. Juřica</i> MICROSTRUCTURE PROPERTIES OF TiAl-Nb ALLOY
16:40 – 17:00	<i>J. Lipka</i> PARAMETERS OF SPENT RADIOACTIVE SOURCE

EVENING PROGRAMME:

WELCOME PARTY..... 19:30

Tuesday, September 1, 2009

BREAKFAST..... 08:00

LECTURES

09:00 – 09:20	<i>P. Demo</i> STIMULATED NUCLEATION ON POLYMER NANOFIBRES
09:20 – 09:40	<i>Z. Kožíšek</i> NUCLEATION BARRIER IN SMALL VOLUMES
09:40 – 10:00	<i>K. Nitsch</i> GROWTH OF RARE EARTH GARNET LAYERS BY LIQUID PHASE EPITAXY
10:00 – 10:30	COFFEE BREAK
10:30 – 10:50	<i>M. Rodová</i> PREPARATION AND PROPERTIES OF LITHIUM YTTRIUM PHOSPHATE - $\text{LiY}(\text{PO}_3)_4$ GLASS
10:50 – 11:10	<i>R. Král</i> STUDY ON GROWTH OF LEAD HALIDES SINGLE CRYSTALS FOR SOLID-STATE LASERS IN MID-IR
11:10 – 11:30	<i>J.A. Mareš</i> SCINTILLATION PROPERTIES OF Ce^{3+}-DOPED (Y-Lu) ALUMINUM GARNETS GROWN BY LPE METHOD IN DIFFERENT FLUXES
11:30 – 11:50	<i>I. Čulák</i> ANAMET s.r.o. INSTRUMENTS FOR MATERIAL TESTING

LUNCH..... 12:30

LECTURES

14:00 – 14:20	<i>M. Behúlová</i> APPROACHES TO THE MODELLING OF METALLIC MATERIAL PROCESSING IN SEMI-SOLID STATE
14:20 – 14:40	<i>M. Martinkovič</i> COMPARISON OF PLASTIC DEFORMATION AND GRAIN BOUNDARIES ORIENTATION OF STEEL
14:40 – 15:00	<i>P. Nemeč</i> MATHEMATICAL CALCULATION OF TOTAL HEAT POWER OF THE SODIUM HEAT PIPE
15:00 – 15:20	<i>I. Pilarčíková</i> MODELLING OF CONSTRICTION PHENOMENON IN COMPOSITE CONTAINING CONDUCTIVE CARBON PARTICLES
15:20 – 16:00	COFFEE BREAK
16:00 – 16:20	<i>L. Válek</i> ENGINEERING OF DEFECTS IN HEAVILY BORON-DOPED SILICON
16:20 – 16:40	<i>O. Blahož</i> EFFECT OF THERMOMECHANICAL CYCLING ON CHARACTERISTIC OF Ni – Ti SHAPE MEMORY ALLOYS
16:40 – 17:00	<i>P. Nemeč</i> PROPOSAL OF HEAT EXCHANGER IN MICRO-COGENERATION UNIT, CONFIGURATION WITH BIOMASS COMBUSTION
17:00 – 17:20	<i>J. Šik</i> BOND AND ETCH-BACK SOI

DINNER..... 18:00
FREE EVENING

Wednesday, September 2, 2009

BREAKFAST..... 08:00

**PANEL DISCUSSION
AND
JOINT MEETING OF THE
SLOVAK EXPERT GROUP OF SOLID STATE CHEMISTRY AND PHYSICS
AND
CZECH AND SLOVAK ASSOCIATION FOR CRYSTAL GROWTH**

DINNER..... 18:00

Thursday, September 3, 2009

BREAKFAST..... 08:00

LECTURES

09:00 – 09:20	<i>S. Lalíková</i> THE PROPERTIES OF NATURAL RUBBER/CLAY COMPOUNDS
09:20 – 09:40	<i>V. Jorík</i> ZEOLITES AND POWDER DIFFRACTION
09:40 – 10:00	<i>T. Bazyláková</i> STUDY OF ZEOLITES AS FILLER IN THE RUBBER COMPOUNDS
10:00 – 10:30	COFFEE BREAK
10:30 – 10:50	<i>V. Brožek</i> COMPATIBILITY OF PLASMA SPRAYED TUNGSTEN BASED MATERIALS WITH GRAPHITE SUBSTRATES
10:50 – 11:10	<i>J. Sedláček</i> STRUCTURE AND ELECTRIC RESISTIVITY OF SINTERED AND PLASMA SPRAYED TUNGSTEN – BASED CERMETS
11:10 – 11:30	<i>P. Štěpán</i> SHAPE MEMORY ALLOYS ON THE BASE OF TiNb
11:30 – 11:50	<i>R. Yatskiv</i> INFLUENCE OF RARE-EARTH ELEMENTS ON ELECTRICAL AND OPTICAL PROPERTIES OF INP BULK CRYSTALS
11:50 – 12:10	<i>J. Nováček</i> COMPREHENSIVE TESTING OF STRUCTURAL POWDER MASS WATER REPELLENTS BASED ON SILICONE

LUNCH..... 12:30

LECTURES

14:00 – 14:20	<i>I. Šabová</i> HETEROBIMETALLIC COORDINATION COMPOUNDS BASED ON COPPER AND NICKEL
14:20 – 14:40	<i>A. Pavlová</i> COMPLEXES OF Ni(II) WITH 2,2'-DIPYRIDYLAMINE
14:40 – 15:00	<i>M. Vavra</i> SPECTRAL-STRUCTURAL CORRELATIONS IN COPPER(II) TETRACYANIDOPLATINATE COMPLEXES WITH BI- AND TRIDENTATE N-DONOR LIGANDS
15:00 – 15:20	<i>B. Papánková</i> THE ZERO FIELD SPLITTING OF PARAMAGNETIC TRANSITION METAL COMPLEXES
15:20 – 15:50	COFFEE BREAK
15:50 – 16:10	<i>L. Dlháň</i> SPIN CROSSOVER IN Fe(II) COMPLEXES MONITORED BY DSC CALORIMETRY
16:10 – 16:30	<i>M. Koman</i> NEW HALOGENCARBOXYLATES OF Cu(II) WITH NICOTINAMIDE
16:30	CLOSING

EVENING PROGRAMME:

FAREWELL PARTY..... 19:30

Friday, September 4, 2003

BREAKFAST..... 08:00

DEPARTURE (*individual*)..... 09:00

Programming Committee is authorized to necessary changes in the time table.

AUTHORS INDEX

B

Bazyláková T., 12, 40
Behúlová M., 14
Beitlerová A., 48
Blahož O., 16
Boča R., 22, 58
Boldyryeva H., 18
Brožek V., 18, 68

C,Č

Cihlář A., 38, 54, 64
Ctibor P., 18, 68
Černák J., 60, 66
Čulák I., 82

D

Demo P., 20, 36
Dlháň L., 22, 58
Drápala J., 24
Dvorský R., 44

F

Frumar M., 26

G

Gutwirth J., 26

H

Hassan N., 22
Hampl J., 62
Hužvár J., 28, 52

CH

Cheong D.-I., 18, 68

J

Jirků S., 62
Jorík V., 30
Juřica J., 32

K

Koman M., 34
Kostelník P., 72
Kožíšek Z., 20, 36
Král R., 38, 54, 64
Krňanský J., 20

Kroupa A., 24
Kučera M., 48
Kursa M., 16

L,Ľ

Ľalíková S., 12, 40
Liner W., 22
Lipka J., 70
Lipták J., 42
Lorenc M., 72
Losertová M., 32, 74
Luňáček J., 44
Lysáček D., 46, 76

M

Mareš J. A., 48
Martinkovič M., 50
Moncol' J., 34

N

Nemec P., 28, 52
Nikl M., 48
Nitsch K., 48, 54, 64
Nováček J., 56

O

Olšovský M., 12, 40,
Ondrušová D., 12, 40,

P

Pajtášová M., 12, 40
Papánková B., 58
Pavlišáková N., 60
Pavlová A., 60
Piksová K., 44
Pilarčíková I., 62
Pekarek L., 80
Potočňák I., 78
Průša P., 48

R

Rodová M., 54, 64

S,Š

Sabová I., 66
Sedláček J., 68
Sitek J., 70
Slíva A., 44
Smetana B., 24
Sveshnikov A. M., 20, 36
Svoboda I., 58
Šik J., 72, 76
Šťastník S., 56
Štěpán P., 74

T

Tichá P., 20, 36
Titiš J., 58

U

Urbánek J., 24

V

Válek L., 46, 76
Vavra M., 78

W

Wágner T., 26
Weinberger P., 22

Y

Yang S.-H., 18, 68
Yatskiv R., 80

Z

Zavadil J., 80

REMARKS

POST DEADLINE ABSTRACT

THIN-FILM THICKNESS DETERMINATION FROM A SPECTRAL REFLECTANCE MEASUREMENT BY USING AN ALTERNATIVE ENVELOPE METHOD

M. Luňáčková^(a), J. Luňáček^(b), Z. Potůček^(c), P. Hlubina^(b)

- (a) Department of Mathematics and Descriptive Geometry, VŠB - Technical University of Ostrava, 17. listopadu 15, 708 33 Ostrava - Poruba, Czech Republic
- (b) Department of Physics, VŠB - Technical University of Ostrava, 17. listopadu 15, 708 33 Ostrava - Poruba, Czech Republic
- (c) Department of Solid State Engineering, Faculty of Nuclear Sciences and Physical Engineering, CTU in Prague, Trojanova 13, 120 00 Praha 2, Czech Republic

This paper deals with an alternative envelope method of determining the thickness of a non-absorbing thin film on an absorbing substrate (the wavelength-dependent optical parameters of the thin film and the substrate are known) from only one extreme of the reflectance spectrum.

If we assume air as the ambient medium, the non-absorbing thin film and the absorbing substrate, we can write the well-known equation for reflectance of the thin-film structure [1]:

$$R(\lambda) = \frac{R_1(\lambda) + R_2(\lambda) + 2[R_1(\lambda)R_2(\lambda)]^{1/2} \cos[2\beta(\lambda) + \phi(\lambda)]}{1 + R_1(\lambda)R_2(\lambda) + 2[R_1(\lambda)R_2(\lambda)]^{1/2} \cos[2\beta(\lambda) + \phi(\lambda)]}, \quad (1)$$

where the reflectance $R_1(\lambda)$ and $R_2(\lambda)$ correspond to both boundaries of the thin-film structure and the phase change $\beta(\lambda)$ and the phase shift $\phi(\lambda)$ are given by:

$$\beta(\lambda) = \frac{2\pi}{\lambda} n_1(\lambda) d \cos \alpha, \quad (2)$$

$$\tan \phi(\lambda) = \frac{2n_1(\lambda)\kappa_2(\lambda)}{n_1^2(\lambda) - n_2^2(\lambda) - \kappa_2^2(\lambda)}, \quad (3)$$

where d is a thin-film thickness and α is an angle of refraction.

Knowing the optical constants of the thin-film structure, we can construct one envelope tangent to the spectrum around the reflection maxima and the second one around the reflection minima. The two envelopes correspond to the conditions:

$$\cos[2\beta(\lambda) + \phi(\lambda)] = \pm 1. \quad (4)$$

These equations contain the relationship between the thin-film thickness and the tangent wavelengths $\lambda_{\tan, m}$ of the reflectance spectrum to the outer envelopes [2]:

$$d = \frac{\lambda_{\tan, m}}{4\pi n_1(\lambda)} \left(m\pi - \tan^{-1} \left[\frac{2n_1(\lambda)\kappa_2(\lambda)}{n_1^2(\lambda) - n_2^2(\lambda) - \kappa_2^2(\lambda)} \right] \right), \quad (5)$$

where m is an integer which is referred to the interference order. A simple linear relation (see Fig. 1) between the tangent wavelengths $\lambda_{\tan, m}$ and thin-film thickness d_{\tan} is revealed:

$$d_{\tan} = A + B\lambda_{\tan, m}, \quad (6)$$

where the characteristic parameters A and B are connected with the known wavelength-dependent optical parameters of the thin-film structure and interference order only.

This method was applied to the SiO₂ thin films prepared on the Si wafers. Silicon wafers were supplied by company ON Semiconductor Czech Republic. SiO₂ thin films were prepared on

Si wafers by dry oxidation technique at furnace at temperature 1200 C (Deal-Grove model). The reflectance measurements were performed by standard procedure with spectrophotometer Shimadzu UV-3600 in the spectral region 185 – 3100 nm [3].

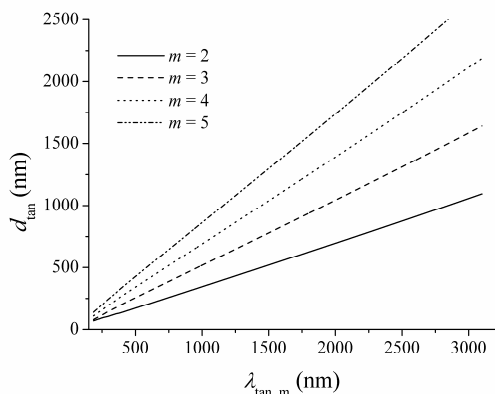


Fig. 1 Linear dependence between the thin thickness d_{tan} and the tangent wavelength $\lambda_{\text{tan}, m}$ for interference orders $m = 2, 3, 4$ and 5 .

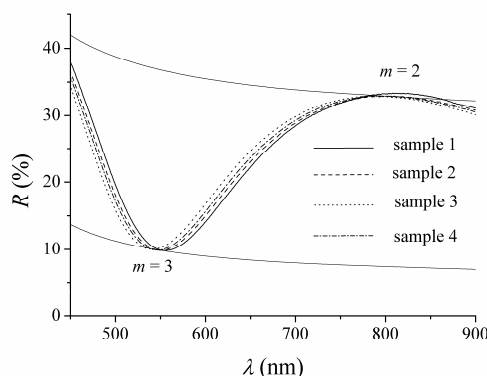


Fig. 2 Part of the experimental reflectance spectra of the samples with two suitable interference orders $m = 2$ and 3 .

The efficiency of this method is shown in Tab. 1 which demonstrates a very good agreement between the thicknesses determined by the fitting method [3] with the ones determined by using Eq. (6), to the exclusion of the sample 1 for $m = 2$ due to the inaccurate measurement evidently (see Fig. 2).

Table 1. Comparison of the values d_{fit} [3] and $d_{\text{tan}, m}$ for SiO_2 thin films for interference orders $m = 2$ and 3 . Wavelength range is 450 – 900 nm.

sample	d_{fit} (nm)	C_{fit}	$d_{\text{tan}, 2}$ (nm)	$d_{\text{tan}, 3}$ (nm)
1	283,5	0.9998	296,1	283,6
2	280,9	0.9999	283,6	280,7
3	276,0	0.9999	276,0	276,0
4	278,2	0.9996	278,8	279,1

This simple method could be well applied in the following cases; e.g. when the reflectance spectra indicate only one clear extreme due to either a too narrow wavelength interval of the recording or a small thin-film thickness. The method could be also used for fast measurement of small thin-film thickness changes.

This work was partially supported by the projects MSM 6198910016 and MSM 6840770021.

- [1] M. Born, E. Wolf, Principles of Optics, Cambridge University Press, Cambridge, 1999.
- [2] J. Luňáček, P. Hlubina, M. Luňáčková, Applied Optics, 48 (2009) 985.
- [3] J. Luňáček, Z. Potůček, M. Luňáčková, P. Hlubina, D. Ciprian, Proceedings of the 18th joint seminar DMSRE, September 1-5, 2008, Hnanice, 2008, p. 39.